



Growth yields and light-capture in PhycoCyanin and PhycoErythrin-rich picocyanobacteria, across photic regimes and growth phases

Journal:	<i>Limnology and Oceanography</i>
Manuscript ID:	Draft
Wiley - Manuscript type:	Original Article
Date Submitted by the Author:	n/a
Complete List of Authors:	Śliwińska-Wilczewska, Sylwia; Mount Allison University Department of Biology; University of Gdańsk, Department of Marine Ecosystems Functioning, Faculty of Oceanography and Geography Konik, Marta; University of Victoria, Department of Geography; Polish Academy of Sciences, Institute of Oceanology Savoie, Mireille; Mount Allison University Department of Biology Aguilera, Anabella; Linnaeus University, Department of Biology and Environmental Science, Centre for Ecology and Evolution in Microbial Model Systems (EEMiS); Swedish University of Agricultural Sciences, Department of Aquatic Sciences and Assessment Omar, Naaman; Mount Allison University Department of Biology Campbell, Douglas; Mount Allison University Department of Biology
Keywords:	Cumulative diel photon dose, Light-capture, PAR, Photic regime, Phase of growth, Photoperiod, Picocyanobacteria, PUR
Abstract:	The genus <i>Synechococcus</i> occurs from tropical to arctic zones, with climate scenarios forecasting range expansions of this picocyanobacteria into new photic regimes. We found that coastal PhycoCyanin(PC)-rich and PhycoErythrin(PE)-rich <i>Synechococcus</i> strains grew fastest under moderate photosynthetically active radiation, and a 24-hour photoperiod, despite a cumulative diel photon dose equivalent to conditions where growth was slower, under higher light and shorter photoperiods. Under optimal conditions, a PE-rich <i>Synechococcus</i> sp. achieved a highest recorded cyanobacterial chlorophyll-specific exponential growth rate of 4.5 d ⁻¹ . PE-rich strains demonstrated wider ability to modulate light capture capacity, whereas PC-rich strains showed less change in light capture across increasing cumulative diel photon dose. We found the coastal picocyanobacteria show consistent patterns of an exponential decay of effective absorption cross section for PSII photochemistry, versus increasing cumulative diel PAR doses. Effective absorption cross section for PSII excited through phycobilisome absorbance at 590 nm was positively correlated with phycobiliprotein:Chl a, particularly during pre-stationary growth phase. Within each strain, μ showed consistent saturating responses to increasing cumulative diel PSII electron flux. As photoperiod opportunists coastal picocyanobacteria show potential to expand into longer photic regimes at warming higher latitudes.



SCHOLARONE™
Manuscripts

Scientific Significance Statement Topic

In PhycoCyanin(PC)-rich, and particularly in PhycoErythrin(PE)-rich phenotypes of *Synechococcus*, photoperiod alters the responses of growth rates to cumulative diel photons, with both 8 and 24 h photoperiods provoking increased photoinhibition of growth. In contrast, growth rates show simpler saturating responses to cumulative diel reductant generation, accessed through a chlorophyll fluorescence measure of electron flux, across a matrix of photoperiods and photosynthetically active radiation levels.

Under optimal conditions of 24 h photoperiod and moderate photosynthetically active radiation, a PE-rich *Synechococcus* sp. reached a chlorophyll-specific exponential growth rate of 4.5 d^{-1} , a record for cyanobacteria, comparable with genetically-modified industrial strains.

As photoperiod opportunitists, with capacity to grow rapidly under 24 h photoperiod, coastal *Synechococcus* sp. show potential to emerge as phytoplankton components during summer in future, warmed, polar regions.

Scientific Significance Statement Outlet

Dear Editor-in-Chief

K. David Hambright,

Our work indicating that picocyanobacteria have the potential to expand into new photic regimes while PE-rich picocyanobacteria may emerge as the dominant phytoplankton.

The findings of this study are helpful for further research on picocyanobacteria ecophysiology, and should be of interest to readers of Limnology and Oceanography, which has previously published articles on similar topics.

1 **Growth yields and light-capture in PhycoCyanin and**
2 **PhycoErythrin-rich picocyanobacteria, across photic**
3 **regimes and growth phases**

4

5 **Sylwia Śliwińska-Wilczewska^{1,2}, Marta Konik^{3,4}, Mireille Savoie¹, Anabella**
6 **Aguilera^{5,6}, Naaman M. Omar¹, and Douglas A. Campbell^{1,*}**

7

8 ¹ Department of Biology, Mount Allison University, 53 York St., Sackville, NB, E4L 1C9,
9 Canada

10 ² Institute of Oceanography, University of Gdańsk, 46 Piłsudskiego St, 80-378, Gdynia, Poland

11 ³ Department of Geography, University of Victoria, Victoria, BC, V8P 5C2, Canada

12 ⁴ Institute of Oceanology, Polish Academy of Sciences, 81-712 Sopot, Poland

13 ⁵ Department of Biology and Environmental Science, Centre for Ecology and Evolution in
14 Microbial Model Systems (EEMiS), Linnaeus University, Kalmar, Sweden

15 ⁶ Department of Aquatic Sciences and Assessment, Swedish University of Agricultural Sciences,
16 Uppsala, Sweden (present address)

17 * Correspondence: Douglas A. Campbell <dubhglas.cambeuil@gmail.com>

18

19 **Running head:** *Picocyanobacteria across photic regimes*

20

21 **Abstract**

22 The genus *Synechococcus* occurs from tropical to arctic zones, with climate scenarios
23 forecasting range expansions of this picocyanobacteria into new photic regimes. We found that
24 coastal PhycoCyanin(PC)-rich and PhycoErythrin(PE)-rich *Synechococcus* strains grew fastest
25 under moderate photosynthetically active radiation, and a 24-hour photoperiod, despite a
26 cumulative diel photon dose equivalent to conditions where growth was slower, under higher
27 light and shorter photoperiods. Under optimal conditions, a PE-rich *Synechococcus* sp. achieved
28 a highest recorded cyanobacterial chlorophyll-specific exponential growth rate of 4.5 d^{-1} . PE-
29 rich strains demonstrated wider ability to modulate light capture capacity, whereas PC-rich
30 strains showed less change in light capture across increasing cumulative diel photon dose. We
31 found the coastal picocyanobacteria show consistent patterns of an exponential decay of effective
32 absorption cross section for PSII photochemistry, versus increasing cumulative diel PAR doses.
33 Effective absorption cross section for PSII excited through phycobilisome absorbance at 590 nm
34 was positively correlated with phycobiliprotein:Chl *a*, particularly during pre-stationary growth
35 phase. Within each strain, μ showed consistent saturating responses to increasing cumulative diel
36 PSII electron flux. As photoperiod opportunists, coastal picocyanobacteria show potential to
37 expand into longer photic regimes at warming higher latitudes.

38

39 **Introduction**

40 The photic regime, comprised of Photosynthetically Active Radiation (PAR), spectral
41 quality, and photoperiod, is a pivotal influence on the growth and productivity of phytoplankton
42 within aquatic ecosystems. PAR refers to the spectral range of solar radiation, approximately
43 400-700 nm, that is capable of driving photosynthesis. The availability and distribution of PAR

44 in aquatic ecosystems is influenced by cloud cover, water depth, and light attenuation due to
45 water turbidity and suspended particles, including phytoplankton cells (Field et al. 1998;
46 Torremorell et al. 2009). Photosynthetically Usable Radiation (PUR), in turn is the fraction of
47 PAR that can be absorbed for photosynthesis by pigments of a given cyanobacteria or algae
48 (Morel 1978). PUR thus depends upon the interaction of PAR, and the phytoplankter expression
49 of genomic capacities for light capture (Moejes et al. 2017). Cyanobacteria also respond to
50 changes in photoperiod, which serves as a key environmental cue for photosynthesis, growth,
51 reproduction, and nutrient assimilation (LaRoche and Robicheau 2022). Thus, in polar regions,
52 characterized by prolonged periods of wintertime darkness and continuous daylight during
53 summer, cyanobacteria encounter unique challenges. Light is the primary limitation on biomass
54 production in winter, suppressing cyanobacteria growth and metabolic activity, whereas
55 extended daylight in summer boosts photosynthetic activity (Arrigo 2014). In temperate regions,
56 seasonal variation in light-limitation is less pronounced, but cyanobacteria are still influenced by
57 daily and seasonal fluctuations, with a contrast between more favorable conditions for
58 cyanobacteria growth in spring and summer, compared to fall and winter (Huisman et al. 2002;
59 Holtrop et al. 2021). In the tropics, daylight hours remain nearly constant throughout the year
60 (Behrenfeld et al. 2006), and cyanobacteria productivity is rather controlled by nutrients
61 resupplied into the euphotic zone (Li et al. 2015), and mortality through viral lysis (Ortmann et
62 al. 2002) and zooplankton grazing (Christaki et al. 1999).

63 *Synechococcus*, a diverse genus of picocyanobacteria, exhibits a distribution spanning
64 diverse geographical regions (Flombaum et al. 2013), with strains demonstrating a remarkable
65 range of adaptations to environmental conditions (Śliwińska-Wilczewska et al. 2018a; Aguilera
66 et al. 2023). *Synechococcus* capacities to thrive across diverse marine and freshwater habitats

positions it as a pivotal agent in energy and nutrient transfer within food webs, connecting the microbial loop with higher trophic levels, offering direct sustenance to grazers, including zooplankton and small fish (Li 1995). As one of the two dominant picocyanobacterial genera in oceanic waters, *Synechococcus* contribute significantly to light attenuation and light availability for other photosynthetic marine organisms, thereby influencing ocean colour and allowing satellite detection of *Synechococcus*-rich communities (Xi et al. 2020). General relations among optical absorption spectra and pigment compositions have been used to determine diagnostic pigment indices of major phytoplankton functional types (Hirata et al. 2011). Modeling suggests that *Synechococcus* abundance and ranges will increase due to climate warming (Flombaum et al. 2013). The projected changes may vary geographically and may include shifts in the spatial distribution of the main picocyanobacteria, as well as changes in the proportions among *Synechococcus* sp. lineages (Six et al. 2021), potentially pushing lineages into new photic regimes. *Synechococcus* exhibits significant phenotypic diversity across lineages, encompassing strains rich in phycobiliprotein pigments, phycoerythrin (PE-rich) or phycocyanin (PC-rich) (Haverkamp et al. 2009; Aguilera et al. 2023). Phycobiliprotein pigments are pivotal for light absorption during photosynthesis and confer distinctive colours to the picocyanobacteria (Stomp et al. 2007). The disparate light preferences between PC-rich and PE-rich *Synechococcus* sp. strains influence their ecological niches. PC-rich strains thrive in environments with elevated light levels, such as surface waters and coastal regions. PE-rich strains exhibit adaptation to lower-light conditions, primarily inhabiting the deeper layers of the water column. PC-rich and PE-rich *Synechococcus* sp. strains thus predominantly occupy complementary habitats (Six et al. 2007; Haverkamp et al. 2009; Six et al. 2021), although differential responses of *Synechococcus*

89 lineages to photoperiod, have not been studied in detail, except for thermophilic PC-rich
90 *Synechococcus* PCC 6715 (Klepacz-Smółka et al. 2020).

91 Cyanobacteria growth includes lag, exponential growth, stationary, and death phases
92 (Reynolds 2006). During the lag phase, cyanobacteria acclimate to the environment and prepare
93 for active growth by synthesizing essential cellular components. Exponential growth phase is
94 marked by cell division and biomass accumulation, fueled by nutrient and light availability. If
95 growth is limited by declining nutrients, by light, or by accumulation of inhibitory factors, algae
96 enter stationary phase, characterized by a balance between cell division and death, leading to a
97 plateau in population. The death phase occurs when cyanobacteria cell death outruns division,
98 leading to net decomposition, contributing to nutrient recycling in aquatic ecosystems (Reynolds
99 2006). Moreover, Schuurmans et al. (2017) proposed an additional phase between the
100 exponential and stationary phases of picocyanobacteria growth, which is often neglected in
101 physiological studies. Herein, we examined the physiological responses of PC-rich and PE-rich
102 *Synechococcus* sp. in this phase, which we termed the pre-stationary phase of growth.

103 Picocyanobacteria are the most abundant phytoplankters in aquatic ecosystems and are
104 crucial to the optical properties of ocean water, by influencing its colour and transparency. PC-
105 rich and PE-rich *Synechococcus* sp. may have different costs and physiological strategies for
106 growth under different photic regimes, which could drive spatial and temporal variability of
107 picocyanobacteria biomass and community composition, in current and potential future aquatic
108 habitats. Therefore, our aim was to determine whether photic regimes and growth phases
109 differentially affect growth and light-capture, between representative PC-rich and PE-rich
110 *Synechococcus* sp.

111

112 **Materials and Methods**

113 **Experimental setup**

114 Two xenic PhycoCyanin(PC)-rich (CCBA_056 or CCBA_077) strains and two
115 PhycoErythrin(PE)-rich (CCBA_048 or CCBA_127) strains of *Synechococcus* were obtained
116 from the Culture Collection of Baltic Algae (CCBA; <https://ccba.ug.edu.pl/pages/en/home.php>).
117 Pre-cultures of picocyanobacteria strains were maintained in Tissue Culture Flasks (VWR
118 International, Cat. No. 10062-872, PA, USA) and were transferred to fresh f/2 media (Guillard
119 1975) at salinity of 8 PSU (which corresponds to their natural habitat) every two weeks, under a
120 photoperiod of 12 h and Photosynthetically Active Radiation (PAR) of 10 $\mu\text{mol photons m}^{-2}\text{s}^{-1}$
121 supplied from cool white fluorescent tubes, at 22°C.

122 Experimental cultures of each strain were grown in 8 x 80 mL round bottom cylindrical
123 glass tubes in a Multi-Cultivator MC 1000-OD (Photon Systems Instruments, Drásov, Czech
124 Republic). Each culture tube contained 75 mL of f/2 medium inoculated with 5 mL of growing
125 pre-culture, to achieve exponential growth from the beginning of the experiment, with little to no
126 lag phase upon inoculation. Culture tubes were inoculated in the afternoon while the
127 photoregime of a sinusoidal photoperiod commenced the following morning such that peak PAR
128 occurred at noon each day.

129 Cultures grew at 22°C, with photoperiods of 8, 12, 16, or 24 h, with peak PAR of 30, 90,
130 180, 300, 600, or 900 $\mu\text{mol photons m}^{-2}\text{s}^{-1}$ independently supplied to each culture tube from
131 white LED lamps. To approximate diel cycles, the photoperiods of 8 – 16 h were applied in a
132 sinusoidal shape, while the 24-hour photoperiod was applied continuously in a square shape.
133 The area under the sinusoidal curve is 1/2 the area under a square of equal width, therefore at

134 equivalent peak PAR the 24 h square photoperiod cultures received 4 times the diel photon doses
135 of the 12 h sinusoidal photoperiod cultures.

136 Culture tubes were closed with a silicone inert silicone stopper perforated by an aeration
137 input tube extending to the bottom of the culture tube, and a pressure outlet tube. Aeration with a
138 total air flow rate of around $\sim 140 \text{ mL min}^{-1} \text{ tube}^{-1}$ through a $0.2\mu\text{m}$ filter ensured mixing and
139 provided sufficient air/ CO_2 supply to cultures through the entire culture volume. The pH of
140 tested cultures did not fluctuate fiercely during the experiment and remained at approximately 8
141 – 9. Light, temperature, optical density, and aeration gas of the Multi-Cultivator system were
142 monitored and controlled via the Photobioreactor Control Software (Photon Systems
143 Instruments, Drásov, Czech Republic).

144

145 **DNA extractions**

146 Samples for total genomic DNA were collected by harvesting 10 mL of each culture and
147 centrifuging for 8 minutes at 8,000 x. DNA was extracted using the FastDNATM SPIN Kit for
148 Soil (MP Biomedicals) with Matrix E columns following manufacturer instructions with the
149 addition of an incubation with proteinase-K (1% final concentration) at 55°C for one hour. DNA
150 concentration was measured using an Invitrogen Qubit 2.0 fluorometer (Thermo Fisher Scientific
151 Inc.) and purity was assessed using a Thermo ScientificTM NanoDrop 2000 spectrophotometer
152 (Thermo Fisher Scientific Inc.).

153 The phylogenetic placement of CCBA strains (Fig. S1 in Supporting Information) within
154 cluster 5 picocyanobacteria was explored by amplifying and sequencing a fragment of the 16S
155 rRNA gene using universal primers 27F and 1492R (Lane 1991). 16S rRNA gene sequences
156 were aligned with MAFFT v. 7.5 using the G-INS-I algorithm (Katoh et al. 2019). Phylogenetic

157 trees were created using IQ-TREE v. 1.6.12 (Hoang et al. 2018), using GTR+F+I+R3 model
158 determined by ModelFinder (Kalyaanamoorthy et al. 2017). Bootstrap values were calculated
159 with 1000 replicates (Hoang et al. 2018).

160

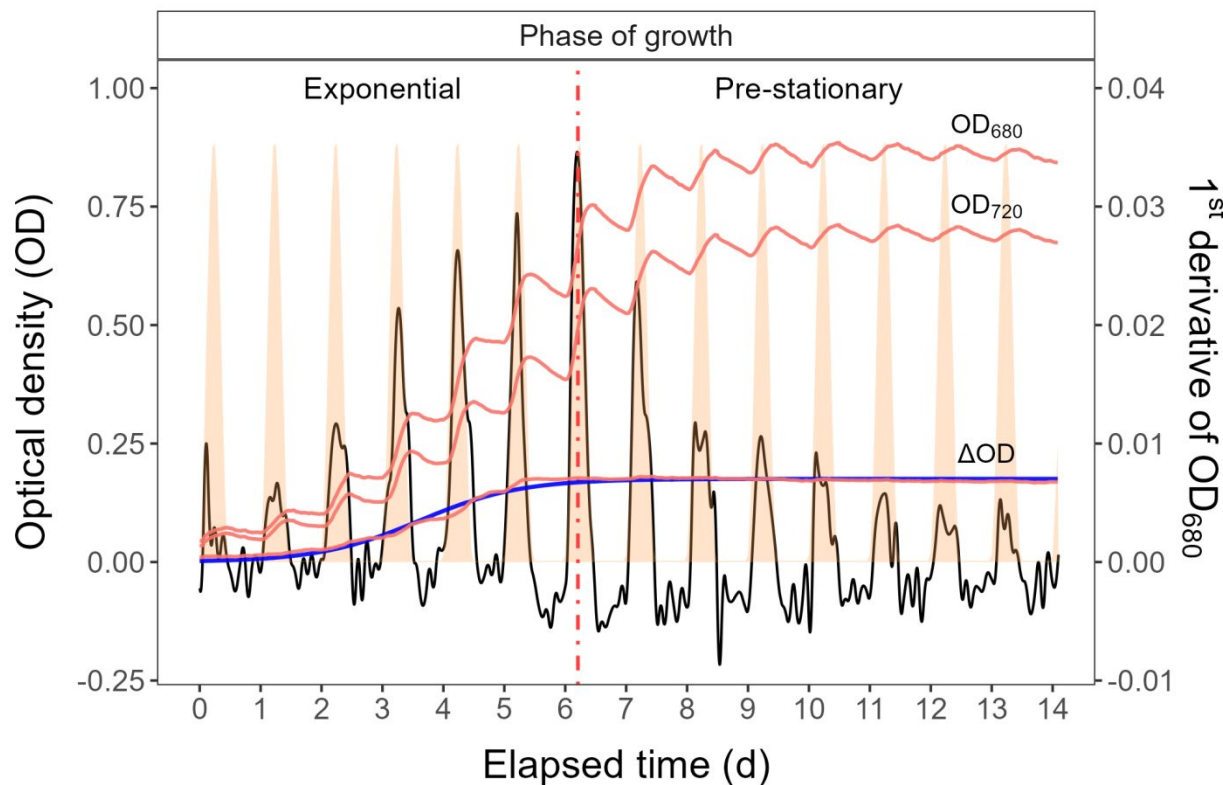
161 **Growth curves and chlorophyll-specific exponential growth rates**

162 Picocyanobacterial growth was monitored every 5 minutes by automatically recording
163 OD₆₈₀, OD₇₂₀, and ΔOD ($\Delta\text{OD} = \text{OD}_{680} - \text{OD}_{720}$) for 14 days, independently for each culture
164 tube. The exceptions were experiments conducted with a photoperiod of 24 h and light of 600 or
165 900 $\mu\text{mol photons m}^{-2}\text{s}^{-1}$, which lasted 7 days (Fig. S2). The chlorophyll-specific exponential
166 growth rates (μ) were determined by fitting logistic growth curves using a modified Levenberg-
167 Marquardt fitting algorithm (Elzhov et al. 2023) to plots of the chlorophyll *a* proxy of ΔOD
168 vs. elapsed time for each combination of strain, photoperiod, and peak PAR (Fig. S3).

169 To summarize the growth responses of the four picocyanobacterial strains we used a
170 Generalized Additive Model (GAM) (Wood 2017) was applied to the relation of chlorophyll-
171 specific μ , d^{-1} to photoperiod and PAR level. The R package *mgcv* (Wood 2017) was used to
172 model the growth rate with smoothing terms and indicate the 90, 50 and 10% quantiles for
173 growth rate across the levels of factors. Only growth rate estimates for which the amplitude of
174 standard error was smaller than 50% of the fitted growth rate were included in the GAM. We
175 visually compared the GAM contours to isolines of equal cumulative diel PAR ($\mu\text{mol photons}$
176 $\text{m}^{-2}\text{d}^{-1}$).

177 The 1st derivative of OD₆₈₀ taken over 1 h increments was computed using *xts*: eXtensible
178 Time Series (Ryan et al. 2024) and *signal*: Signal Processing (Ligges et al. 2024) R packages.
179 The time when the cultures reached their maximum absolute hourly growth (tMaxAHG) of the

180 1st derivative of OD₆₈₀ was taken as the time of transition from exponential to pre-stationary
 181 growth phases (Fig. 1).



182
 183 **Fig. 1.** Example of a growth curve (tracked as OD₇₂₀, OD₆₈₀, or ΔOD; red solid lines, left y-axis) of PE-rich culture
 184 of *Synechococcus* sp. (048) vs. elapsed time (d, x-axis). 1st derivative of OD₆₈₀ taken over 1 h increments (black
 185 solid line, right y-axis); solid blue line shows logistic fits of chlorophyll proxy OD₆₈₀ – OD₇₂₀ (ΔOD) vs. elapsed
 186 time. The vertical red dot dash line represents the time when the culture reached the maximum of the 1st derivative
 187 of OD₆₈₀, or maximum absolute hourly growth (tMaxAHG), taken as the time of transition from exponential to pre-
 188 stationary growth phases.

189

190 Whole-cell absorbance spectra

191 Absorbance measurements on intact cells in suspension were conducted in an integrating
 192 cavity upgrade spectrophotometer (CLARiT^Y 17 UV/Vis/NIR, On-Line Instrument Systems,
 193 Inc., Bogart, GA, USA). 8 mL of f/2 medium were added to both the sample and reference

194 observation cavities of the spectrophotometer. After recording a baseline from 375 to 710 nm, 1
195 mL was withdrawn from the sample cavity and replaced with 1 mL of picocyanobacteria cell
196 suspension. The pathlength corrected absorbance per cm was performed by determining the
197 Jávorfi coefficients (Jávorfi et al. 2006) as described in the equipment manual.

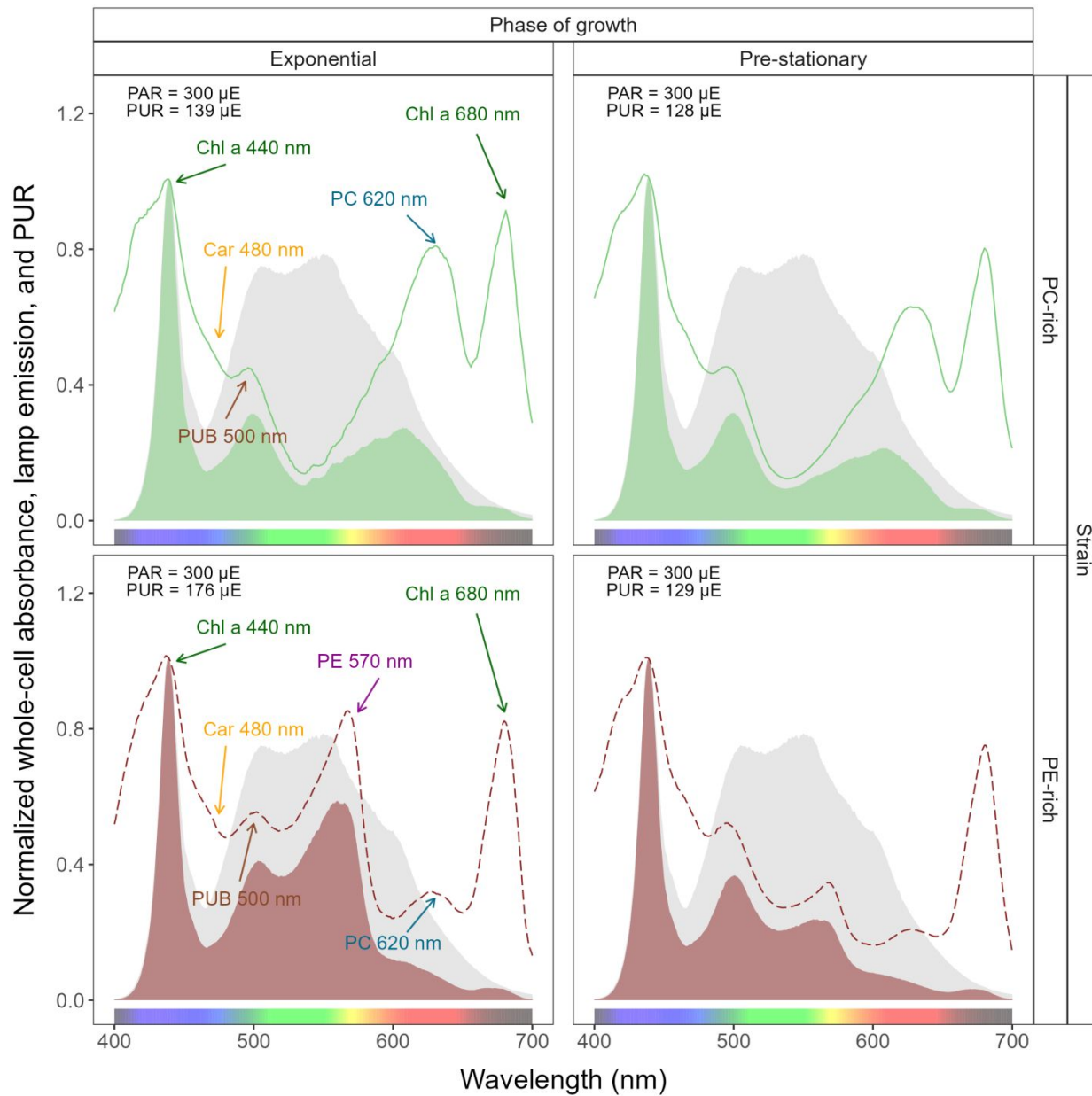
198

199 Photosynthetically Usable Radiation (PUR)

200 Using whole-cell absorbance spectra of *Synechococcus* sp. cultures (Fig. 2, we estimated
201 Photosynthetically Usable Radiation (PUR; $\mu E = \mu\text{mol photons m}^{-2}\text{s}^{-1}$) according to (Morel
202 1978). We normalized the obtained whole-cell Absorbances (A) and the Emission spectra of the
203 white LED lamps (Em) from 400 nm to 700 nm to a reference wavelength of 440 nm. PUR is
204 then the ratio of the sum of Absorbance Normalized to 440 nm (NormA₄₄₀) multiplied by the
205 sum of Emission spectra Normalized to 440 nm (NormEm₄₄₀) to the sum of the Emission spectra
206 Normalized to 440 nm (NormEm₄₄₀), multiplied by the PAR (Eq. (1)).

$$207 PUR (\mu E) = \frac{\sum(NormA_{440} \times NormEm_{440})}{\sum(NormEm_{440})} \times PAR (\mu E) \quad (1)$$

208



209

210 **Fig. 2.** Whole-cell absorbance spectra of PC-rich (solid green lines) or PE-rich (dashed red lines) cultures of
 211 *Synechococcus* sp. Representative absorbance spectra, normalized to 440 nm (NormA_{440}), were measured from the
 212 exponential or pre-stationary phases of growth, together with emission spectra of the white LED lamp used for PAR,
 213 normalized to emission at 440 nm (NormEm_{440} , light gray area), in this example PAR was $300 \mu\text{mol photons m}^{-2}\text{s}^{-1}$.
 214 Estimated Photosynthetically Usable Radiation (PUR) is shown as a darker green area for the PC-rich strain and a
 215 darker red area for the PE-rich strain, with PUR given for each culture ($\mu\text{E} = \mu\text{mol photons m}^{-2}\text{s}^{-1}$). Peaks

216 characteristic of known pigments are labeled; Chl *a*, chlorophyll *a*; PC, phycocyanin; PE, phycoerythrin; PUB,
217 phycobilin; Car, carotenoids.

218

219 Cumulative diel PAR and PUR

220 Based on the length and shape of the photoperiod (sinusoidal wave for photoperiods of 8,
221 12, 16 h; square for photoperiod of 24 h) and the peak PAR ($\mu\text{E} = \mu\text{mol photons m}^{-2}\text{s}^{-1}$), we
222 estimated the value of the cumulative diel PAR ($\mu\text{mol photons m}^{-2}\text{d}^{-1}$). For sinusoidal
223 photoperiods we used Eq. (2); for the continuous 24 h photoperiod we used Eq. (3). Cumulative
224 diel PUR was estimated similarly after estimation of peak PUR from peak PAR.

$$225 \frac{\text{Cumulative diel PAR } (\mu\text{mol photons m}^{-2} \text{ d}^{-1})}{\text{PAR } (\mu\text{E}) \times 60 \text{ (s min}^{-1}\text{)} \times 60 \text{ (min h}^{-1}\text{)} \times \text{photoperiod (h d}^{-1}\text{)}}{2} \quad (2)$$

$$226 \frac{\text{Cumulative diel PAR } (\mu\text{mol photons m}^{-2} \text{ d}^{-1})}{\text{PAR } (\mu\text{E}) \times 60 \text{ (s min}^{-1}\text{)} \times 60 \text{ (min h}^{-1}\text{)} \times \text{photoperiod (h d}^{-1}\text{)}} \quad (3)$$

227

228 Pigment content

229 Chlorophyll *a* (Chl *a*) ($\mu\text{g mL}^{-1}$) was measured using Trilogy Laboratory Fluorometer
230 (Turner Designs, Inc., CA, USA) equipped with Chlorophyll In-Vivo Module, previously
231 calibrated using 20 mL ampoules with known Chl *a* concentrations in 3:2 90% acetone:DMSO
232 solution. Quantitative analysis of Chl *a* was obtained after adding 50 μL of culture and 2 mL of a
233 90% acetone:DMSO solution in a 3:2 ratio.

234 We also estimated the pigment content ($\mu\text{g mL}^{-1}$): chlorophyll *a* (Chl *a*), carotenoids (Car),
235 phycoerythrin (PE), phycocyanin (PC), and allophycocyanin (APC) in *Synechococcus* sp.
236 cultures over time using previously determined linear correlations between pigment content
237 obtained by extraction (Strickland and Parsons 1972; Bennett and Bogorad 1973) and absorbance

values of individual pigment peaks (Car; 480, PE; 565, PC; 620, APC; 650, and Chl *a*; 665 nm) obtained from the whole-cell absorbance spectra using integrating cavity upgrade spectrophotometer (CLARiTY 17 UV/Vis/NIR, On-Line Instrument Systems, Inc., Bogart, GA, USA) (Tab. S1 in Supporting Information). The sum of phycobiliproteins (PE, PC, APC protein) to Chl *a* ratio ($\mu\text{g}:\mu\text{g}$) for individual strains was also calculated.

243

244 **PSII effective absorption cross section of PSII and electron flux**

245 We harvested 2 mL of cultures for photophysiological characterizations repeatedly across
246 the growth trajectories. We used Fast Repetition Rate fluorometry (Kolber et al. 1998) (FRRf,
247 Solisense, USA), with a lab built temperature control jacket (22°C), to apply series of flashlets to
248 drive saturation induction/relaxation trajectories, fit using the onboard Solisense LIFT software
249 (Falkowski and Kolber 1993; Kolber et al. 1998). From the model fits we took the initial
250 fluorescence before induction (F_0 , F_0' , or F_S , depending upon the level of actinic light and step
251 in the light response curve); the maximum fluorescence (F_M or F_M') once Photosystem II (PSII)
252 was driven to closure; and the effective absorption cross section for PSII photochemistry (σ_{PSII} or
253 σ_{PSII}' ; $\text{nm}^2 \text{ quanta}^{-1}$) (Tortell and Suggett 2021). We used a double tap protocol (Xu et al. 2017),
254 where FRRf induction/relaxation trajectories were collected during a rapid light curve sequence
255 increasing in steps of 10 s at 0, 20, 40, 80, 160, and 320 $\mu\text{mol photons m}^{-2}\text{s}^{-1}$ PAR, delivered
256 from LED emitters centred at 445, preferentially exciting chlorophyll, or 590 nm, preferentially
257 exciting phycobiliproteins. Flash Power for 445 nm excitation was 60000 $\mu\text{mol photons m}^{-2}\text{s}^{-1}$
258 PAR, while for 590 nm excitation power was 14000 $\mu\text{mol photons m}^{-2}\text{s}^{-1}$, calibrated using a
259 quantum sensor (LI-250, LI-COR, Inc.). We applied 1 s darkness between sequential light steps,

260 to allow re-opening of PSII. FRRf excitation flashlets were applied at the same wavebands, 445
261 or 590 nm, as the actinic light steps.

262 We calculated (Eq. (4)) an uncalibrated fluorescence based estimator for volumetric
263 electron transport, JV_{PSII} , ($\text{km} \times \text{e}^- \text{ L}^{-1} \text{ s}^{-1}$) under both 445 and 590 nm excitation bands
264 (Oxborough et al. 2012; Boatman et al. 2019; Tortell and Suggett 2021).

265

$$JV_{PSII} = \frac{\sigma_{PSII}' \times qP \times I \times F_O}{\sigma_{PSII}} \quad (4)$$

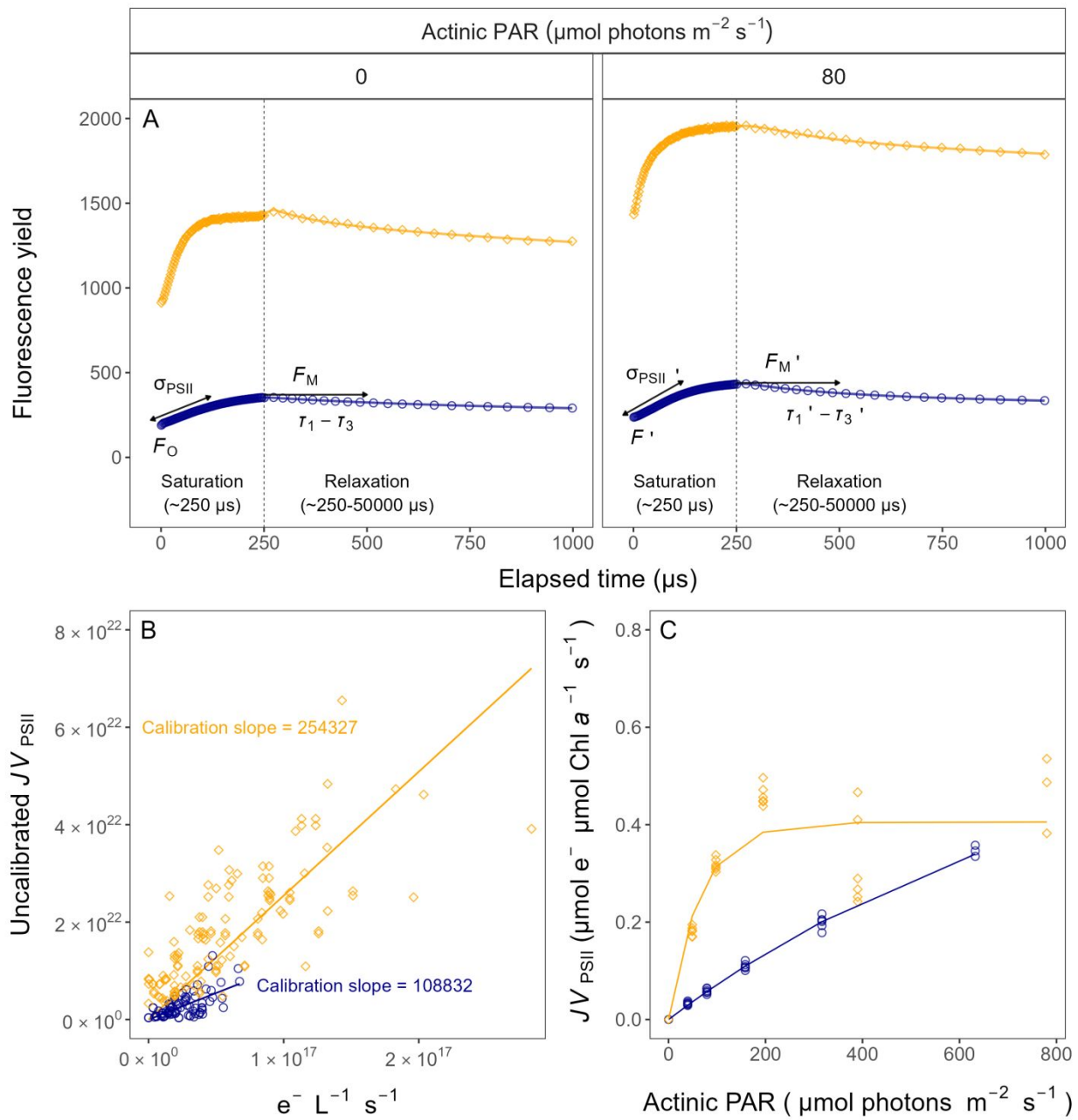
266 where σ_{PSII}' is effective absorption cross section for PSII photochemistry under the relevant
267 actinic PAR step ($\text{nm}^2 \text{ quanta}^{-1}$); qP is an estimate of the fraction of PSII open for
268 photochemistry estimated according to Oxborough and Baker (1997); I is the applied PAR (μmol
269 photons $\text{m}^{-2}\text{s}^{-1}$); F_O is the minimum fluorescence from a given sample and excitation bandwidth
270 (relative fluorescence) and σ_{PSII} is the maximum effective absorption cross section for PSII
271 photochemistry from a given sample and excitation bandwidth ($\text{nm}^2 \text{ quanta}^{-1}$). We compared
272 several other algorithms for JV_{PSII} (Tortell and Suggett 2021) and found similar results.

273 We calibrated the JV_{PSII} estimator to absolute rates of electron transport (Eq. (5)) using
274 parallel measures of oxygen evolution ($\mu\text{mol O}_2 \text{ L}^{-1} \text{ s}^{-1}$), captured simultaneously with the FRRf
275 measures, below light saturation of electron transport, using a FireSting robust oxygen probe
276 (PyroScience, Germany) inserted in the cuvette for select Rapid Light Curve (RLC) runs (Fig. 3).
277 For the blue LED ($\text{Ex}_{445\text{nm}}$) excitation we used a calibration slope of 108832, while for orange
278 LED ($\text{Ex}_{590\text{nm}}$) excitation we used a calibration slope of 254327

279

$$JV_{PSII}(\text{e}^- \text{ L}^{-1} \text{ s}^{-1}) = \frac{\text{Uncalibrated } JV_{PSII}(\text{e}^- \text{ L}^{-1} \text{ s}^{-1})}{\text{Calibration slope}} \quad (5)$$

280



281

282 **Fig. 3.** Single turnover (ST) fluorescence induction by Fast Repetition Rate fluorometry (FRRf). (A) Examples of
 283 fluorescence yield vs. elapsed time (μs) for PE-rich culture of *Synechococcus* sp. (048) in the dark (dark-relaxed; 0
 284 $\mu\text{mol photons m}^{-2}\text{s}^{-1}$) and under actinic PAR (in this example 80 $\mu\text{mol photons m}^{-2}\text{s}^{-1}$) using blue LED (Ex_{445nm};
 285 open blue circles) or orange (Ex_{590nm}; open orange diamonds) excitation. The ST technique delivers a series of
 286 flashlets for non-intrusive, repeated monitoring of chlorophyll fluorescence parameters (including F_O , F' , F_M , F_M' ,
 287 $\tau_1 - \tau_3$, $\tau_1' - \tau_3'$, σ_{PSII} , and σ_{PSII}'). (B) Linear regressions of uncalibrated PSII electron flux (JV_{PSII}) vs. $e^- L^{-1} s^{-1}$ derived

288 from simultaneously measured oxygen evolution Light Response Curves (LRC) under blue LED ($\text{Ex}_{445\text{nm}}$; open blue
289 circles) or orange ($\text{Ex}_{590\text{nm}}$; open orange diamonds) excitation. (C) Rapid Light Curve (RLC), fit with a three
290 parameter model (Harrison and Platt 1986), for PSII electron flux (JV_{PSII} ; $\mu\text{mol e}^{-} \mu\text{mol Chl } a^{-1} s^{-1}$) vs. actinic PAR
291 measured under blue LED ($\text{Ex}_{445\text{nm}}$; open blue circles) or orange ($\text{Ex}_{590\text{nm}}$; open orange diamonds) excitation.
292

293 Statistical analysis

294 We used R version 4.3.0 (R Core Team 2023) running under RStudio (Posit team 2022).
295 We performed three-way factorial ANOVA (*aov()* function; R Base package) to determine
296 whether peak PAR, photoperiod, strain, and their interactions, significantly influence the
297 chlorophyll-specific exponential growth rate (μ ; d^{-1}), estimated from logistic fits (*nlsLM()*
298 function; Elzhov et al. (2023)) of chlorophyll proxy $OD_{680} - OD_{720}$ vs. cumulative diel PUR
299 (Table S2). We also used the *nlsLM()* function to fit a three parameter light response model
300 (Harrison and Platt 1986) of growth rates (α , initial slope of curve; β , reflecting the
301 photoinhibition process; P_{max} , the maximum rate of growth curve).

302 To examine statistical differences between fits of light responses, we performed one-way
303 ANOVA (*aov()* function) of the three parameter model (Harrison and Platt 1986) fit to pooled
304 data for each taxa, compared to separate fits for each different photoperiod (8, 12, 16, or 24); or
305 to separate fits for each different peak PAR (30, 90, 180, 300, 600 together with 900). These
306 comparisons were run for chlorophyll-specific exponential growth rate vs. cumulative diel PUR
307 (Table S3, S4); vs. cumulative diel PAR (Table S5, S6) or vs. PSII electron flux (JV_{PSII} ; $\mu\text{mol e}^{-}$
308 $\mu\text{mol Chl } a^{-1} d^{-1}$; Table S7, S8). One-way ANOVA was also used to examine statistical
309 differences between single phase exponential decay fits (*SSasymp()* function; Serway et al.
310 (2004)) of pooled data across different strains for a given phase of growth and across different
311 phase of growth for a given strain for PUR/PAR ratio (Table S9); Phycobiliprotein to Chl a ratio

312 (Table S10); or effective absorption cross section of PSII (σ_{PSII}' ; nm² quanta⁻¹) measured under
313 diel peak PAR growth light under Ex_{590nm} (orange) excitation in relation to the cumulative diel
314 PAR ($\mu\text{mol photons m}^{-2}\text{d}^{-1}$) (Table S11).

315 We used *t*-tests (*t.test()* function; R Base package) of linear fits (*lm()* function) to compare
316 pooled data across different strains for a given phase of growth, and across different phases of
317 growth, for a given strain, for effective absorption cross section of PSII (σ_{PSII}' ; nm² quanta⁻¹)
318 measured under diel peak PAR growth light under Ex_{445nm} (blue) excitation vs. the cumulative
319 diel PAR ($\mu\text{mol photons m}^{-2}\text{d}^{-1}$; Table S12); or vs. the Phycobiliprotein to Chl *a* ratio (Table
320 S13). The same *t*-test analyses were performed for effective absorption cross section of PSII
321 (σ_{PSII}' or σ_{PSII} ; nm² quanta⁻¹) measured under Ex_{590nm} (orange) excitation vs. the Phycobiliprotein
322 to Chl *a* ratio (Table S14, S15).

323 Statistical differences for all analyses were determined at significance level $\alpha = 0.05$. The
324 manuscript was prepared as a Rmarkdown document (Handel 2020) with figures plotted using
325 ggplot2 (Wickham 2016) and patchwork (Pedersen 2024) packages. All metadata, data and code
326 is available on GitHub (<https://github.com/FundyPhytoPhys/BalticPhotoperiod>).

327

328 **Results**

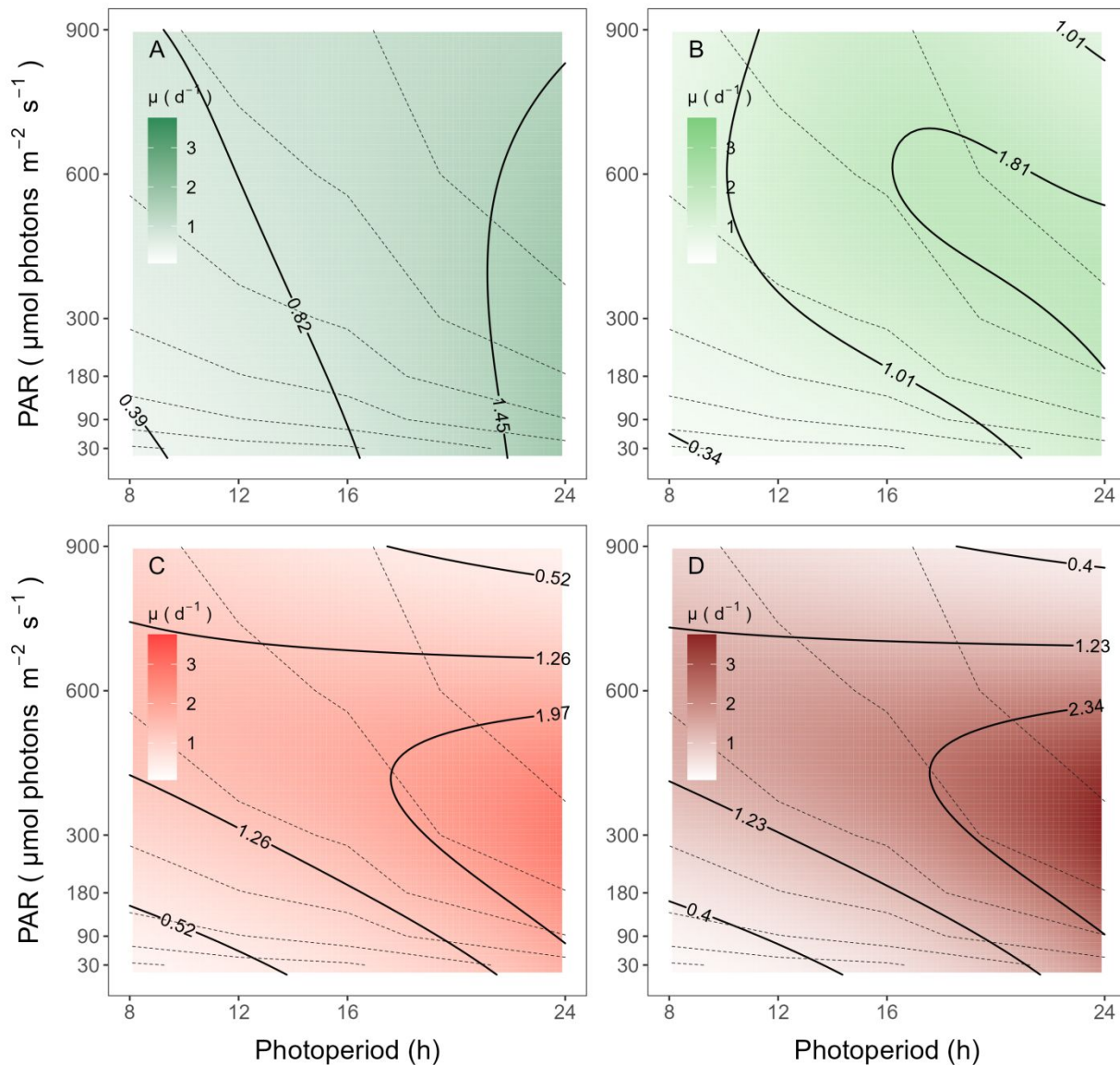
329 **Chlorophyll-specific exponential growth rate**

330 We used logistic curve fits (Fig. S3B) to determine chlorophyll-specific exponential
331 growth rates (μ ; d⁻¹), for two PhycoCyanin(PC)-rich cultures (056, 077) and two
332 PhycoErythrin(PE)-rich cultures (048, 127) of *Synechococcus* sp. grown at 30, 90, 180, 300, 600,
333 or 900 peak PAR $\mu\text{mol photons m}^{-2}\text{s}^{-1}$ (μE); and photoperiods of 8, 12, 16, or 24 h. Three-way
334 factorial ANOVA showed that peak PAR, photoperiod, strain, and their interactions,

335 significantly affected μ (ANOVA, $p < 0.05$ for all; Table S2). All tested strains, except PE-
336 rich_048, grew even under peak PAR 900 $\mu\text{mol photons m}^{-2}\text{s}^{-1}$ and 24 h photoperiod. The
337 highest growth rate was recorded for *Synechococcus* sp. PE-rich_127 ($\mu = 4.5 \text{ d}^{-1}$; 3.7 h doubling
338 time) and PC-rich_056 ($\mu = 3.4 \text{ d}^{-1}$; 4.9 h doubling time) at 180 $\mu\text{mol photons m}^{-2}\text{s}^{-1}$ peak PAR
339 and photoperiod of 24 h.

340 The GAM model in Fig. 4 summarizes the growth responses of the PC-rich and PE-rich
341 picocyanobacteria to peak PAR and photoperiod. PC-rich_056 *Synechococcus* sp. showed
342 highest growth rates under a photoperiod of 24 h, across a wide range of peak PAR indicated by
343 the contour line labeled 1.45 d^{-1} , representing the 90th percentile of achieved growth rates for the
344 strain. On the other hand, the other tested PC-rich strain (077) showed highest growth rates in the
345 range of photoperiod 16-24 h and peak PAR between 300 – 700 $\mu\text{mol photons m}^{-2}\text{s}^{-1}$, indicated
346 by the 1.81 d^{-1} contour line again representing the 90th percentile of maximum achieved growth
347 rates for the strain. For both PC-rich strains, growth was slowest under 30 $\mu\text{mol photons m}^{-2}\text{s}^{-1}$
348 and a photoperiod of 8 h.

349 Both PE-rich strains achieved fastest growth rates above peak PAR of ~300 $\mu\text{mol photons}$
350 $\text{m}^{-2}\text{s}^{-1}$, under the longest photoperiod of 24 h, indicated by the 1.97 d^{-1} for PE-rich_048, and
351 2.34 d^{-1} for PE-rich_127, contour lines. For the PE-rich strains growth decreased with decreasing
352 photoperiod and decreasing peak PAR. Moreover, PE-rich strains showed photoinhibition of
353 growth at peak PAR of 900 $\mu\text{mol photons m}^{-2}\text{s}^{-1}$ and photoperiods of 16- 24 h. The growth rate
354 contours for PC-rich and PE-rich *Synechococcus* sp. did not generally follow isoclines of
355 cumulative diel photon dose ($\mu\text{mol photons m}^{-2}\text{d}^{-1}$, dashed lines), showing that photoperiod, and
356 peak PAR influenced growth rates beyond cumulative diel photon dose.



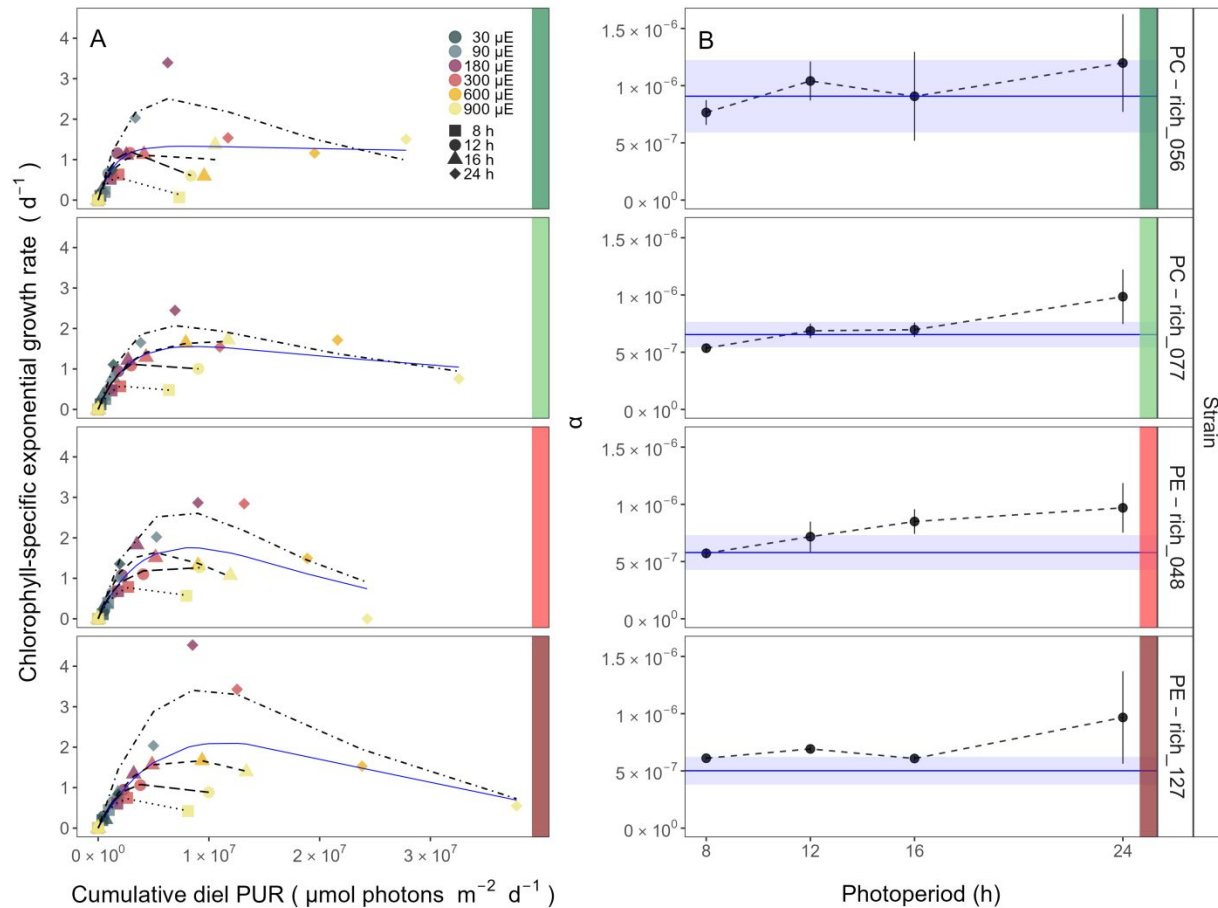
357

358 **Fig. 4.** A contour plot of a Generalized Additive Model (GAM) of chlorophyll-specific growth rates (d^{-1}) for two
 359 PC-rich cultures: **(A)** 056, **(B)** 077 and two PE-rich cultures: **(C)** 048, **(D)** 127 of *Synechococcus* sp. grown at 30, 90,
 360 180, 300, 600, or 900 peak PAR $\mu\text{mol photons m}^{-2}\text{s}^{-1}$; and photoperiods of 8, 12, 16, or 24 h. Legends show colour
 361 gradients of growth rate ($\mu; d^{-1}$) from no growth (white) to 3.0 d^{-1} (dark green for PC-rich_056, light green for PC-
 362 rich_077, light red for PE-rich_048 or dark red for PE-rich_127 strains). Labeled contour lines indicate the 90%,
 363 50%, and 10% quantiles for achieved growth rate. Dotted lines show isoclines of cumulative diel photon dose (μmol
 364 $\text{photons m}^{-2}d^{-1}$).

365

366 A three parameter light response model fit (Harrison and Platt 1986) of chlorophyll-
367 specific exponential growth rates vs. cumulative diel PUR dose for two PC-rich and two PE-rich
368 cultures of *Synechococcus* sp. showed significant differences between model fits of the pooled
369 data vs. fits for all tested photoperiods (8, 12, 16, or 24 h; ANOVA, $p < 0.05$; Fig. 5A, Table S3).
370 The alpha parameters of the initial rise of growth rate (α) vs. cumulative diel PUR, estimated
371 from data pooled for each photoperiod increased with increasing photoperiod for all strains. The
372 highest increase (>2-fold) of α with increasing photoperiod was recorded for PC-rich_056 (Fig.
373 5B). Strains also showed distinct growth rate responses to cumulative diel PUR, depending upon
374 peak PAR (Fig. S4A, Table S4), that differ from a single light response model fit to the pooled
375 data across all peak PAR from a strain. Exceptions were observed in the strains PC-rich_077 and
376 PE-rich_048 with the peak PAR of 600 or 900 $\mu\text{mol photons m}^{-2}\text{s}^{-1}$, which were not
377 significantly different from the pooled data model. A caveat to these findings is that cumulative
378 diel photon dose is a product of photoperiod and PAR, so the highest levels of cumulative PUR
379 dose are only achieved under the 600 or 900 $\mu\text{mol photons m}^{-2}\text{s}^{-1}$. The alpha parameters of the
380 initial rise of growth rate (α) vs. cumulative diel PUR, estimated from data pooled for each peak
381 PAR decreased across peak PAR for all tested strains (Fig. S4B).

382 Growth rate saturated under increasing cumulative diel PUR for all strains, however, the
383 achieved estimates of μ_{\max} varied depending upon photoperiod and peak diel PAR. Growth rates
384 vs. cumulative diel PAR relationships, estimated for exponential phase cultures, followed similar
385 patterns (Fig. S5, Fig. S6 and Table S5, S6 in Supporting Information).



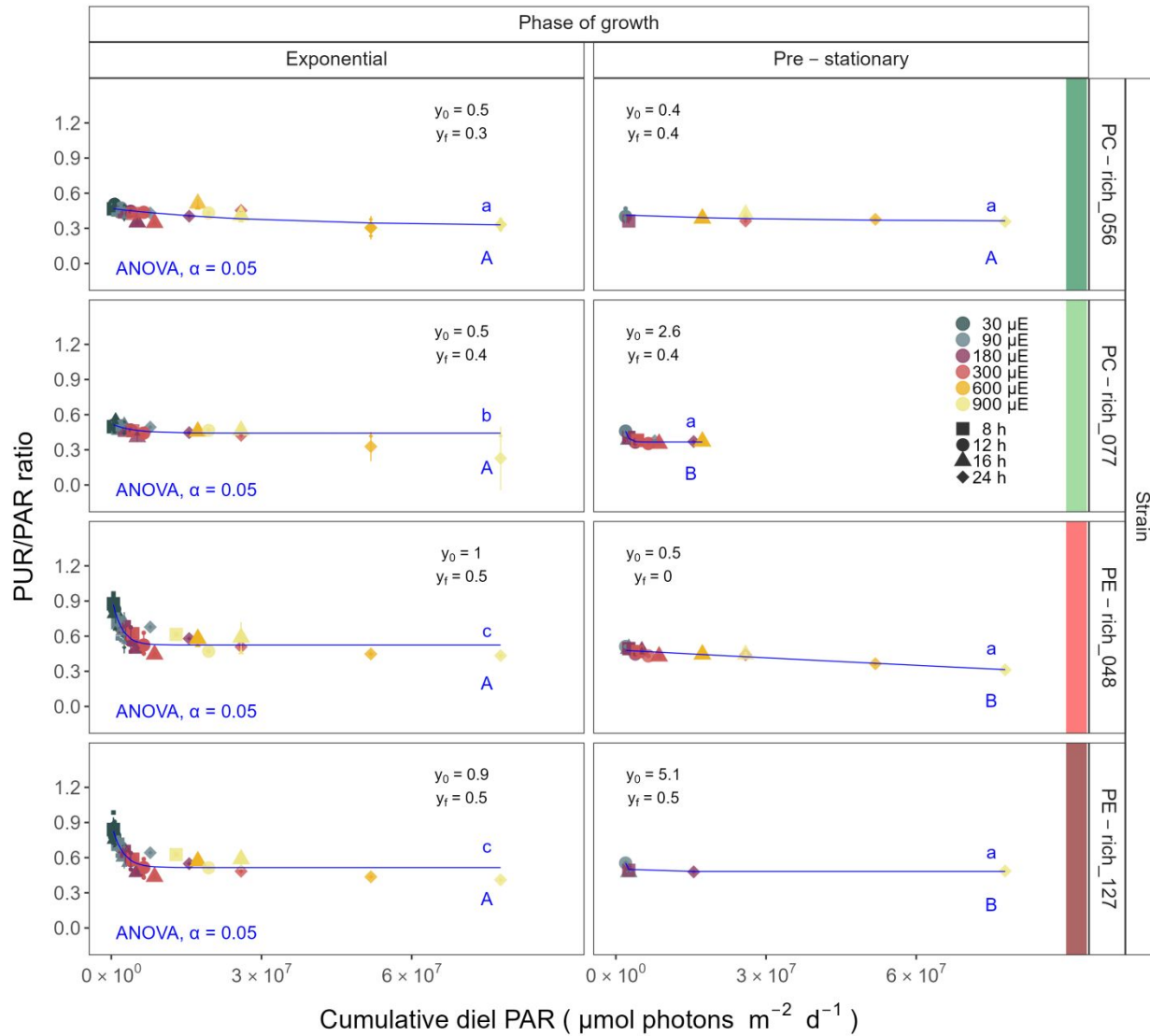
386

387 **Fig. 5.** (A) Chlorophyll-specific exponential growth rates (d^{-1}) vs. cumulative diel Photosynthetically Usable
 388 Radiation (PUR, $\mu\text{mol photons m}^{-2}\text{d}^{-1}$). Growth rates (\pm SE falling within symbols) were estimated from logistic fits
 389 of chlorophyll proxy $\text{OD}_{680} - \text{OD}_{720}$ (ΔOD) vs. elapsed time (Fig. 1, Fig. S3B), for two PC-rich cultures (056; dark
 390 green, 077; light green) and two PE-rich cultures (048; light red, 127; dark red) of *Synechococcus* sp. grown at 30
 391 (μE); and photoperiods of 8 (square), 12 (circle), 16 (triangle), or 24 (diamond) h. Solid blue line shows a fit of the
 392 pooled growth rates through photoperiods for each strain, with a three parameter model (Harrison and Platt 1986).
 393 We also fit the same model separately for 8 (dotted line), 12 (long dash line), 16 (dashed line), or 24 (two dash line)
 394 h photoperiods, since for all strains they were each significantly different (ANOVA, $p < 0.05$) from the fit of pooled
 395 data. (B) Alpha parameters of the initial rise of growth rate (α) vs. cumulative diel Photosynthetically Usable
 396 Radiation (PUR), estimated from data pooled for each photoperiod (points (\pm SE) connected by dashed lines), and
 397 estimated for all data across photoperiods (solid blue horizontal line \pm SE), for each strain.

399

400 **PUR/PAR ratio vs. cumulative diel PAR**

401 The PUR/PAR ratio is an index of the efficacy of light capture for a culture under a given
402 growth condition; showing the fraction of PAR that can be captured by the absorbance of the
403 cells (Fig. 6). For the two PC-rich and, particularly, for the two PE-rich cultures of
404 *Synechococcus* sp. PUR/PAR decayed exponentially to a plateau, with increasing cumulative
405 diel PAR, when pooling PUR/PAR data across different combinations of photoperiod and peak
406 PAR. Although all strains followed a similar trend, the single phase exponential decay model fit
407 parameters varied significantly among strains, during their exponential phase of growth
408 (ANOVA, $p < 0.05$), except the model fits from PE-rich_048 and PE-rich_127 (ANOVA, $p >$
409 0.05; Table S9). Moreover, the PUR/PAR ratio was higher in the PE-rich strains under low
410 cumulative diel photon dose during their exponential phase of growth (y_0 greater or equal to 0.9),
411 but decayed towards a plateau close to the PC-rich strains as cumulative diel photon dose
412 increases ($y_f = 0.5$). On the other hand, the single phase exponential decay model fits did not
413 differ significantly among strains, during their pre-stationary phase of growth (ANOVA, $p >$
414 0.05; Table S9). During this phase, response of PUR/PAR ratio to increasing cumulative diel
415 PAR exhibits damping, maintaining a consistent trend across all strains within the y_f range of 0.4
416 to 0.5, with the exception of the PE-rich_048 strain. We also find that model fits from different
417 phases of growth differed within a given strain, with the exception of PC-rich_056 (ANOVA; p
418 < 0.05 , Table S9). A similar decay trend was observed for Phycobiliprotein to Chl *a* ratio
419 ($\mu\text{g}:\mu\text{g}$) across cumulative diel PAR (Fig. S7).



420

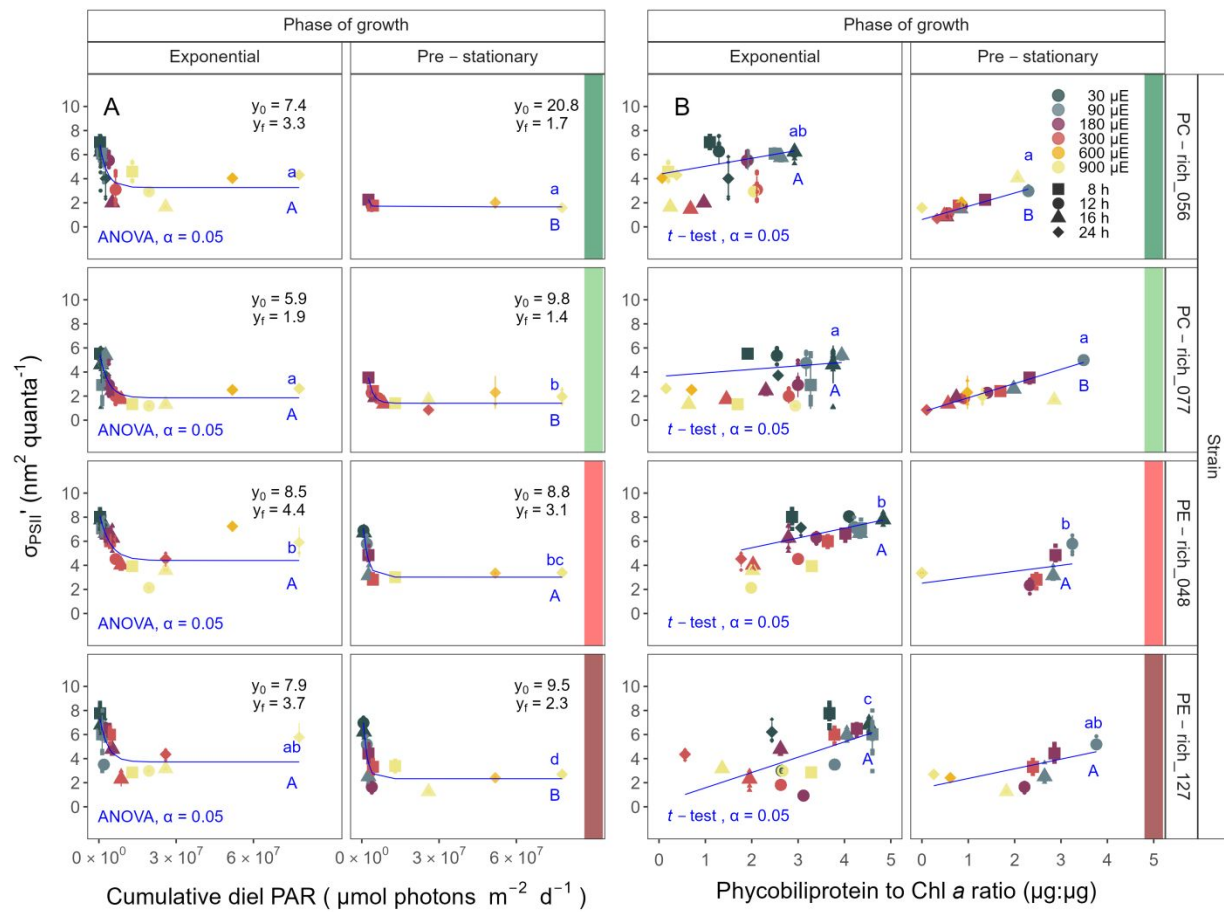
421 **Fig. 6.** Changes in PUR/PAR ratio vs. cumulative diel PAR ($\mu\text{mol photons m}^{-2}\text{d}^{-1}$). PUR/PAR ratio was estimated
422 for two PC-rich cultures (056; dark green, 077; light green) and two PE-rich cultures (048; light red, 127; dark red)
423 of *Synechococcus* sp. grown at 30 (dark gray), 90 (light gray), 180 (purple), 300 (red), 600 (orange), or 900 (yellow)
424 peak PAR $\mu\text{mol photons m}^{-2}\text{s}^{-1}$ (μE); and photoperiods of 8 (square), 12 (circle), 16 (triangle), or 24 (diamond) h.
425 Figure presents data (smaller symbols) and means (bigger symbols) from exponential or pre-stationary phase of
426 growth. Blue solid line shows single phase exponential decay fit for data from each strain and growth phase, with fit
427 parameters presented. Different lowercase letters indicate statistically significant differences between the fit models
428 for different strains within a given phase of growth. Different uppercase letters indicate statistically significant
429 differences between the fit models for different phases of growth within a given strain (ANOVA; $p < 0.05$).

430

431 **Effective absorption cross section of PSII of picocyanobacteria**

432 The effective absorption cross section of PSII (σ_{PSII}' , $\text{nm}^2 \text{ quanta}^{-1}$), was estimated using
433 FRRf induction curves using $\text{Ex}_{590\text{nm}}$ (orange) excitation, for two PC-rich (056, 077) and two PE-
434 rich (048, 127) cultures of *Synechococcus* sp. grown at 30, 90, 180, 300, 600, or 900 peak PAR
435 $\mu\text{mol photons m}^{-2}\text{s}^{-1}$ (μE); and photoperiods of 8, 12, 16, or 24 h (Fig. 7). The σ_{PSII}' measured
436 under diel peak PAR growth light under $\text{Ex}_{445\text{nm}}$ (blue) excitation vs. cumulative diel photon
437 dose is shown in Supporting Information (Fig. S8, Table S12).

438 All strains showed consistent patterns of sharp, exponential decay of effective absorption
439 cross section for PSII photochemistry vs. cumulative diel photon doses, across different
440 combinations of photoperiod and peak PAR (Fig. 7A). Although all strains showed this response
441 pattern, the exponential decay fits differed significantly among two PC-rich strains and PE-
442 rich_048 strains during their exponential phase of growth (ANOVA, $p < 0.05$; Table S11). PE-
443 rich strains showed higher σ_{PSII}' under low cumulative diel photon dose (y_0 about 0.8 and y_f
444 about 4) than did PC-rich strains. During pre-stationary phase this response dampens in the PC-
445 rich strains but persists in the PE-rich strains (Table S11). σ_{PSII}' for the PE-rich strains during
446 pre-stationary phase of growth still remain higher (y_f between 2.3 – 3.0) than in the PC-rich
447 strains (y_f between 1.4 – 1.7) even as cumulative diel photon dose increases. Model fits from
448 different phases of growth differed within a given strain, with the exception of PE-rich_048
449 (ANOVA; $p < 0.05$, Table S11).



450

451 **Fig. 7. (A)** Effective absorption cross section of PSII (σ_{PSII}' ; nm² quanta⁻¹) measured under diel peak PAR growth
 452 light vs. cumulative diel PAR ($\mu\text{mol photons m}^{-2} \text{d}^{-1}$); blue solid line shows single phase exponential decay fit for
 453 data from each strain and growth phase. **(B)** Changes of σ_{PSII}' measured under diel peak PAR growth light vs. the
 454 ratio of sum of μg phycobilins (PE, PC, APC protein, Phycobiliprotein) to $\mu\text{g Chl a}$; blue solid line shows linear
 455 model fit for data from each strain and growth phase. σ_{PSII}' was estimated using FRRf induction curves with
 456 excitation of phycobilisomes (Ex_{590nm}, orange), for two PC-rich cultures (056; dark green, 077; light green) and two
 457 PE-rich cultures (048; light red, 127; dark red) of *Synechococcus* sp. grown at 30 (dark gray), 90 (light gray), 180
 458 (purple), 300 (red), 600 (orange), or 900 (yellow) peak PAR $\mu\text{mol photons m}^{-2} \text{s}^{-1}$ (μE); and photoperiods of 8
 459 (square), 12 (circle), 16 (triangle), or 24 (diamond) h. Figure presents data (smaller symbols) and means (bigger
 460 symbols) from exponential or pre-stationary phase of growth. Different lowercase letters indicate statistically
 461 significant differences between the fit models for different strains within a given phase of growth. Different

462 uppercase letters indicate statistically significant differences between the fit models for different phases of growth
463 within a given strain ($p < 0.05$).

464

465 Effective absorption cross section of PSII (σ_{PSII}' ; $\text{nm}^2 \text{ quanta}^{-1}$), measured under diel peak
466 PAR growth light with $\text{Ex}_{590\text{nm}}$ (orange) excitation, varies with Phycobiliprotein to Chl *a* ratio
467 (Fig. 7B). σ_{PSII}' excited through phycobilisome absorbance at $\text{Ex}_{590\text{nm}}$ shows positive linear
468 correlations with the Phycobiliprotein to Chl *a* ratio, although strains in exponential growth show
469 significant scatter around this positive relation, likely related to regulatory control of σ_{PSII}' under
470 different measurement PAR, beyond pigment composition. Under pre-stationary phase the
471 relationship between σ_{PSII}' and Phycobiliprotein to Chl *a* ratio was more consistent, suggesting
472 increased reliance upon compositional regulation to control light delivery to PSII, as opposed to
473 shorter-term physiological regulation under changing light. The linear fits of σ_{PSII}'
474 vs. Phycobiliprotein to Chl *a* ratio also vary significantly between PC-rich_077 and two PE-rich
475 strains during their exponential phase of growth. During pre-stationary phase we noted
476 significant differences between two PC-rich strains and PE-rich_048. Moreover, significant
477 differences between the fit models for varying phases of growth were noted for PC-rich strains
478 056 and 077 (*t*-test; $p < 0.05$, Table S14).

479 Changes in effective absorption cross section of PSII (σ_{PSII} ; $\text{nm}^2 \text{ quanta}^{-1}$) measured in the
480 dark with $\text{Ex}_{590\text{nm}}$ (orange) excitation vs. Phycobiliprotein to Chl *a* ratio (Fig. S9A, Table S15)
481 and σ_{PSII}' measured under diel peak PAR growth light under $\text{Ex}_{445\text{nm}}$ (blue) excitation
482 vs. Phycobiliprotein to Chl *a* ratio (Fig. S9B and Table S13) are shown in Supporting
483 Information.

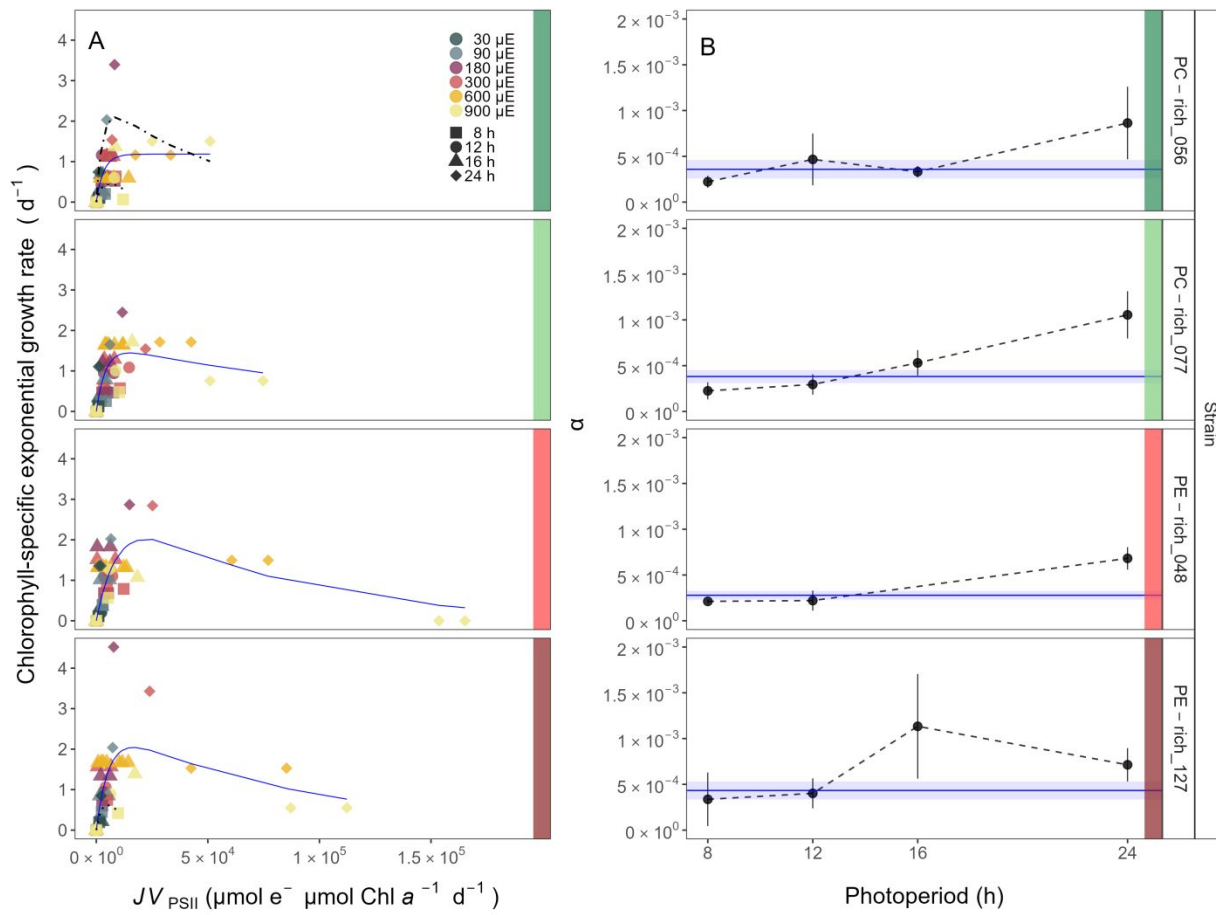
484

485 **Growth rates vs. cumulative diel PSII electron flux**

486 Chlorophyll-specific exponential growth rates (d^{-1}), within each strain, show fairly
487 consistent saturating responses to increasing cumulative diel PSII electron flux (JV_{PSII} ; $\mu\text{mol e}^-$
488 $\mu\text{mol Chl } a^{-1} d^{-1}$) estimated under diel peak PAR growth light, and estimated using FRRf
489 induction curves with excitation of chlorophyll (Ex_{445nm}, blue), although photoperiod (Fig. 8A,
490 Table S7) and peak PAR (Fig. S10, Table S8) retained a secondary influence on achieved growth
491 responses for some growth conditions.

492 A three parameter model fit of (Harrison and Platt 1986) vs. cumulative diel PSII electron
493 flux (JV_{PSII} ; $\mu\text{mol e}^- \mu\text{mol Chl } a^{-1} d^{-1}$) for two PC-rich and two PE-rich cultures of
494 *Synechococcus* sp. showed no significant differences between fits of the pooled data vs. fits for
495 different photoperiods (8, 12, 16, or 24 h; ANOVA, $p < 0.05$), with exception of 8 and 24 h
496 photoperiod for PC-rich_056 and 8 h photoperiod for PE-rich_127 strains (ANOVA, $p > 0.05$;
497 Table S7).

498 Alpha parameters of the initial rise of growth rate (α) vs. cumulative diel JV_{PSII} , estimated
499 from data pooled for each photoperiod showed an increase across increasing photoperiods for
500 each strain except for PE-rich_0127. The highest increase (>2-fold) of α from the lowest to the
501 highest photoperiod was recorded for PC-rich_077 (Fig. 8B).



502

503 **Fig. 8.** (A) Chlorophyll-specific exponential growth rates (d^{-1}) vs. cumulative diel PSII electron flux (JV_{PSII} ; $\mu\text{mol e}^-$
 504 $\mu\text{mol Chl } a^{-1} d^{-1}$) measured under diel peak PAR growth light. Growth rates (\pm SE falling within symbols) were
 505 estimated from logistic fits of chlorophyll proxy $OD_{680} - OD_{720}$ (ΔOD) vs. elapsed time (Fig. S3B). JV_{PSII} was
 506 estimated using FRRf induction curves with excitation of chlorophyll ($Ex_{445\text{nm}}$, blue), for two PC-rich cultures (056;
 507 dark green, 077; light green) and two PE-rich cultures (048; light red, 127; dark red) of *Synechococcus* sp. grown at
 508 30 (dark gray), 90 (light gray), 180 (purple), 300 (red), 600 (orange), or 900 (yellow) peak PAR $\mu\text{mol photons}$
 509 $\text{m}^{-2}\text{s}^{-1}$ (μE); and photoperiods of 8 (square), 12 (circle), 16 (triangle), or 24 (diamond) h. Solid blue line shows a fit
 510 of the pooled growth rates for each strain, with a three parameter model (Harrison and Platt 1986). We also fit the
 511 same model separately for 8 (dotted line) and 24 (two dash line) h photoperiods, when they were significantly
 512 different (ANOVA, $p < 0.05$) from the fit of pooled data. (B) Alpha parameters of the initial rise of growth rate (α)
 513 vs. cumulative diel JV_{PSII} , estimated from data pooled for each photoperiod (points (\pm SE) connected by dashed
 514 lines), and estimated for all data across photoperiods (horizontal line \pm SE), for each strain.

515

516 **Discussion**517 **Photic regimes - implications for picocyanobacteria growth and distribution**

518 Light regimes, including photoperiod, and peak PAR, are major factors affecting the
519 distribution and seasonality of phytoplankters (Erga and Heimdal 1984). Changes in photoperiod
520 trigger acclimation responses, shaping the temporal dynamics and community structure of
521 phytoplankton (Theus et al. 2022; Longobardi et al. 2022). Each tested picocyanobacterial strain
522 showed influences of photoperiod upon the responses of growth rate to cumulative diel PUR
523 (Fig. 5) and PAR (Fig. S5). To our surprise, increasing photoperiod increased the ranges of
524 response to PAR and PUR. Both the PC-rich and the PE-rich strains of *Synechococcus* sp.
525 exhibited their highest initial responses of growth to increasing PUR and PAR (alpha, (Fig. 5B),
526 Fig. S5B), and their fastest growth rates under continuous light (24 h photoperiod), consistent
527 with some other strains (Jacob-Lopes et al. 2009; Klepacz-Smólka et al. 2020). Yet, 24 h
528 photoperiod also exacerbated eventual photoinhibition under excess cumulative diel PUR and
529 PAR. Our temperate strains do not experience direct selective pressures to exploit a continuous
530 24 photoperiod (Brand and Guillard 1981), so achieving maximum growth under a 24 h
531 photoperiod rather suggests lack of a requirement for a dark period, and lack of requirement for a
532 regular photoperiod. Coastal phytoplankton strains are selected to exploit instantaneous light
533 (Brand and Guillard 1981), of whatever duration, to cope with fluctuating light and nutrients in
534 coastal environments (MacIntyre et al. 2000; Litchman et al. 2009), leading to a pleiotropic
535 capacity for exploiting continuous light. The ability of both PC-rich and PE-rich coastal
536 picocyanobacteria to exploit continuous light means they could, potentially, grow rapidly at
537 higher latitudes, in a future warmer polar summer water.

538 Light level is another key driver of picocyanobacteria productivity (Pick 1991; Six et al.
539 2007; Aguilera et al. 2023). The spatial and temporal distribution of PAR within aquatic
540 ecosystems is influenced by solar angle, water depth, water clarity, and the presence of light-
541 absorbing substances such as dissolved organic matter (Morel 1978, 1988) and phytoplankton
542 cells. PUR then represents the light potentially available for phytoplankton to photosynthesize.
543 PUR is always smaller than PAR ($\text{PUR} < \text{PAR}$), and depends on the spectral composition of the
544 PAR, versus the phytoplankton pigment composition, determining cellular spectral absorption
545 (Morel 1978), which changes depending upon growth conditions and the phase of growth.

546 PE-rich and PC-rich *Synechococcus* sp. strains show distinct growth responses to
547 cumulative diel photon dose, depending upon the peak PAR of the applied photoregime (Fig. S4,
548 Fig. S6). Chlorophyll-specific exponential growth rates of the PE-rich and PC-rich
549 *Synechococcus* sp. strains increased with increasing light levels, to a plateau in the range of 180
550 – 300 $\mu\text{mol photons m}^{-2}\text{s}^{-1}$. Growth above 600 $\mu\text{mol photons m}^{-2}\text{s}^{-1}$ occurred with a growth
551 yield per cumulative diel photon lower than under moderate light, particularly when combined
552 with short 8 h or long 24 h photoperiods. Even though PE-rich *Synechococcus* sp. are more
553 adapted to lower-light conditions deeper in the water column (Stomp et al. 2007), our findings
554 show that PE-rich strains will grow under higher irradiance.

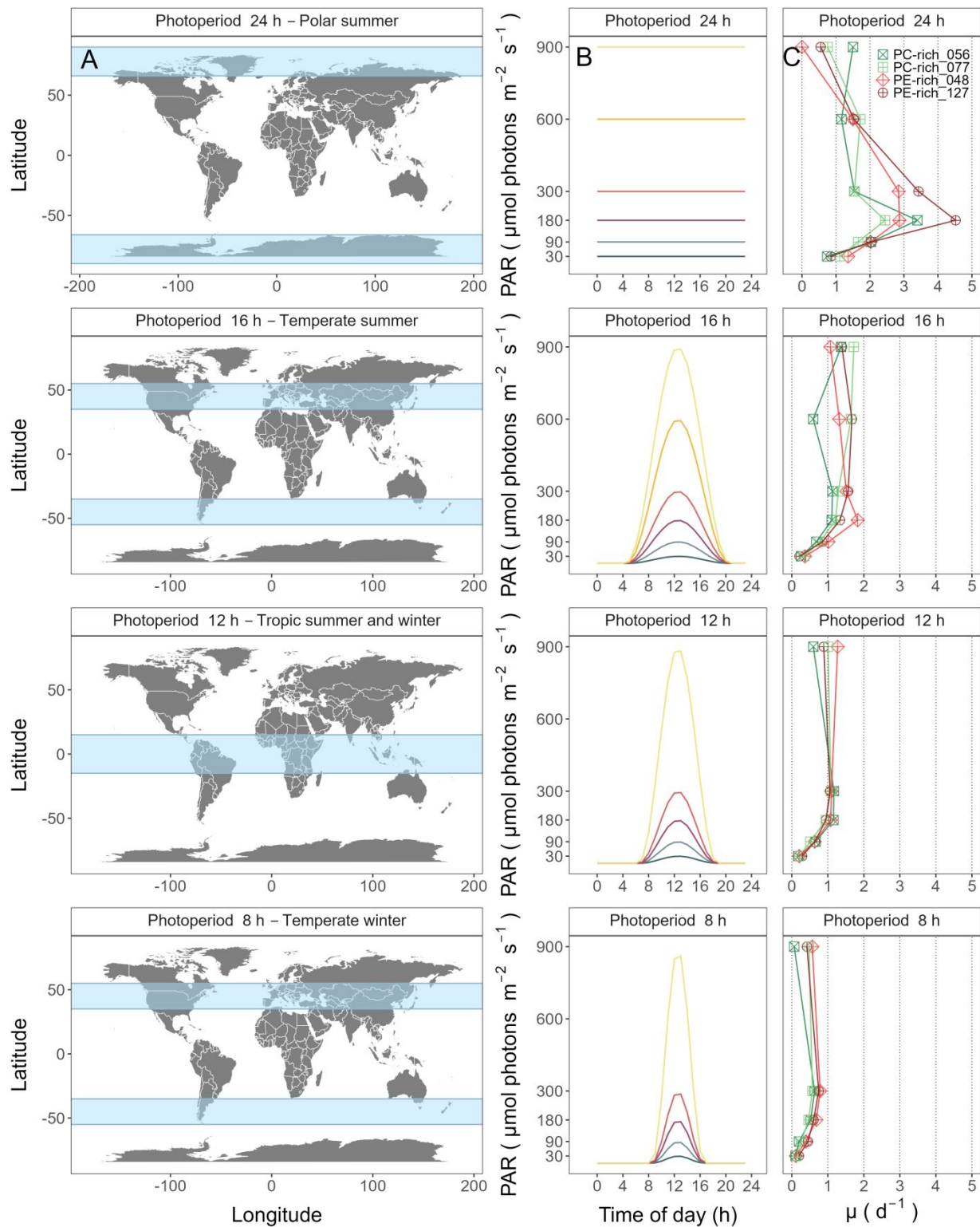
555 The maximum growth rate of *Synechococcus* sp. PE-rich_127 strain under 24 h
556 photoperiod and peak PAR of 180 $\mu\text{mol photons m}^{-2}\text{s}^{-1}$ was 4.5 d^{-1} ($\mu = 0.187 \text{ h}^{-1}$),
557 corresponding to a doubling time of 3.7 h (Fig. 5, Fig. S4); faster than previously reported for
558 marine picocyanobacteria, and indeed faster than for the model freshwater cyanobacteria
559 *Synechococcus* sp. PCC6301 (doubling time of 4.5–5 h under constant illumination and 250 μmol
560 $\text{photons m}^{-2}\text{s}^{-1}$) (Sakamoto and Bryant 1999), or *Synechocystis* sp. PCC 6803 (doubling time of

561 4.3 h) (van Alphen et al. 2018). The fastest growth rate as yet achieved for any phytoplankton
562 occurs in a genetically modified green algae *Picochlorum celeri*, with a maximum of about 6.8
563 d⁻¹ and ~2.5 h doubling time, in bioreactors (Krishnan et al. 2021). The Baltic *Synechococcus* sp.
564 strains, not genetically modified, preferred 24 h photoperiod and moderate peak PAR of 180
565 μmol photons m⁻²s⁻¹, suggesting they could, potentially, thrive in warming polar latitude waters.
566 *Synechococcus* sp. strains indeed already occur across geographical regions (Śliwińska-
567 Wilczewska et al. 2018b) with different photic regimes, including polar regions (reviewed by
568 Velichko et al. (2021)), exceeding latitude 80°S and 80°N. The prolonged daylight hours of polar
569 summers, coupled with nutrient-rich waters, promote growth of genetically diverse
570 *Synechococcus* populations (Vincent et al. 2000), contributing significantly to primary
571 productivity. Gradinger and Lenz (1989) suggested that *Synechococcus*-type picocyanobacteria
572 may serve as indicator organisms for the advection of warm water masses into polar regions,
573 important in the context of monitoring upcoming climate changes.

574 The coastal PC-rich and PE-rich strains of *Synechococcus* showed saturation, and then
575 photoinhibition of growth rates under increasing cumulative diel PUR, although the achieved
576 estimates of μ_{\max} , and the onset of photoinhibition of growth, varied depending upon strain,
577 photoperiod and peak PAR (Fig. 4). The tested strains were generally opportunistic in exploiting
578 longer photoperiods to achieve faster μ , although PE-rich strains suffered strong photoinhibition
579 of growth under peak PAR above 600 μmol photons m⁻²s⁻¹ and 24 h photoperiod (Fig. 5, Fig.
580 S4), suggesting the PE-rich strains are better adapted to lower light and deeper parts of the water
581 column. The least favorable growth conditions for both PE-rich and PC-rich strains of
582 *Synechococcus* sp. were under high light (> 600 μmol photons m⁻²s⁻¹) and the shortest
583 photoperiod (8 h), even though the cumulative diel PUR dose was equivalent to conditions where

584 the light intensity was lower and the photoperiod was longer. Thus these Baltic
585 picocyanobacteria are prone to photoinhibition under both the longest, and the shortest,
586 photoperiod regimes, with flatter light responses of growth under intermediate photoperiods.
587 Thus, in regions and periods with a longer photoperiod, both PC-rich and PE-rich *Synechococcus*
588 sp. could become dominant species in surface waters, but could suffer under shorter
589 photoperiods (Fig. 9).

For Review Only



590

591 **Fig. 9.** Latitudinal bands, equivalent summer or winter photoperiods, and picocyanobacterial growth responses. **(A)**
 592 Latitudinal bands corresponding to tested growth photoperiods. **(B)** Tested photoperiod and peak PAR regimes used

593 for growth experiments. (C) Chlorophyll specific exponential growth rates (\pm SE falling within symbols) for two
594 PhycoCyanin(PC)-rich cultures (056; dark green, 077; light green) and two PhycoErythrin(PE)-rich cultures (048;
595 light red, 127; dark red) of *Synechococcus* sp. under tested photoperiod and peak PAR regimes.

596

597 **Photic regimes and growth phase both influence cellular absorbance and light
598 use**

599 Under nutrient replete exponential growth the picocyanobacterial strains show consistent
600 patterns of an exponential decline in PUR/PAR ratio versus cumulative diel photon doses, across
601 different combinations of photoperiod and peak PAR. Thus, under nutrient repletion the
602 picocyanobacteria balance pigment composition to match light conditions (Fig. 6). In addition to
603 chlorophyll *a*, picocyanobacteria use phycobilins, including phycocyanin (harvesting red light at
604 620 nm) and phycoerythrin (harvesting yellow light at 570 nm), as accessory pigments to
605 enhance light harvesting efficiency. Picocyanobacteria enhance phycobilin production to
606 compensate for limited irradiance, thereby optimizing their photosynthetic capabilities
607 (Śliwińska-Wilczewska et al. 2018a) and increasing their PUR/PAR.

608 The effective absorption cross section for photochemistry of PSII in the light (σ_{PSII}')
609 comprises the probability of light capture by PSII and the quantum yield for subsequent
610 photochemistry. PC-rich and PE-rich strains of *Synechococcus* again show consistent patterns of
611 an exponential decay to a plateau with increasing cumulative diel PAR doses, for σ_{PSII}' (nm^2
612 quanta $^{-1}$, measured under diel peak PAR growth light under Ex_{590nm} (orange) excitation), without
613 detectable influences of photoperiod, nor of peak PAR (Fig. 7A). σ_{PSII}' excited through
614 chlorophyll absorbance at 445 nm was, in contrast, consistently small across strains and growth
615 conditions (Fig. S8, Fig. S9), since in cyanobacteria the number of chlorophyll serving each PSII
616 is nearly fixed (Xu et al. 2018). σ_{PSII}' excited through phycobilisome absorbance at 590 nm

617 shows, as expected, a positive correlation with Phycobiliprotein:Chl *a*. Growth under low
618 cumulative diel PAR results in an increased Phycobiliprotein:Chl *a*, as the picocyanobacteria
619 allocate protein resources towards phycobiliprotein-mediated light capture (Beale 1994;
620 Stadnichuk et al. 2015; Chakdar and Pabbi 2016). PC-rich and PE-rich strains of *Synechococcus*
621 sp. in exponential growth nonetheless show significant scatter around this pattern, likely related
622 to regulatory control of σ_{PSII}' , beyond pigment composition. In pre-stationary phase σ_{PSII}'
623 vs. Phycobiliprotein:Chl *a* was better aligned, suggesting reliance upon fixed compositional
624 regulation of phycobiliprotein content to control light delivery to PSII, as opposed to shorter-
625 term regulation.

626 A phylogeny 16S rRNA gene phylogeny (amplicon average 1385 bp) placed the tested
627 strains in order Synechoccales and family Synechoccaceae, within the cluster 5
628 picocyanobacterial lineage, in sub-cluster 5.2 together with freshwater, brackish and halotolerant
629 strains, separated from marine sub-clusters 5.1 and 5.3 (Fig. 1S). The 16S rRNA of the strains
630 showed ~100% identity with strains assigned to *Synechococcus* spp. or to *Cyanobium* spp. It is
631 worth emphasizing that light capture and light absorption abilities differed significantly among
632 tested strains (Six et al. 2021). The PE-rich strains show a much higher PUR/PAR ratio under
633 low cumulative diel photon doses during exponential phase, but decay towards a plateau and
634 reach a similar value to the PC-rich strains as cumulative diel photon dose increases. Thus the
635 PE-rich strains in exponential phase demonstrated higher ability to modulate light absorbance
636 capacity, whereas PC-rich strains retained a more stable PUR/PAR across cumulative diel
637 photon doses. What is more, during exponential phase, the PE-rich strains show a much higher
638 σ_{PSII}' under low cumulative diel photon dose, and their σ_{PSII}' remains higher than the PC-rich
639 strains, even as cumulative diel photon dose increases. Hence, PE-rich strains exhibit higher light

640 harvesting efficiency, at the expense of susceptibility to higher light levels, particularly under the
641 shortest (8h) and longest (24h) photoperiods.

642 *Synechococcus* exhibits remarkable acclimation within a strain to different environmental
643 conditions (Śliwińska-Wilczewska et al. 2018a, 2020; Aguilera et al. 2023). Under high
644 cumulative diel photon dose, *Synechococcus* employs photoprotective mechanisms to prevent the
645 harmful effects of excess light energy. These include the dissipation of excess energy as heat via
646 non-photochemical quenching (NPQ) and the regulation of phycobilisome antenna pigments, to
647 balance light absorption and energy transfer. In contrast, under conditions of low cumulative diel
648 PAR dose, *Synechococcus* sp. increases the expression of light-harvesting complexes to enhance
649 light absorption (Fig. 6) and capture (Fig. 7).

650 Available photic regimes, combining photoperiod and peak PAR, may determine the
651 occurrences of PC-rich and PE-rich picocyanobacterial phenotypes. Nitrogen (N) is an essential
652 element for cyanobacteria, while the N costs to produce photosynthetic pigments varies. The
653 molecular weight of the two phycoerythrin (PE; phycoerythrobilin) subunits is about 20,000 and
654 18,300 g mol⁻¹, while the two phycocyanin (PC; phycocyanobilin) subunits are about 17,600 and
655 16,300 g mol⁻¹, and allophycocyanin (APC) is lower still, about 16,000 g mol⁻¹ (Bennett and
656 Bogorad 1971) and cell-specific content of this pigment is usually low in both phenotypes
657 (Śliwińska-Wilczewska et al. 2020). It follows that N-cost of producing PE is higher than that of
658 PC, even though PE-rich picocyanobacteria capture light better than PC-rich phenotypes (Fig. 6;
659 Fig. 7. Our results confirm that PE-rich strains are stronger light-harvesting competitors, while
660 the PC-rich strains have lower N-quotients for their phycobilin light capture system.

661

662 **Photic regimes - implications for cumulative diel PSII electron flux**

663 Algal dynamics respond rapidly to changes in environmental conditions (Connor 2018).
664 We used Fast Repetition Rate fluorometry (FRRf; Fig. 3) (Kolber et al. 1998) to generate an
665 index of PSII electron transport rate per unit volume (JV_{PSII}) (Oxborough et al. 2012; Tortell and
666 Suggett 2021; Berman-Frank et al. 2023), calibrated to absolute rates of electron transport
667 measured through oxygen evolution. Across different photic regimes the growth rates, μ , of PC-
668 rich and PE-rich picocyanobacteria show fairly consistent saturating responses to increasing
669 cumulative diel PSII electron flux (JV_{PSII} ; $\mu\text{mol e}^- \mu\text{mol Chl } \alpha^{-1} \text{ d}^{-1}$; Fig. 8). As previously found
670 for diatoms (Li et al. 2017) cumulative diel reductant generation was indeed a better predictor of
671 μ than was cumulative diel PUR, although photoperiod and peak PAR retain secondary
672 influences on achieved growth responses of the picocyanobacteria under some conditions.

673

674 **Conclusions**

675 Coastal picocyanobacteria show different growth responses to photoperiod and light level,
676 even under combinations giving equivalent cumulative diel PUR. Both PE-rich and PC-rich
677 strains of *Synechococcus* sp., grew fastest under moderate light and a 24 h photoperiod.
678 Consequently, *Synechococcus* sp. has the potential to emerge as components of the
679 phytoplankton during the Arctic or Antarctic summer under future, warmed, polar regions. In
680 optimal conditions (24 h of photoperiod and a peak PAR of 180 $\mu\text{mol photons m}^{-2}\text{s}^{-1}$), one of the
681 PE-rich *Synechococcus* sp., reached a chlorophyll-specific exponential growth rate of 4.5 d^{-1} (3.7
682 h doubling time), a record for a cyanobacteria. PE-rich strains in the exponential phase of growth
683 also demonstrated high ability to modulate their PUR/PAR ratio by adjusting pigment
684 composition, giving an advantage in the competition for light. We determined that growth yields

685 of PC-rich and PE-rich picocyanobacteria are well predicted by cumulative diel PSII electron
686 fluxes, across different photic regimes. PE-rich phenotypes of picocyanobacteria currently
687 predominate in abundance and genetic diversity in the Baltic Sea (Aguilera et al. 2023). This
688 dominance may be the result of eutrophication in the Baltic Sea, providing higher nitrogen for
689 phycobiliprotein synthesis, and leading to lower light even in near-surface waters. Our results
690 suggest possible expansion of the range of picocyanobacteria to new photic regimes in a warmed
691 future and indicate that PE-rich *Synechococcus* sp. may be a dominant component of
692 picophytoplankton in nutrient-rich environments.

693

694 **Additional Supporting Information may be found in the online version of this article.**

695

696 **Authors Contribution Statement:** S.S-W. designed the study with input from D.A.C. M.K.
697 estimated the transition point between exponential and pre-stationary phase of growth. M.S.
698 ensured the proper operation of the photobioreactors. A.A. conducted genetic analysis. N.M.O.
699 solved technical problems related to computer operation and software. S.S-W., M.S., N.M.O.,
700 D.A.C. contributed to R coding and data analysis. S.S-W. conducted the experiments, created
701 plots and wrote the manuscript, with support from D.A.C. All authors contributed to the
702 discussion of the results, supported manuscript preparation, and approved the final submitted
703 manuscript.

704

705 **Data availability statement**

706 Data supporting this study is available on:

707 <https://github.com/FundyPhytoPhys/BalticPhotoperiod> (public GitHub Repository) and

708 <https://docs.google.com/spreadsheets/d/1ZXpwR7Gfto->
709 [uRzVdXzMpQF4frbrvMLH_IyLqonFZRSw/edit#gid=0](https://docs.google.com/spreadsheets/d/1ZXpwR7Gfto-) (URL for MetaDataCatalog).
710 Code to perform data processing and analyses is available at
711 <https://github.com/FundyPhytoPhys/BalticPhotoperiod>.
712 16S rRNA sequences used in this study are available in GenBank under the accession
713 numbers PP034393, PP034394, PP034396 and PP034403.

714

715 **Acknowledgements**

716 We thank Maximilian Berthold for the code for the GAM model; Miranda Corkum who
717 maintained cultures and trained personnel in culture handling; Laurel Genge, and Carlie Barnhill
718 (Mount Allison students) who assisted with R code. This work was supported by Canada
719 Research Chair in Phytoplankton Ecophysiology (D.A.C) and Latitude & Light; NSERC of
720 Canada Discovery Grant (D.A.C).

721

722 **Conflict of Interest**

723 None declared.

724

725 **References**

726 Aguilera, A., J. Alegria Zufia, L. Bas Conn, and others. 2023. Ecophysiological analysis reveals
727 distinct environmental preferences in closely related Baltic Sea picocyanobacteria.
728 Environmental Microbiology **25**: 1674–1695. doi:10.1111/1462-2920.16384

- 729 Arrigo, K. R. 2014. Sea ice ecosystems. *Annual Review of Marine Science* **6**: 439–467.
- 730 doi:10.1146/annurev-marine-010213-135103
- 731 Beale, S. I. 1994. Biosynthesis of cyanobacterial tetrapyrrole pigments: Hemes, chlorophylls,
732 and phycobilins, p. 519–558. In D.A. Bryant [ed.], *The Molecular Biology of Cyanobacteria*.
733 Springer Netherlands.
- 734 Behrenfeld, M. J., R. T. O'Malley, D. A. Siegel, and others. 2006. Climate-driven trends in
735 contemporary ocean productivity. *Nature* **444**: 752–755. doi:10.1038/nature05317
- 736 Bennett, A., and L. Bogorad. 1971. Properties of subunits and aggregates of blue-green algal
737 biliproteins. *Biochemistry* **10**: 3625–3634. doi:10.1021/bi00795a022
- 738 Bennett, A., and L. Bogorad. 1973. Complementary Chromatic Adaptation in a filamentous blue-
739 green alga. *Journal of Cell Biology* **58**: 419–435. doi:10.1083/jcb.58.2.419
- 740 Berman-Frank, I., D. Campbell, A. Ciotti, and others. 2023. Application of Single Turnover
741 Active Chlorophyll Fluorescence for Phytoplankton Productivity Measurements. Version 2.0,
742 June, 26, 2023. Report Scientific Committee on Oceanic Research (SCOR) Working Group 156.
- 743 Boatman, T. G., R. J. Geider, and K. Oxborough. 2019. Improving the accuracy of Single
744 Turnover Active Fluorometry (STAF) for the estimation of Phytoplankton Primary Productivity
745 (PhytoPP). *Frontiers in Marine Science* **6**. doi:10.3389/fmars.2019.00319
- 746 Brand, L. E., and R. R. L. Guillard. 1981. The effects of continuous light and light intensity on
747 the reproduction rates of twenty-two species of marine phytoplankton. *Journal of Experimental
748 Marine Biology and Ecology* **50**: 119–132. doi:10.1016/0022-0981(81)90045-9

- 749 Chakdar, H., and S. Pabbi. 2016. Cyanobacterial phycobilins: Production, purification, and
750 regulation, p. 45–69. In P. Shukla [ed.], *Frontier Discoveries and Innovations in Interdisciplinary*
751 *Microbiology*. Springer India.
- 752 Christaki, U., S. Jacquet, J. R. Dolan, D. Vaultot, and F. Rassoulzadegan. 1999. Growth and
753 grazing on *Prochlorococcus* and *Synechococcus* by two marine ciliates. *Limnology and*
754 *Oceanography* **44**: 52–61. doi:10.4319/lo.1999.44.1.0052
- 755 Connor, D. 2018. Investigating the use of fast repetition rate fluorometry in understanding algal
756 physiology in optically complex oceans.
- 757 Elzhov, T. V., K. M. Mullen, A.-N. Spiess, and B. Bolker. 2023. Minpack.lm: R Interface to the
758 Levenberg-Marquardt Nonlinear Least-Squares Algorithm Found in MINPACK, Plus Support
759 for Bounds.
- 760 Erga, S. R., and B. R. Heimdal. 1984. Ecological studies on the phytoplankton of Korsfjorden,
761 western Norway. The dynamics of a spring bloom seen in relation to hydrographical conditions
762 and light regime. *Journal of Plankton Research* **6**: 67–90. doi:10.1093/plankt/6.1.67
- 763 Falkowski, P., and Z. Kolber. 1993. Estimation of phytoplankton photosynthesis by active
764 fluorescence. *ICES Marine Science Symposium* **197**: 92–103.
- 765 Field, C. B., M. J. Behrenfeld, J. T. Randerson, and P. Falkowski. 1998. Primary production of
766 the biosphere: Integrating terrestrial and oceanic components. *Science* **281**: 237–240.
767 doi:10.1126/science.281.5374.237

- 768 Flombaum, P., J. L. Gallegos, R. A. Gordillo, and others. 2013. Present and future global
769 distributions of the marine Cyanobacteria *Prochlorococcus* and *Synechococcus*. Proceedings of
770 the National Academy of Sciences **110**: 9824–9829. doi:10.1073/pnas.1307701110
- 771 Gradinger, R., and J. Lenz. 1989. Picocyanobacteria in the high Arctic. Marine Ecology Progress Series
772 **52**: 99–101. doi:10.3354/meps052099
- 773 Guillard, R. R. L. 1975. Culture of phytoplankton for feeding marine invertebrates, p. 29–60. In
774 W.L. Smith and M.H. Chanley [eds.], Culture of Marine Invertebrate Animals: Proceedings —
775 1st Conference on Culture of Marine Invertebrate Animals Greenport. Springer US.
- 776 Handel, A. 2020. Andreas Handel - Custom Word formatting using R Markdown.
- 777 Harrison, W. G., and T. Platt. 1986. Photosynthesis-irradiance relationships in polar and
778 temperate phytoplankton populations. Polar biology **5**: 153–164.
- 779 Haverkamp, T. H. A., D. Schouten, M. Doeleman, U. Wollenzien, J. Huisman, and L. J. Stal.
780 2009. Colorful microdiversity of *Synechococcus* strains (picocyanobacteria) isolated from the
781 Baltic Sea. The ISME Journal **3**: 397–408. doi:10.1038/ismej.2008.118
- 782 Hirata, T., N. J. Hardman-Mountford, R. J. W. Brewin, and others. 2011. Synoptic relationships
783 between surface Chlorophyll-*a* and diagnostic pigments specific to phytoplankton functional
784 types. Biogeosciences **8**: 311–327. doi:10.5194/bg-8-311-2011
- 785 Hoang, D. T., O. Chernomor, A. von Haeseler, B. Q. Minh, and L. S. Vinh. 2018. UFBoot2:
786 Improving the Ultrafast Bootstrap Approximation. Molecular Biology and Evolution **35**: 518–
787 522. doi:10.1093/molbev/msx281

- 788 Holtrop, T., J. Huisman, M. Stomp, and others. 2021. Vibrational modes of water predict spectral
789 niches for photosynthesis in lakes and oceans. *Nature Ecology & Evolution* **5**: 55–66.
790 doi:10.1038/s41559-020-01330-x
- 791 Huisman, J., M. Arrayás, U. Ebert, and B. Sommeijer. 2002. How do sinking phytoplankton
792 species manage to persist? *The American Naturalist* **159**: 245–254. doi:10.1086/338511
- 793 Jacob-Lopes, E., C. H. G. Scoparo, L. M. C. F. Lacerda, and T. T. Franco. 2009. Effect of light
794 cycles (night/day) on CO₂ fixation and biomass production by microalgae in photobioreactors.
795 *Chemical Engineering and Processing: Process Intensification* **48**: 306–310.
796 doi:10.1016/j.cep.2008.04.007
- 797 Jávorfi, T., J. Erostyák, J. Gál, A. Buzády, L. Menczel, G. Garab, and K. Razi Naqvi. 2006.
798 Quantitative spectrophotometry using integrating cavities. *Journal of Photochemistry and
799 Photobiology B: Biology* **82**: 127–131. doi:10.1016/j.jphotobiol.2005.10.002
- 800 Kalyaanamoorthy, S., B. Q. Minh, T. K. F. Wong, A. von Haeseler, and L. S. Jermiin. 2017.
801 ModelFinder: Fast model selection for accurate phylogenetic estimates. *Nature Methods* **14**:
802 587–589. doi:10.1038/nmeth.4285
- 803 Katoh, K., J. Rozewicki, and K. D. Yamada. 2019. MAFFT online service: Multiple sequence
804 alignment, interactive sequence choice and visualization. *Briefings in Bioinformatics* **20**: 1160–
805 1166. doi:10.1093/bib/bbx108
- 806 Klepacz-Smólka, A., D. Pietrzyk, R. Szeląg, P. Głuscz, M. Daroch, J. Tang, and S. Ledakowicz.
807 2020. Effect of light colour and photoperiod on biomass growth and phycocyanin production by

- 808 *Synechococcus* PCC 6715. Bioresource Technology **313**: 123700.
809 doi:10.1016/j.biortech.2020.123700
- 810 Kolber, Z. S., O. Prášil, and P. G. Falkowski. 1998. Measurements of variable chlorophyll
811 fluorescence using fast repetition rate techniques: Defining methodology and experimental
812 protocols. Biochimica et Biophysica Acta (BBA) - Bioenergetics **1367**: 88–106.
813 doi:10.1016/S0005-2728(98)00135-2
- 814 Krishnan, A., M. Likhogrud, M. Cano, and others. 2021. *Picochlorum Celere* as a model system
815 for robust outdoor algal growth in seawater. Scientific Reports **11**: 11649. doi:10.1038/s41598-
816 021-91106-5
- 817 Lane, D. J. 1991. 16S/23S rRNA sequencing. Nucleic acid techniques in bacterial systematics
818 115–175.
- 819 LaRoche, J., and B. M. Robicheau. 2022. The Pelagic Light-Dependent Microbiome, p. 395–
820 423. In L.J. Stal and M.S. Cretoiu [eds.], The Marine Microbiome. Springer International
821 Publishing.
- 822 Li, G., D. Talmy, and D. A. Campbell. 2017. Diatom growth responses to photoperiod and light
823 are predictable from diel reductant generation. Journal of Phycology **53**: 95–107.
824 doi:10.1111/jpy.12483
- 825 Li, Q., L. Legendre, and N. Jiao. 2015. Phytoplankton responses to nitrogen and iron limitation
826 in the tropical and subtropical Pacific Ocean. Journal of Plankton Research **37**: 306–319.
827 doi:10.1093/plankt/fbv008

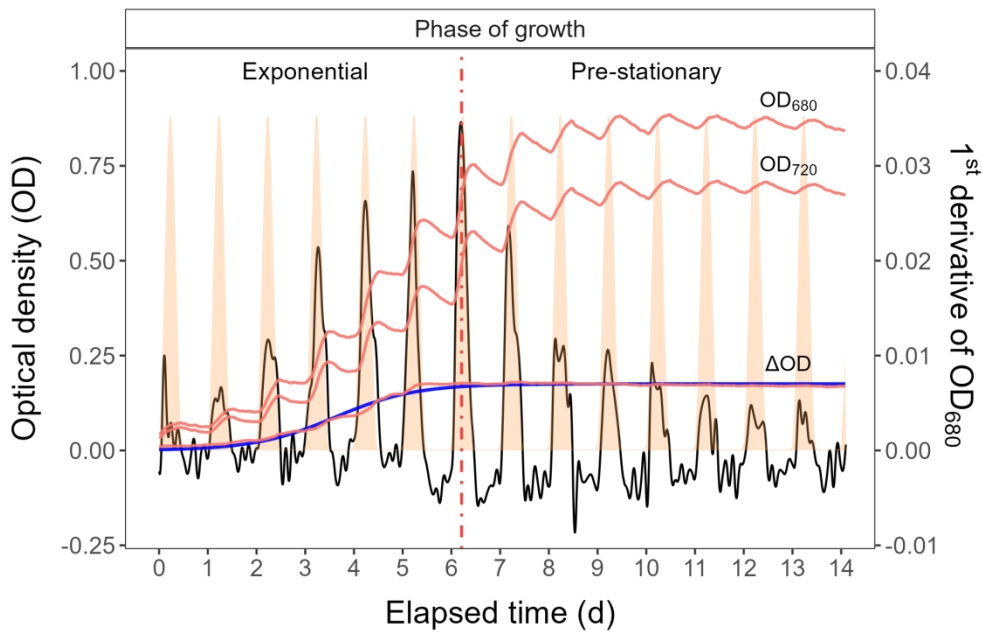
- 828 Li, W. K. W. 1995. Composition of ultraphytoplankton in the central North Atlantic. *Marine
829 Ecology Progress Series* **122**: 1–8.
- 830 Ligges, U., T. Short, P. Kienzle, and others. 2024. Signal: Signal Processing.
- 831 Litchman, E., C. A. Klausmeier, and K. Yoshiyama. 2009. Contrasting size evolution in marine
832 and freshwater diatoms. *Proceedings of the National Academy of Sciences* **106**: 2665–2670.
833 doi:10.1073/pnas.0810891106
- 834 Longobardi, L., L. Dubroca, F. Margiotta, D. Sarno, and A. Zingone. 2022. Photoperiod-driven
835 rhythms reveal multi-decadal stability of phytoplankton communities in a highly fluctuating
836 coastal environment. *Scientific Reports* **12**: 3908. doi:10.1038/s41598-022-07009-6
- 837 MacIntyre, H. L., T. M. Kana, R. J. Geider, H. L. MacIntyre, T. M. Kana, and R. J. Geider. 2000.
838 The effect of water motion on short-term rates of photosynthesis by marine phytoplankton.
839 *Trends in Plant Science* **5**: 12–17. doi:10.1016/S1360-1385(99)01504-6
- 840 Moejes, F. W., A. Matuszyńska, K. Adhikari, and others. 2017. A systems-wide understanding
841 of photosynthetic acclimation in algae and higher plants. *Journal of Experimental Botany* **68**:
842 2667–2681. doi:10.1093/jxb/erx137
- 843 Morel, A. 1978. Available, usable, and stored radiant energy in relation to marine
844 photosynthesis. *Deep Sea Research* **25**: 673–688. doi:10.1016/0146-6291(78)90623-9
- 845 Morel, A. 1988. Optical modeling of the upper ocean in relation to its biogenous matter content
846 (case I waters). *Journal of Geophysical Research: Oceans* **93**: 10749–10768.
847 doi:10.1029/JC093iC09p10749

- 848 Oxborough, K., and N. R. Baker. 1997. Resolving chlorophyll *a* fluorescence images of
849 photosynthetic efficiency into photochemical and non-photochemical components – calculation
850 of qP and Fv-/Fm-; without measuring Fo-; *Photosynthesis Research* **54**: 135–142.
851 doi:10.1023/A:1005936823310
- 852 Oxborough, K., C. M. Moore, D. J. Suggett, T. Lawson, H. G. Chan, and R. J. Geider. 2012.
853 Direct estimation of functional PSII reaction center concentration and PSII electron flux on a
854 volume basis: A new approach to the analysis of Fast Repetition Rate fluorometry (FRRf) data.
855 *Limnology and Oceanography: Methods* **10**: 142–154. doi:10.4319/lom.2012.10.142
- 856 Pedersen, T. L. 2024. Patchwork: The Composer of Plots.
- 857 Pick, F. R. 1991. The abundance and composition of freshwater picocyanobacteria in relation to
858 light penetration. *Limnology and Oceanography* **36**: 1457–1462. doi:10.4319/lo.1991.36.7.1457
- 859 Posit team. 2022. RStudio: Integrated development environment for r, Posit Software, PBC.
- 860 R Core Team. 2023. R: A language and environment for statistical computing, R Foundation for
861 Statistical Computing.
- 862 Reynolds, C. S. 2006. *The Ecology of Phytoplankton*, Cambridge University Press.
- 863 Ryan, J. A., J. M. Ulrich, R. Bennett, and C. Joy. 2024. Xts: eXtensible Time Series.
- 864 Sakamoto, T., and D. A. Bryant. 1999. Nitrate transport and not photoinhibition limits growth of
865 the freshwater cyanobacterium *Synechococcus* species PCC 6301 at low temperature. *Plant
866 Physiology* **119**: 785–794. doi:10.1104/pp.119.2.785

- 867 Schuurmans, R. M., J. C. P. Matthijs, and K. J. Hellingwerf. 2017. Transition from exponential
868 to linear photoautotrophic growth changes the physiology of *Synechocystis* sp. PCC 6803.
869 Photosynthesis Research **132**: 69–82. doi:10.1007/s11120-016-0329-8
- 870 Serway, R. A., C. J. Moses, and C. A. Moyer. 2004. Modern Physics, Cengage Learning.
- 871 Six, C., Z. V. Finkel, A. J. Irwin, and D. A. Campbell. 2007. Light variability illuminates niche-
872 partitioning among marine picocyanobacteria. PLOS ONE **2**: e1341.
873 doi:10.1371/journal.pone.0001341
- 874 Six, C., M. Ratin, D. Marie, and E. Corre. 2021. Marine *Synechococcus* picocyanobacteria: Light
875 utilization across latitudes. Proceedings of the National Academy of Sciences **118**: e2111300118.
876 doi:10.1073/pnas.2111300118
- 877 Śliwińska-Wilczewska, S., A. Cieszyńska, J. Maculewicz, and A. Latała. 2018a.
878 Ecophysiological characteristics of red, green, and brown strains of the Baltic
879 picocyanobacterium *Synechococcus* sp. – a laboratory study. Biogeosciences **15**: 6257–6276.
880 doi:10.5194/bg-15-6257-2018
- 881 Śliwińska-Wilczewska, S., Z. Konarzewska, K. Wiśniewska, and M. Konik. 2020.
882 Photosynthetic pigments changes of three phenotypes of picocyanobacteria *Synechococcus* sp.
883 Under different light and temperature conditions. Cells **9**: 2030. doi:10.3390/cells9092030
- 884 Śliwińska-Wilczewska, S., J. Maculewicz, A. Barreiro Felpeto, and A. Latała. 2018b.
885 Allelopathic and bloom-forming picocyanobacteria in a changing world. Toxins **10**: 48.
886 doi:10.3390/toxins10010048

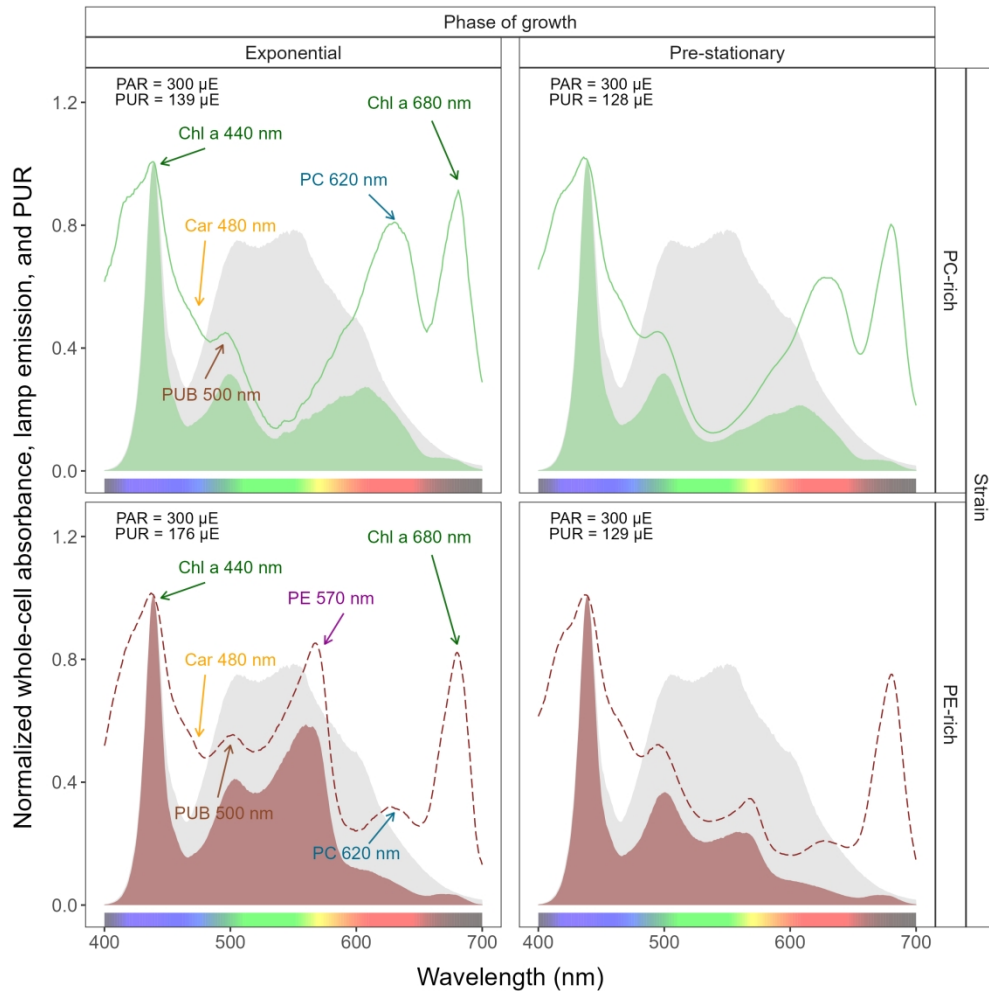
- 887 Stadnichuk, I. N., P. M. Krasilnikov, and D. V. Zlenko. 2015. Cyanobacterial phycobilisomes
888 and phycobiliproteins. *Microbiology* **84**: 101–111. doi:10.1134/S0026261715020150
- 889 Stomp, M., J. Huisman, L. Vörös, F. R. Pick, M. Laamanen, T. Haverkamp, and L. J. Stal. 2007.
890 Colourful coexistence of red and green picocyanobacteria in lakes and seas. *Ecology Letters* **10**:
891 290–298. doi:10.1111/j.1461-0248.2007.01026.x
- 892 Strickland, J. D., and T. R. Parsons. 1972. Practical Hand Book of Seawater Analysis. Fisheries
893 Research Board of Canada **167 (2nd edition)**: 1–311. doi:DOI: <http://dx.doi.org/10.25607/OBP-1791>
- 895 Theus, M. E., T. J. Layden, N. McWilliams, S. Crafton-Tempel, C. T. Kremer, and S. B. Fey.
896 2022. Photoperiod influences the shape and scaling of freshwater phytoplankton responses to
897 light and temperature. *Oikos* **2022**: e08839. doi:10.1111/oik.08839
- 898 Torremorell, A., M. E. Llames, G. L. Pérez, R. Escaray, J. Bustingorry, and H. Zagarese. 2009.
899 Annual patterns of phytoplankton density and primary production in a large, shallow lake: The
900 central role of light. *Freshwater Biology* **54**: 437–449. doi:10.1111/j.1365-2427.2008.02119.x
- 901 Tortell, P., and D. J. Suggett. 2021. A user guide for the application of Single Turnover active
902 chlorophyll fluorescence for phytoplankton productivity measurements. Version 1. Report
903 Scientific Committee on Oceanic Research (SCOR) Working Group 156.
- 904 van Alphen, P., H. Abedini Najafabadi, F. Branco dos Santos, and K. J. Hellingwerf. 2018.
905 Increasing the photoautotrophic growth rate of *Synechocystis* sp. PCC 6803 by identifying the
906 limitations of its cultivation. *Biotechnology Journal* **13**: 1700764. doi:10.1002/biot.201700764

- 907 Velichko, N., S. Smirnova, S. Averina, and A. Pinevich. 2021. A survey of Antarctic
908 cyanobacteria. *Hydrobiologia* **848**: 2627–2653.
- 909 Vincent, W. F., J. P. Bowman, L. M. Rankin, and T. A. McMeekin. 2000. Phylogenetic diversity
910 of picocyanobacteria in Arctic and Antarctic ecosystems. *Microbial biosystems: new frontiers.*
911 Proceedings of the 8th International Symposium on Microbial Ecology 317–322.
- 912 Wickham, H. 2016. Data Analysis, p. 189–201. *In* H. Wickham [ed.], *Ggplot2: Elegant Graphics*
913 for Data Analysis. Springer International Publishing.
- 914 Wood, S. N. 2017. Generalized Additive Models: An Introduction with R, Second Edition, 2nd
915 ed. Chapman and Hall/CRC.
- 916 Xi, H., S. N. Losa, A. Mangin, and others. 2020. Global retrieval of phytoplankton functional
917 types based on empirical orthogonal functions using CMEMS GlobColour merged products and
918 further extension to OLCI data. *Remote Sensing of Environment* **240**: 111704.
919 doi:10.1016/j.rse.2020.111704
- 920 Xu, K., J. L. Grant-Burt, N. Donaher, and D. A. Campbell. 2017. Connectivity among
921 Photosystem II centers in phytoplankters: Patterns and responses. *Biochimica et Biophysica Acta*
922 (*BBA*) - *Bioenergetics* **1858**: 459–474. doi:10.1016/j.bbabi.2017.03.003
- 923 Xu, K., J. Lavaud, R. Perkins, E. Austen, M. Bonnanfant, and D. A. Campbell. 2018.
924 Phytoplankton σ PSII and excitation dissipation; implications for estimates of primary
925 productivity. *Frontiers in Marine Science* **5**. doi:10.3389/fmars.2018.00281



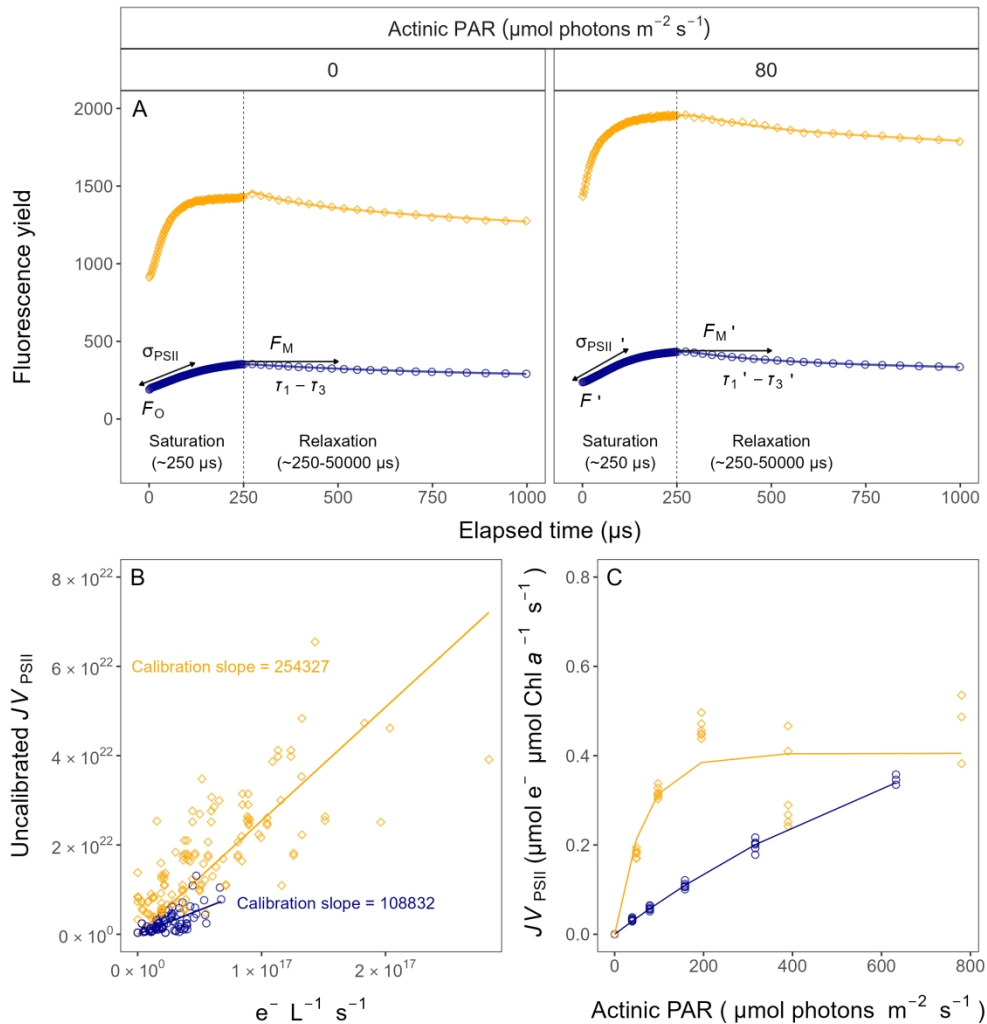
Example of a growth curve (tracked as OD₇₂₀, OD₆₈₀, or Δ OD; red solid lines, left y-axis) of PE-rich culture of *Synechococcus* sp. (048) vs. elapsed time (d, x-axis).

452x290mm (118 x 118 DPI)



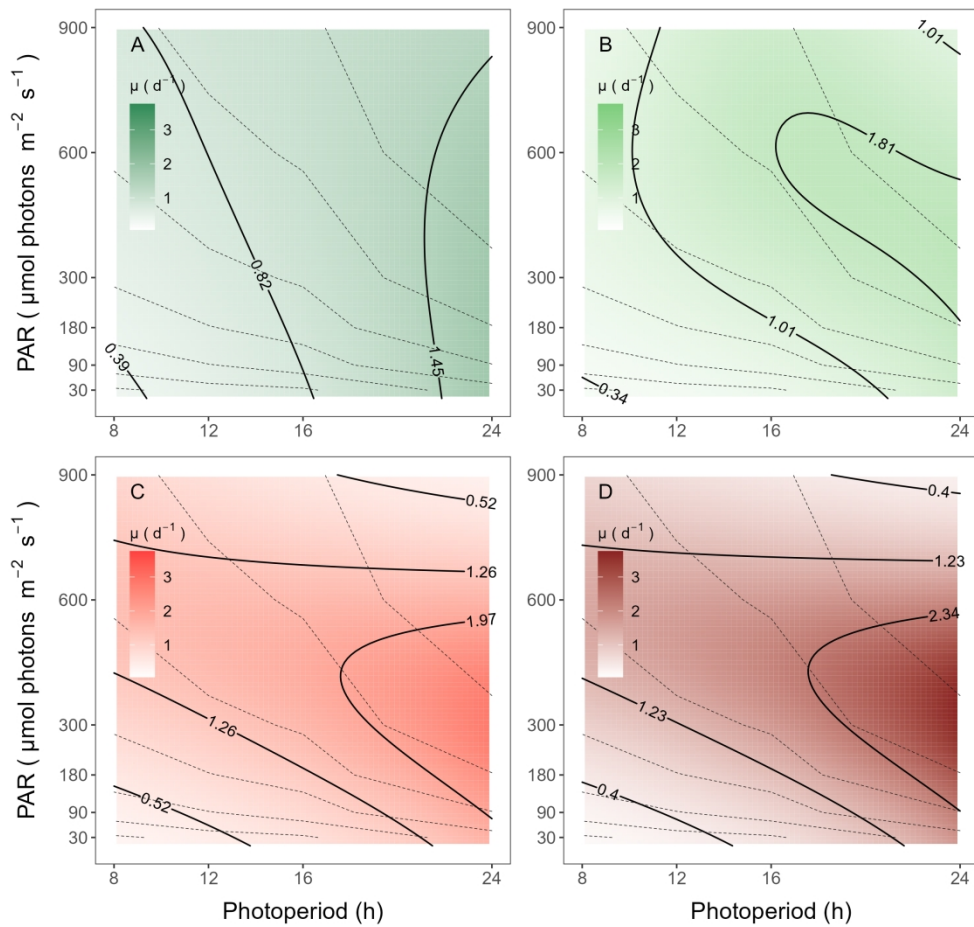
Whole-cell absorbance spectra of PC-rich (solid green lines) or PE-rich (dashed red lines) cultures of *Synechococcus* sp.

581x581mm (118 x 118 DPI)



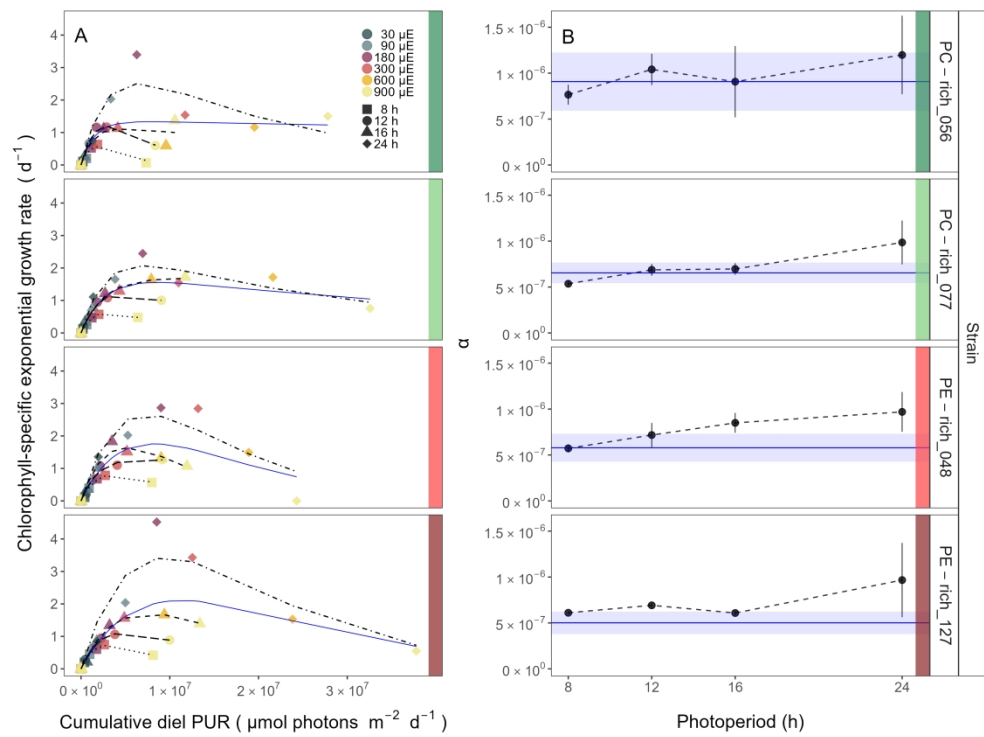
Single turnover (ST) fluorescence induction by Fast Repetition Rate fluorometry (FRRf).

613x645mm (118 x 118 DPI)



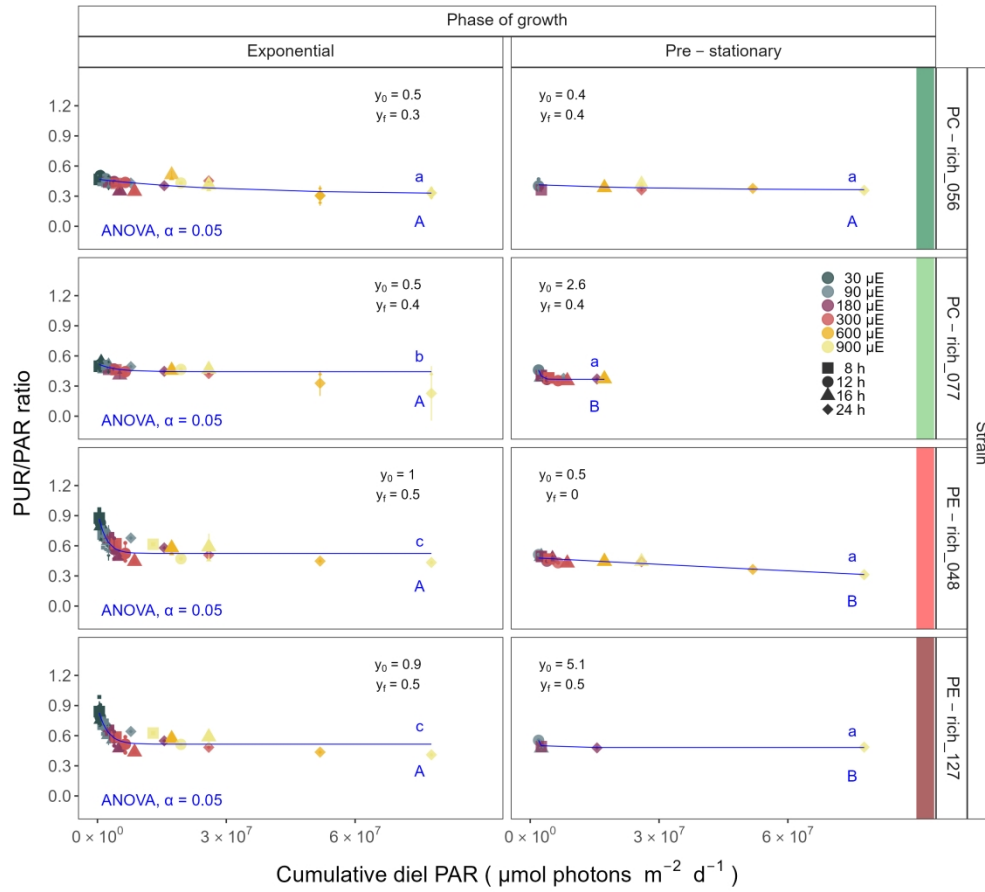
A contour plot of a Generalized Additive Model (GAM) of chlorophyll-specific growth rates (d⁻¹) for two PC-rich cultures: (A) 056, (B) 077 and two PE-rich cultures: (C) 048, (D) 127 of *Synechococcus* sp. originating from the Baltic Sea.

613x581mm (118 x 118 DPI)



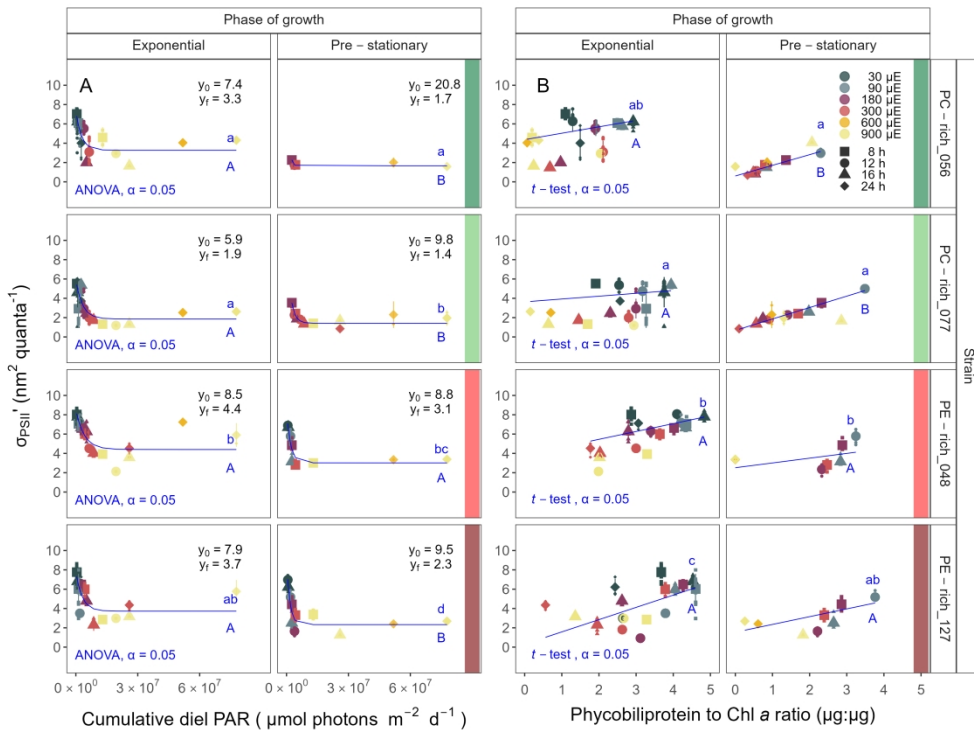
Chlorophyll-specific exponential growth rates (d^{-1}) vs. cumulative diel Photosynthetically Usable Radiation (PUR, $\mu\text{mol photons m}^{-2} \text{d}^{-1}$).

774x581mm (118 x 118 DPI)



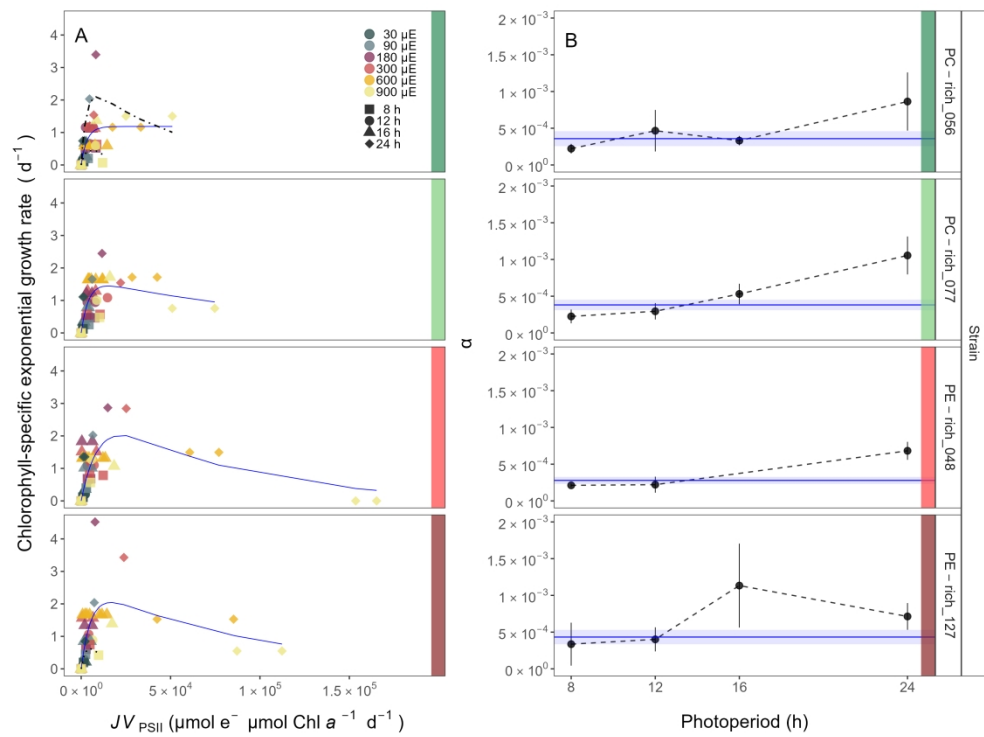
Changes in PUR/PAR ratio vs. cumulative diel PAR ($\mu\text{mol photons m}^{-2}\text{d}^{-1}$).

645x581mm (118 x 118 DPI)



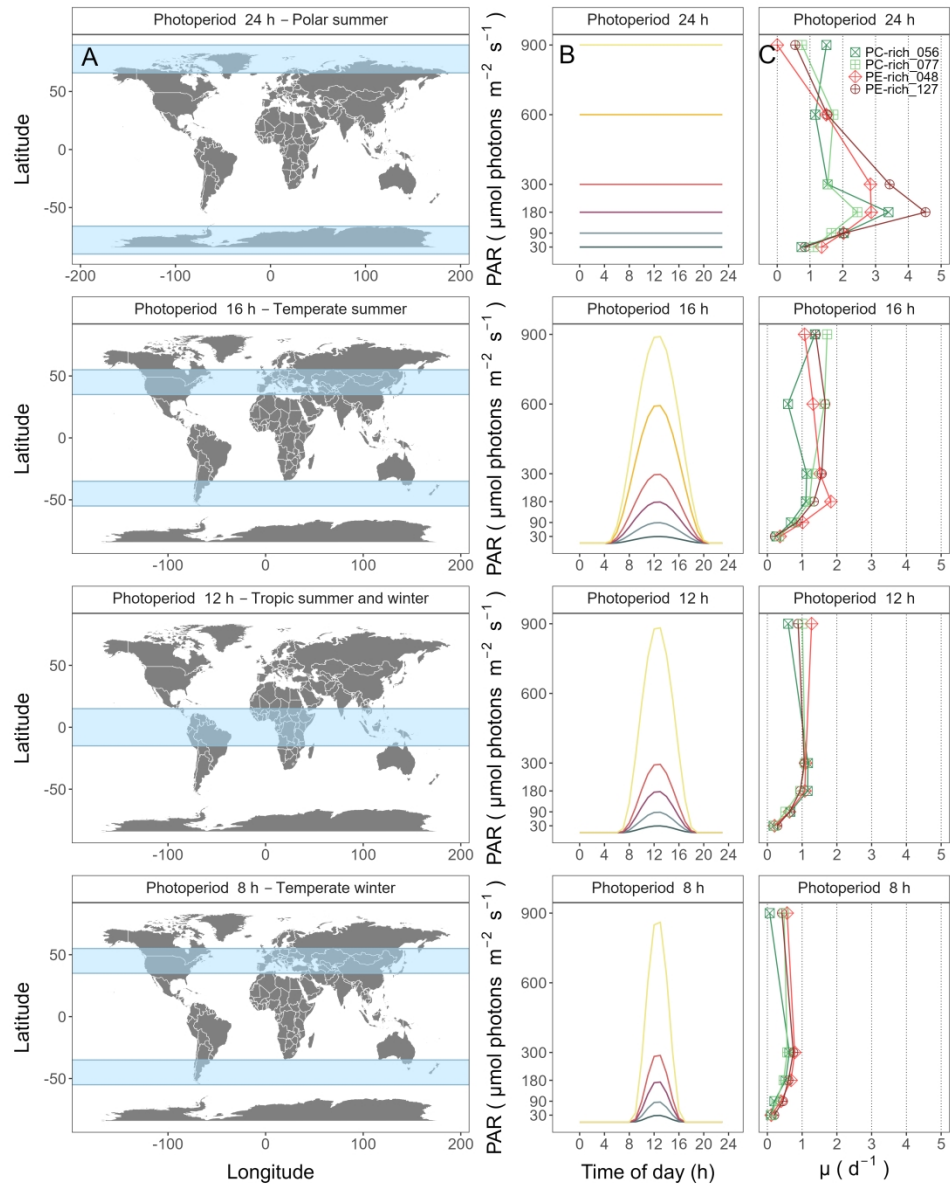
Effective absorption cross section of PSII (σ_{PSII}' ; nm² quanta⁻¹) measured under diel peak PAR growth light.

774x581mm (118 x 118 DPI)



Chlorophyll-specific exponential growth rates (d^{-1}) vs. cumulative diel PSII electron flux (JV_{PSII} ; $\mu\text{mol e}^- \mu\text{mol Chl } a^{-1} d^{-1}$) measured under diel peak PAR growth light.

774x581mm (118 x 118 DPI)



Latitudinal bands, equivalent summer or winter photoperiods, and picocyanobacterial growth responses.

774x968mm (118 x 118 DPI)

1 **Growth yields and light-capture in PhycoCyanin and**
2 **PhycoErythrin-rich picocyanobacteria, across photic**
3 **regimes and growth phases**

4

5 **Sylwia Śliwińska-Wilczewska^{1,2}, Marta Konik^{3,4}, Mireille Savoie¹, Anabella**
6 **Aguilera^{5,6}, Naaman M. Omar¹, and Douglas A. Campbell^{1,*}**

7

8 ¹ Department of Biology, Mount Allison University, 53 York St., Sackville, NB, E4L 1C9,
9 Canada

10 ² Institute of Oceanography, University of Gdańsk, 46 Piłsudskiego St, 80-378, Gdynia, Poland

11 ³ Department of Geography, University of Victoria, Victoria, BC, V8P 5C2, Canada

12 ⁴ Institute of Oceanology, Polish Academy of Sciences, 81-712 Sopot, Poland

13 ⁵ Department of Biology and Environmental Science, Centre for Ecology and Evolution in
14 Microbial Model Systems (EEMiS), Linnaeus University, Kalmar, Sweden

15 ⁶ Department of Aquatic Sciences and Assessment, Swedish University of Agricultural Sciences,
16 Uppsala, Sweden (present address)

17 * Correspondence: Douglas A. Campbell <dubhglas.cambeuil@gmail.com>

18

19 ***Supporting Information***

20

22 **Tab. S1.** Linear regression, coefficient of determination (R^2), Pearson correlation coefficients (R), and p -value
 23 used to calculate the pigment content ($\mu\text{g mL}^{-1}$) of two PhycoCyanin(PC)-rich cultures (056, 077) and two
 24 PhycoErythrin(PE)-rich cultures (048, 127) (Culture Collection of Baltic Algae) of *Synechococcus* sp. based on
 25 absorbance (A) measurements.
 26

Pigment	Abs	Linear_regression	R^2	R	p _value
Chl a	665	Chl a $\mu\text{g/mL} = (\text{Abs}_{665} * 13.411029) + 0.154793$	0.865	0.930	0.000
Car	480	Car $\mu\text{g/mL} = (\text{Abs}_{480} * 5.469880) + 0.089971$	0.791	0.890	0.000
PE	565	PE $\mu\text{g/mL} = (\text{Abs}_{565} * 26.760737) - 0.143872$	0.698	0.840	0.000
PC	620	PC $\mu\text{g/mL} = (\text{Abs}_{620} * 29.979866) - 0.182611$	0.807	0.900	0.000
APC	650	APC $\mu\text{g/mL} = (\text{Abs}_{650} * 3.873803) + 0.021964$	0.087	0.300	0.000

27
 28 **Tab. S2.** Three-way factorial ANOVA testing whether peak PAR, photoperiod, strain, and their interactions
 29 (Source_of_variation), significantly influence the chlorophyll specific exponential growth rate ($\mu; \text{d}^{-1}$), estimated
 30 from logistic fits of chlorophyll proxy $\text{OD}_{680} - \text{OD}_{720}$ vs. cumulative diel PUR, for two PhycoCyanin(PC)-rich
 31 cultures (056, 077) and two PhycoErythrin(PE)-rich cultures (048, 127) (Culture Collection of Baltic Algae) of
 32 *Synechococcus* sp., grown at 30, 90, 180, 300, 600, or 900 peak PAR $\mu\text{mol photons m}^{-2}\text{s}^{-1}$; and photoperiods of 8,
 33 12, 16, or 24 h. Df – degrees of freedom; Sum Sq – sum of squares; Mean Sq – mean sum of squares; F _value –
 34 Fisher's F -test statistic; p _value - level of significance.
 35

Source_of_variation	Df	Sum Sq	Mean Sq	F _value	p _value
Par_ue	5	0.049	0.010	3.276e+30	0.000
Photoperiod	3	0.076	0.025	8.367e+30	0.000
Strain	3	0.003	0.001	3.151e+29	0.000
Par_ue:Photoperiod	13	0.040	0.003	1.025e+30	0.000
Par_ue:Strain	15	0.007	0.000	1.593e+29	0.000
Photoperiod:Strain	9	0.004	0.000	1.306e+29	0.000
Par_ue:Photoperiod:Strain	39	0.017	0.000	1.434e+29	0.000
Residuals	88	0.000	0.000	NA	N/A

36

38 **Tab. S3.** One-way ANOVA of a three parameter model (Harrison and Platt 1986) from pooled data (All) and data fit
 39 across different photoperiods (8, 12, 16, or 24) from chlorophyll specific exponential growth rate vs. cumulative diel
 40 PUR (Fit_model), for two PhycoCyanin(PC)-rich cultures (056, 077) and two PhycoErythrin(PE)-rich cultures (048,
 41 127) of *Synechococcus* sp., grown at 30, 90, 180, 300, 600, or 900 peak PAR $\mu\text{mol photons m}^{-2}\text{s}^{-1}$; and
 42 photoperiods of 8, 12, 16, or 24 h. Res.Df - residual degrees of freedom for each model; Res.Sum Sq - residual sum
 43 of squares for each model; F _value – Fisher's F -test statistic; p _value - level of significance.
 44

Strain	Fit_model	Res.Df	Res.Sum Sq	F _value	p _value
PC-rich_056	8_All	41	8.063	1.807e+03	0.000
PC-rich_056	12_All	41	8.063	2.822e+01	0.001
PC-rich_056	16_All	41	8.063	8.566e+00	0.012
PC-rich_056	24_All	41	8.063	2.333e+01	0.001
PC-rich_077	8_All	41	3.015	6.193e+01	0.000
PC-rich_077	12_All	41	3.015	2.477e+01	0.001
PC-rich_077	16_All	41	3.015	1.855e+01	0.002
PC-rich_077	24_All	41	3.015	1.073e+01	0.007
PE-rich_048	8_All	41	6.731	1.443e+01	0.004
PE-rich_048	12_All	41	6.731	8.361e+01	0.000
PE-rich_048	16_All	41	6.731	8.403e+00	0.013
PE-rich_048	24_All	41	6.731	8.234e+01	0.000
PE-rich_127	8_All	41	13.016	1.453e+02	0.000
PE-rich_127	12_All	41	13.016	2.060e+03	0.000
PE-rich_127	16_All	41	13.016	6.908e+00	0.020
PE-rich_127	24_All	41	13.016	7.812e+01	0.000



45
 46
 47
 48
 49
 50
 51
 52
 53
 54
 55

57 **Tab. S4.** One-way ANOVA of a three parameter model (Harrison and Platt 1986) from pooled data (All) and data fit
 58 across different peak PAR (30, 90, 180, 300, 600 together with 900) from chlorophyll specific exponential growth
 59 rate vs. cumulative diel PUR (Fit_model), for two PhycoCyanin(PC)-rich cultures (056, 077) and two
 60 PhycoErythrin(PE)-rich cultures (048, 127) of *Synechococcus* sp., grown at 30, 90, 180, 300, 600, or 900 peak PAR
 61 $\mu\text{mol photons m}^{-2}\text{s}^{-1}$; and photoperiods of 8, 12, 16, or 24 h. Res.Df - residual degrees of freedom for each model;
 62 Res.Sum Sq - residual sum of squares for each model; F_{value} – Fisher's F -test statistic; p_{value} - level of
 63 significance.

64

Strain	Fit_model	Res.Df	Res.Sum Sq	F_{value}	p_{value}
PC-rich_056	30_All	41	8.063	1.807e+03	0.000
PC-rich_056	90_All	41	8.063	2.822e+01	0.001
PC-rich_056	180_All	41	8.063	8.566e+00	0.012
PC-rich_056	300_All	41	8.063	2.333e+01	0.001
PC-rich_056	900_All	41	8.063	3.360e+00	0.030
PC-rich_077	30_All	41	3.015	6.193e+01	0.000
PC-rich_077	90_All	41	3.015	2.477e+01	0.001
PC-rich_077	180_All	41	3.015	1.855e+01	0.002
PC-rich_077	300_All	41	3.015	1.073e+01	0.007
PC-rich_077	900_All	41	3.015	6.508e-01	0.822
PE-rich_048	30_All	41	6.731	1.443e+01	0.004
PE-rich_048	90_All	41	6.731	8.361e+01	0.000
PE-rich_048	180_All	41	6.731	8.403e+00	0.013
PE-rich_048	300_All	41	6.731	8.234e+01	0.000
PE-rich_048	900_All	41	6.731	1.357e+00	0.328
PE-rich_127	30_All	41	13.016	1.453e+02	0.000
PE-rich_127	90_All	41	13.016	2.060e+03	0.000
PE-rich_127	180_All	41	13.016	6.908e+00	0.020
PE-rich_127	300_All	41	13.016	7.812e+01	0.000
PE-rich_127	900_All	41	13.016	3.523e+00	0.026

65

66

68 **Tab. S5.** One-way ANOVA of a three parameter model (Harrison and Platt 1986) from pooled data (All) and data fit
 69 across different photoperiods (8, 12, 16, or 24) from chlorophyll specific exponential growth rate vs. cumulative diel
 70 PAR (Fit_model), for two PhycoCyanin(PC)-rich cultures (056, 077) and two PhycoErythrin(PE)-rich cultures (048,
 71 127) of *Synechococcus* sp., grown at 30, 90, 180, 300, 600, or 900 peak PAR $\mu\text{mol photons m}^{-2}\text{s}^{-1}$; and
 72 photoperiods of 8, 12, 16, or 24 h. Res.Df - residual degrees of freedom for each model; Res.Sum Sq - residual sum
 73 of squares for each model; F _value – Fisher's F -test statistic; p _value - level of significance.
 74

Strain	Fit_model	Res.Df	Res.Sum Sq	F _value	p _value
PC-rich_056	8_All	135	18.854	1.089e+03	0.000
PC-rich_056	12_All	135	18.854	1.412e+01	0.000
PC-rich_056	16_All	135	18.854	7.420e+00	0.000
PC-rich_056	24_All	135	18.854	1.279e+01	0.000
PC-rich_077	8_All	131	5.672	2.749e+01	0.000
PC-rich_077	12_All	131	5.672	8.972e+00	0.000
PC-rich_077	16_All	131	5.672	5.640e+00	0.000
PC-rich_077	24_All	131	5.672	4.027e+00	0.000
PE-rich_048	8_All	133	16.660	2.122e+01	0.000
PE-rich_048	12_All	133	16.660	1.997e+01	0.000
PE-rich_048	16_All	133	16.660	3.576e+00	0.000
PE-rich_048	24_All	133	16.660	8.068e+01	0.000
PE-rich_127	8_All	133	26.508	6.568e+01	0.000
PE-rich_127	12_All	133	26.508	6.758e+03	0.000
PE-rich_127	16_All	133	26.508	1.515e+01	0.000
PE-rich_127	24_All	133	26.508	5.207e+01	0.000



75

76

78 **Tab. S6.** One-way ANOVA of a three parameter model (Harrison and Platt 1986) from pooled data (All) and data fit
 79 across different peak PAR (30, 90, 180, 300, 600 together with 900) from chlorophyll specific exponential growth
 80 rate vs. cumulative diel PAR (Fit_model), for two PhycoCyanin(PC)-rich cultures (056, 077) and two
 81 PhycoErythrin(PE)-rich cultures (048, 127) of *Synechococcus* sp., grown at 30, 90, 180, 300, 600, or 900 peak PAR
 82 $\mu\text{mol photons m}^{-2}\text{s}^{-1}$; and photoperiods of 8, 12, 16, or 24 h. Res.Df - residual degrees of freedom for each model;
 83 Res.Sum Sq - residual sum of squares for each model; F_{value} – Fisher's F -test statistic; p_{value} - level of
 84 significance.

85

Strain	Fit_model	Res.Df	Res.Sum Sq	F_{value}	p_{value}
PC-rich_056	30_All	135	18.854	1.089e+03	0.000
PC-rich_056	90_All	135	18.854	1.412e+01	0.000
PC-rich_056	180_All	135	18.854	7.420e+00	0.000
PC-rich_056	300_All	135	18.854	1.279e+01	0.000
PC-rich_056	900_All	135	18.854	2.573e+00	0.003
PC-rich_077	30_All	131	5.672	2.749e+01	0.000
PC-rich_077	90_All	131	5.672	8.972e+00	0.000
PC-rich_077	180_All	131	5.672	5.640e+00	0.000
PC-rich_077	300_All	131	5.672	4.027e+00	0.000
PC-rich_077	900_All	131	5.672	7.428e-01	0.844
PE-rich_048	30_All	133	16.660	2.122e+01	0.000
PE-rich_048	90_All	133	16.660	1.997e+01	0.000
PE-rich_048	180_All	133	16.660	3.576e+00	0.000
PE-rich_048	300_All	133	16.660	8.068e+01	0.000
PE-rich_048	900_All	133	16.660	1.893e+00	0.034
PE-rich_127	30_All	133	26.508	6.568e+01	0.000
PE-rich_127	90_All	133	26.508	6.758e+03	0.000
PE-rich_127	180_All	133	26.508	1.515e+01	0.000
PE-rich_127	300_All	133	26.508	5.207e+01	0.000
PE-rich_127	900_All	133	26.508	2.800e+00	0.002

86

87

89 **Tab. S7.** One-way ANOVA of a three parameter model (Harrison and Platt 1986) from pooled data (All) and data fit
 90 across different photoperiods (8, 12, 16, or 24) from chlorophyll specific exponential growth rate vs. PSII electron
 91 flux (JV_{PSII} ; $\mu\text{mol e}^- \mu\text{mol Chl } a^{-1} d^{-1}$) (Fit_model), for two PhycoCyanin(PC)-rich cultures (056, 077) and two
 92 PhycoErythrin(PE)-rich cultures (048, 127) of *Synechococcus* sp., grown at 30, 90, 180, 300, 600, or 900 peak PAR
 93 $\mu\text{mol photons m}^{-2}\text{s}^{-1}$; and photoperiods of 8, 12, 16, or 24 h. Res.Df - residual degrees of freedom for each model;
 94 Res.Sum Sq - residual sum of squares for each model; F _value – Fisher's F -test statistic; p _value - level of
 95 significance.
 96

Strain	Fit_model	Res.Df	Res.Sum Sq	F _value	p _value
PC-rich_056	8_All	61	11.802	3.972e+00	0.016
PC-rich_056	12_All	61	11.802	7.712e-01	0.730
PC-rich_056	16_All	61	11.802	2.287e-01	1.000
PC-rich_056	24_All	61	11.802	3.332e+00	0.037
PC-rich_077	8_All	61	9.014	1.125e+00	0.459
PC-rich_077	12_All	61	9.014	1.377e+00	0.350
PC-rich_077	16_All	61	9.014	6.146e-01	0.861
PC-rich_077	24_All	61	9.014	1.562e+00	0.260
PE-rich_048	8_All	61	16.583	1.332e+00	0.339
PE-rich_048	12_All	61	16.583	1.977e+00	0.174
PE-rich_048	16_All	61	16.583	5.540e-01	0.903
PE-rich_048	24_All	61	16.583	6.716e-01	0.817
PE-rich_127	8_All	53	21.117	7.994e+00	0.004
PE-rich_127	12_All	53	21.117	4.159e+00	0.057
PE-rich_127	16_All	53	21.117	5.525e-01	0.882
PE-rich_127	24_All	53	21.117	1.100e+00	0.504

97

98

100 **Tab. S8.** One-way ANOVA of a three parameter model (Harrison and Platt 1986) from pooled data (All) and data fit
 101 across different peak PAR (30, 90, 180, 300, 600 together with 900) from chlorophyll specific exponential growth
 102 rate vs. PSII electron flux (JV_{PSII} ; $\mu\text{mol e}^{-} \mu\text{mol Chl } a^{-1} d^{-1}$) (Fit_model), for two PhycoCyanin(PC)-rich cultures
 103 (056, 077) and two PhycoErythrin(PE)-rich cultures (048, 127) of *Synechococcus* sp., grown at 30, 90, 180, 300,
 104 600, or 900 peak PAR $\mu\text{mol photons m}^{-2}s^{-1}$; and photoperiods of 8, 12, 16, or 24 h. Res.Df - residual degrees of
 105 freedom for each model; Res.Sum Sq - residual sum of squares for each model; F_value – Fisher's F-test statistic;
 106 p_value - level of significance.
 107

Strain	Fit_model	Res.Df	Res.Sum Sq	F_value	p_value
PC-rich_056	30_All	61	11.802	3.972e+00	0.016
PC-rich_056	90_All	61	11.802	7.712e-01	0.730
PC-rich_056	180_All	61	11.802	2.287e-01	1.000
PC-rich_056	300_All	61	11.802	3.332e+00	0.037
PC-rich_056	900_All	61	11.802	2.156e+00	0.044
PC-rich_077	30_All	61	9.014	1.125e+00	0.459
PC-rich_077	90_All	61	9.014	1.377e+00	0.350
PC-rich_077	180_All	61	9.014	6.146e-01	0.861
PC-rich_077	300_All	61	9.014	1.562e+00	0.260
PC-rich_077	900_All	61	9.014	1.295e+00	0.287
PE-rich_048	30_All	61	16.583	1.332e+00	0.339
PE-rich_048	90_All	61	16.583	1.977e+00	0.174
PE-rich_048	180_All	61	16.583	5.540e-01	0.903
PE-rich_048	300_All	61	16.583	6.716e-01	0.817
PE-rich_048	900_All	61	16.583	3.125e+00	0.007
PE-rich_127	30_All	53	21.117	7.994e+00	0.004
PE-rich_127	90_All	53	21.117	4.159e+00	0.057
PE-rich_127	180_All	53	21.117	5.525e-01	0.882
PE-rich_127	300_All	53	21.117	1.100e+00	0.504
PE-rich_127	900_All	53	21.117	3.784e+00	0.002

108

109

111 **Tab. S9.** One-way ANOVA of single phase exponential decay fit model (Fit_model) of pooled data across different
 112 strains for a given phase of growth (exponential; _Exp, pre-stationary; _St) and across different phase of growth for
 113 a given strain (_Exp_St) from PUR/PAR ratio in relation to the cumulative diel PAR ($\mu\text{mol photons m}^{-2}\text{d}^{-1}$), for two
 114 PhycoCyanin(PC)-rich cultures (056, 077) and two PhycoErythrin(PE)-rich cultures (048, 127) of *Synechococcus*
 115 sp., grown at 30, 90, 180, 300, 600, or 900 peak PAR $\mu\text{mol photons m}^{-2}\text{s}^{-1}$; and photoperiods of 8, 12, 16, or 24 h.
 116 Res.Df - residual degrees of freedom for each model; Res.Sum Sq - residual sum of squares for each model; F_value
 117 – Fisher's F-test statistic; p_value - level of significance.

118

Fit_model	Res.Df	Res.Sum Sq	F_value	p_value
056_077_Exp	43	0.025	2.813e+01	0.000
048_127_Exp	51	0.217	NA	N/A
056_048_Exp	51	0.307	2.762e+01	0.000
077_048_Exp	51	0.307	5.976e+01	0.000
056_127_Exp	51	0.217	1.607e+01	0.000
077_127_Exp	51	0.217	4.064e+01	0.000
056_077_St	20	0.006	-1.491e-01	1.000
048_127_St	2	0.000	5.386e+00	0.168
056_048_St	17	0.009	9.648e-02	0.999
077_048_St	17	0.009	-2.066e+00	1.000
056_127_St	2	0.000	1.415e+01	0.067
077_127_St	2	0.000	2.812e+00	0.294
056_Exp_St	7	0.008	1.882e+00	0.195
077_Exp_St	20	0.006	3.039e+00	0.007
048_Exp_St	17	0.009	1.681e+01	0.000
127_Exp_St	2	0.000	4.128e+01	0.024

119

120

122 **Tab. S10.** One-way ANOVA of single phase exponential decay fit model (Fit_model) of pooled data across
123 different strains for a given phase of growth (exponential; _Exp, pre-stationary; _St) and across different phase of
124 growth for a given strain (_Exp_St) from Phycobiliprotein to Chl a ratio in relation to the cumulative diel PAR
125 ($\mu\text{mol photons m}^{-2}\text{d}^{-1}$), for two PhycoCyanin(PC)-rich cultures (056, 077) and two PhycoErythrin(PE)-rich
126 cultures (048, 127) of *Synechococcus* sp., grown at 30, 90, 180, 300, 600, or 900 peak PAR $\mu\text{mol photons m}^{-2}\text{s}^{-1}$;
127 and photoperiods of 8, 12, 16, or 24 h. Res.Df - residual degrees of freedom for each model; Res.Sum Sq - residual
128 sum of squares for each model; F _value – Fisher's F -test statistic; p _value - level of significance.
129

Fit_model	Res.Df	Res.Sum Sq	F _value	p _value
056_077_Exp	49	38.089	1.531e+01	0.000
048_127_Exp	52	54.559	NA	N/A
056_048_Exp	52	39.302	4.333e+00	0.005
077_048_Exp	52	39.302	5.202e-01	0.670
056_127_Exp	52	54.559	1.067e+01	0.000
077_127_Exp	52	54.559	7.063e+00	0.000
056_077_St	24	3.580	-1.005e+01	1.000
048_127_St	19	3.343	NA	N/A
056_048_St	19	2.239	-2.229e-01	1.000
077_048_St	19	2.239	2.276e+00	0.088
056_127_St	19	3.343	-1.195e+00	1.000
077_127_St	19	3.343	2.686e-01	0.925
056_Exp_St	25	2.081	1.399e+01	0.000
077_Exp_St	24	3.580	9.255e+00	0.000
048_Exp_St	19	2.239	9.531e+00	0.000
127_Exp_St	19	3.343	8.820e+00	0.000

130

131

133 **Tab. S11.** One-way ANOVA of single phase exponential decay fit model (Fit_model) of pooled data across
 134 different strains for a given phase of growth (exponential; _Exp, pre-stationary; _St) and across different phase of
 135 growth for a given strain (_Exp_St) from effective absorption cross section of PSII (σ_{PSII}' ; nm² quanta⁻¹) measured
 136 under diel peak PAR growth light under Ex590nm (orange) excitation in relation to the cumulative diel PAR (μmol
 137 photons m⁻²d⁻¹), for two PhycoCyanin(PC)-rich cultures (056, 077) and two PhycoErythrin(PE)-rich cultures (048,
 138 127) of *Synechococcus* sp., grown at 30, 90, 180, 300, 600, or 900 peak PAR μmol photons m⁻²s⁻¹; and
 139 photoperiods of 8, 12, 16, or 24 h. Res.Df - residual degrees of freedom for each model; Res.Sum Sq - residual sum
 140 of squares for each model; F_value – Fisher's F-test statistic; p_value - level of significance.

141

Fit_model	Res.Df	Res.Sum Sq	F_value	p_value
056_077_Exp	97	116.359	9.926e-01	0.469
048_127_Exp	72	106.728	-1.652e+00	1.000
056_048_Exp	97	116.359	3.764e+01	0.000
077_048_Exp	112	134.219	8.037e+00	0.000
056_127_Exp	72	106.728	2.599e-01	1.000
077_127_Exp	72	106.728	4.636e-01	0.995
056_077_St	41	3.366	1.522e+01	0.000
048_127_St	45	38.775	3.762e+00	0.001
056_048_St	34	17.489	1.158e+02	0.000
077_048_St	34	17.489	-3.922e+00	1.000
056_127_St	45	38.775	1.566e+02	0.000
077_127_St	45	38.775	1.078e+02	0.000
056_Exp_St	17	0.150	1.650e+02	0.000
077_Exp_St	41	3.366	2.245e+01	0.000
048_Exp_St	34	17.489	1.146e+00	0.339
127_Exp_St	45	38.775	2.921e+00	0.001

142

143

145 **Tab. S12.** *T*-test of linear fit model (Fit_model) of pooled data across different strains for a given phase of growth
 146 (exponential; _Exp, pre-stationary; _St) and across different phase of growth for a given strain (_Exp_St) from
 147 effective absorption cross section of PSII (σ_{PSII}' ; nm² quanta⁻¹) measured under diel peak PAR growth light under
 148 Ex_{445nm} (blue) excitation in relation to the cumulative diel PAR ($\mu\text{mol photons m}^{-2}\text{d}^{-1}$, for two PhycoCyanin(PC)-
 149 rich cultures (056, 077) and two PhycoErythrin(PE)-rich cultures (048, 127) of *Synechococcus* sp., grown at 30, 90,
 150 180, 300, 600, or 900 peak PAR $\mu\text{mol photons m}^{-2}\text{s}^{-1}$; and photoperiods of 8, 12, 16, or 24 h. Estimate - estimation
 151 statistics; Std.Error - standard error of the estimate; *t*_value – *t*-test statistic; *p*_value - level of significance.
 152

Fit_model	Estimate	Std.Error	<i>t</i> _value	<i>p</i> _value
056_077_Exp	-1.451e-09	1.058e-09	-1.372	0.171
056_048_Exp	-2.188e-09	1.313e-09	-1.666	0.097
056_127_Exp	-8.236e-10	1.412e-09	-0.583	0.560
048_127_Exp	1.365e-09	1.603e-09	0.851	0.395
077_048_Exp	-7.373e-10	1.233e-09	-0.598	0.550
077_127_Exp	6.274e-10	1.336e-09	0.470	0.639
056_077_St	2.453e-09	1.349e-09	1.818	0.071
056_048_St	5.254e-09	2.098e-09	2.505	0.014
056_127_St	1.745e-09	1.862e-09	0.937	0.350
048_127_St	-3.509e-09	1.658e-09	-2.116	0.036
077_048_St	2.801e-09	1.263e-09	2.217	0.028
077_127_St	-7.077e-10	1.209e-09	-0.586	0.559
056_Exp_St	2.487e-09	1.643e-09	1.514	0.132
077_Exp_St	6.391e-09	9.166e-10	6.973	0.000
048_Exp_St	9.930e-09	1.695e-09	5.860	0.000
127_Exp_St	5.056e-09	1.621e-09	3.120	0.002

153

154

156 **Tab. S13.** *T*-test of linear fit model (Fit_model) of pooled data across different strains for a given phase of growth
 157 (exponential; _Exp, pre-stationary; _St) and across different phase of growth for a given strain (_Exp_St) from
 158 effective absorption cross section of PSII (σ_{PSII}' ; nm² quanta⁻¹) measured under diel peak PAR growth light under
 159 Ex_{445nm} (blue) excitation in relation to Phycobiliprotein to Chl *a* ratio, for two PhycoCyanin(PC)-rich cultures (056,
 160 077) and two PhycoErythrin(PE)-rich cultures (048, 127) of *Synechococcus* sp., grown at 30, 90, 180, 300, 600, or
 161 900 peak PAR $\mu\text{mol photons m}^{-2}\text{s}^{-1}$; and photoperiods of 8, 12, 16, or 24 h. Estimate - estimation statistics;
 162 Std.Error - standard error of the estimate; *t*_value - *t*-test statistic; *p*_value - level of significance.
 163

Fit_model	Estimate	Std.Error	<i>t</i> _value	<i>p</i> _value
056_077_Exp	0.003	0.008	0.424	0.672
056_048_Exp	0.078	0.009	9.082	0.000
056_127_Exp	0.039	0.009	4.382	0.000
048_127_Exp	-0.039	0.009	-4.416	0.000
077_048_Exp	0.075	0.008	8.954	0.000
077_127_Exp	0.036	0.009	4.117	0.000
056_077_St	-0.023	0.007	-3.495	0.000
056_048_St	-0.062	0.016	-3.788	0.000
056_127_St	-0.037	0.014	-2.606	0.009
048_127_St	0.026	0.023	1.143	0.253
077_048_St	-0.039	0.014	-2.823	0.005
077_127_St	-0.013	0.012	-1.117	0.264
056_Exp_St	0.083	0.013	6.327	0.000
077_Exp_St	0.057	0.009	6.590	0.000
048_Exp_St	-0.057	0.018	-3.217	0.001
127_Exp_St	0.008	0.020	0.389	0.698

164

165

167 **Tab. S14.** *T*-test of linear fit model (Fit_model) of pooled data across different strains for a given phase of growth
 168 (exponential; _Exp, pre-stationary; _St) and across different phase of growth for a given strain (_Exp_St) from
 169 effective absorption cross section of PSII (σ_{PSII}' ; nm² quanta⁻¹) measured under Ex_{590nm} (orange) excitation in
 170 relation to the Phycobiliprotein to Chl *a* ratio, for two PhycoCyanin(PC)-rich cultures (056, 077) and two
 171 PhycoErythrin(PE)-rich cultures (048, 127) of *Synechococcus* sp., grown at 30, 90, 180, 300, 600, or 900 peak PAR
 172 μmol photons m⁻²s⁻¹; and photoperiods of 8, 12, 16, or 24 h. Estimate - estimation statistics; Std.Error - standard
 173 error of the estimate; *t*_value – *t*-test statistic; *p*_value - level of significance.
 174

Fit_model	Estimate	Std.Error	<i>t</i> _value	<i>p</i> _value
056_077_Exp	-0.369	0.092	-4.000	0.000
056_048_Exp	0.149	0.082	1.812	0.070
056_127_Exp	0.606	0.099	6.122	0.000
048_127_Exp	0.457	0.090	5.084	0.000
077_048_Exp	0.518	0.083	6.267	0.000
077_127_Exp	0.976	0.097	10.089	0.000
056_077_St	0.077	0.029	2.669	0.008
056_048_St	-0.610	0.079	-7.751	0.000
056_127_St	-0.299	0.071	-4.191	0.000
048_127_St	0.311	0.177	1.759	0.080
077_048_St	-0.688	0.076	-9.099	0.000
077_127_St	-0.377	0.070	-5.371	0.000
056_Exp_St	0.440	0.117	3.761	0.000
077_Exp_St	0.887	0.091	9.780	0.000
048_Exp_St	-0.319	0.148	-2.164	0.031
127_Exp_St	-0.465	0.247	-1.882	0.060

175

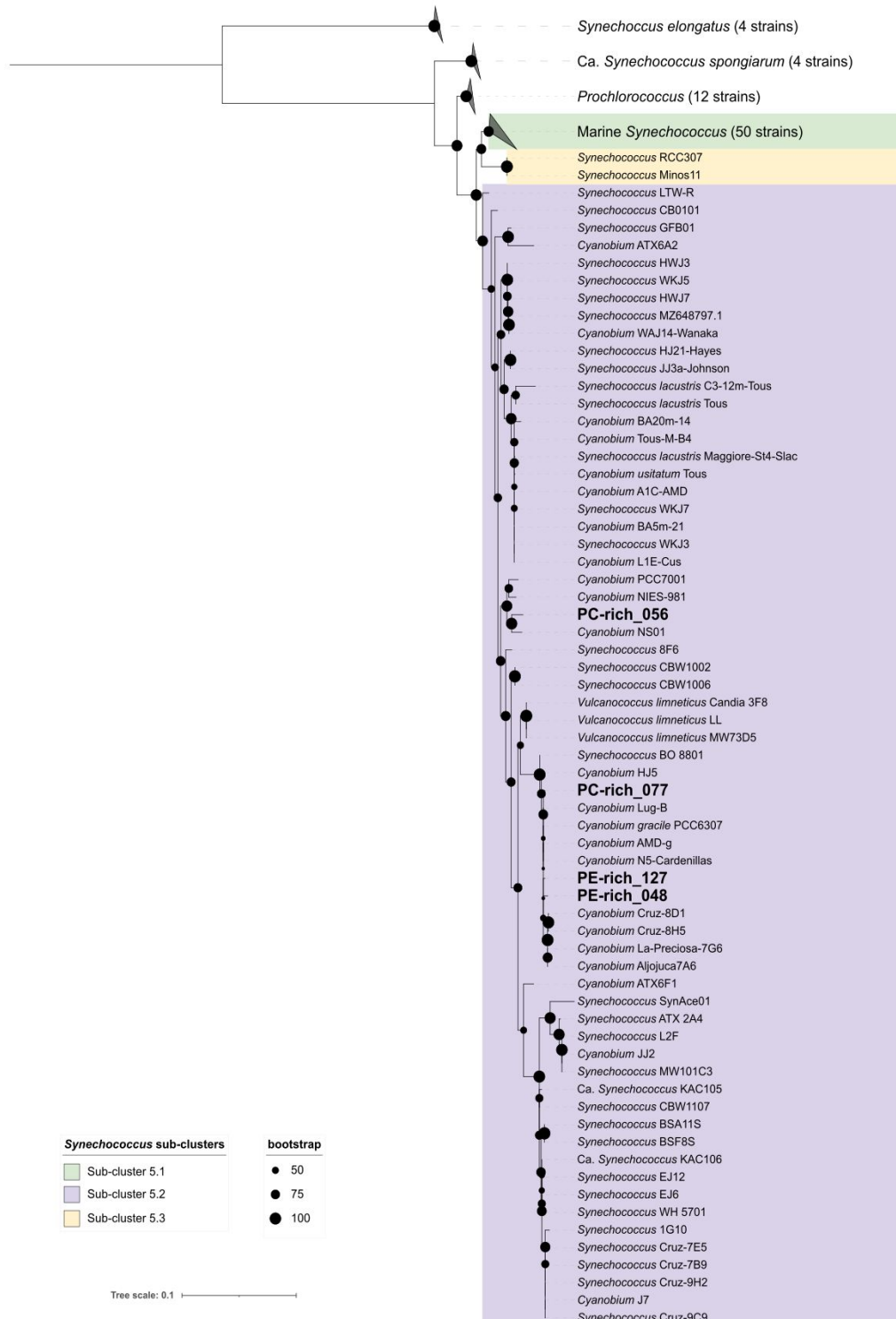
176

178 **Tab. S15.** *T*-test of linear fit model (Fit_model) of pooled data across different strains for a given phase of growth
 179 (exponential; _Exp, pre-stationary; _St) and across different phase of growth for a given strain (_Exp_St) from
 180 effective absorption cross section of PSII (σ_{PSII} ; nm² quanta⁻¹) measured under Ex590nm (orange) excitation in
 181 relation to the Phycobiliprotein to Chl *a* ratio, for two PhycoCyanin(PC)-rich cultures (056, 077) and two
 182 PhycoErythrin(PE)-rich cultures (048, 127) of *Synechococcus* sp., grown at 30, 90, 180, 300, 600, or 900 peak PAR
 183 μmol photons m⁻²s⁻¹; and photoperiods of 8, 12, 16, or 24 h. Estimate - estimation statistics; Std.Error - standard
 184 error of the estimate; *t*_value – *t*-test statistic; *p*_value - level of significance.

185

Fit_model	Estimate	Std.Error	<i>t</i> _value	<i>p</i> _value
056_077_Exp	-0.118	0.060	-1.962	0.050
056_048_Exp	0.216	0.058	3.693	0.000
056_127_Exp	0.841	0.076	11.067	0.000
048_127_Exp	0.625	0.076	8.187	0.000
077_048_Exp	0.334	0.060	5.526	0.000
077_127_Exp	0.959	0.075	12.806	0.000
056_077_St	0.397	0.027	14.566	0.000
056_048_St	-0.120	0.064	-1.873	0.062
056_127_St	0.086	0.061	1.411	0.159
048_127_St	0.206	0.114	1.801	0.073
077_048_St	-0.516	0.048	-10.776	0.000
077_127_St	-0.310	0.044	-7.121	0.000
056_Exp_St	0.317	0.075	4.234	0.000
077_Exp_St	0.831	0.061	13.656	0.000
048_Exp_St	-0.019	0.122	-0.155	0.877
127_Exp_St	-0.438	0.209	-2.099	0.036

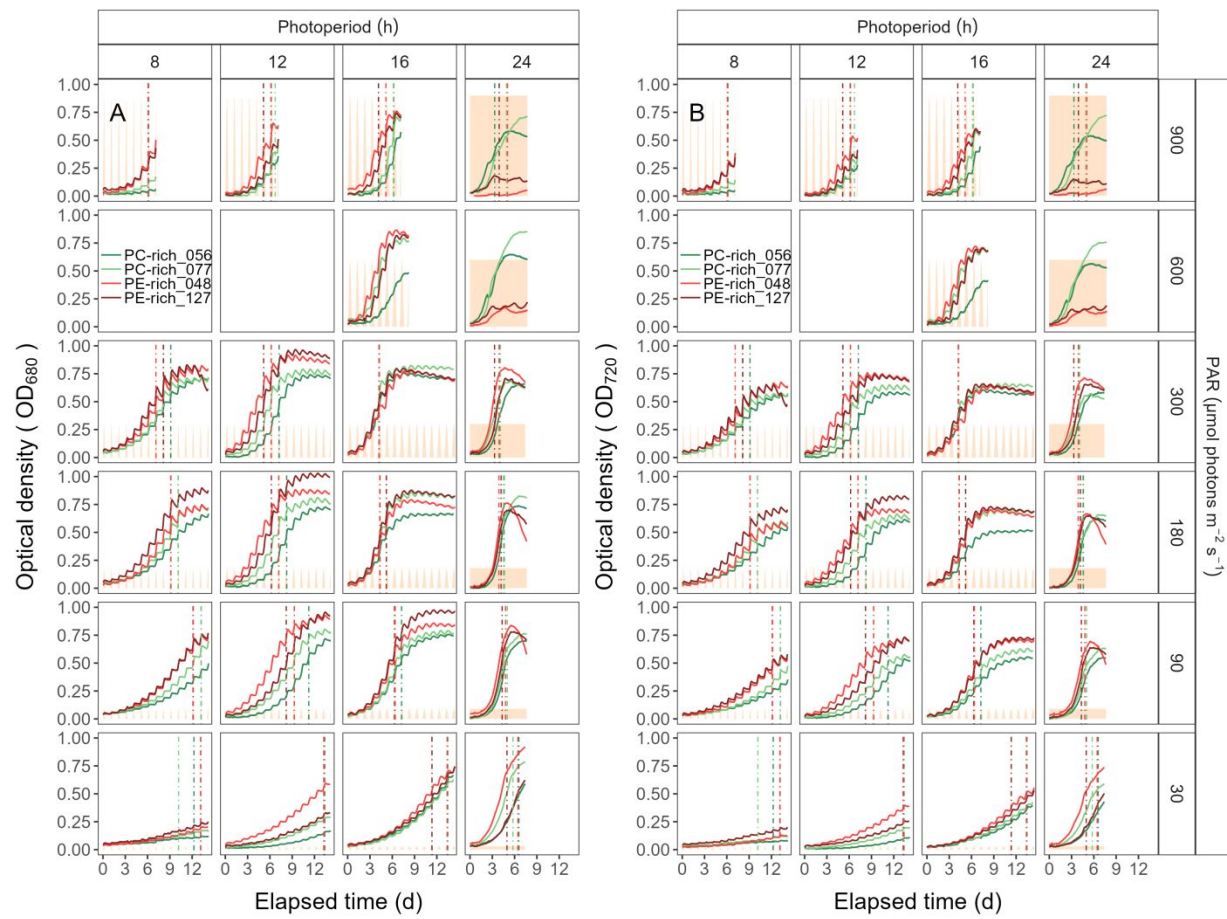
186



187

188 **Fig. S1.** Phylogenetic tree derived from partial 16S rRNA gene sequences using topology given by Maximum
189 Likelihood (1000 bootstraps). Support values are indicated by the size of internal nodes. Strains used in this study
190 are shown in bold.

191



192

193 **Fig. S2.** Growth curves, tracked as OD_{680} (A) and OD_{720} (B) vs. elapsed time (d). Growth curves were estimated
 194 over 5-min intervals for two PC-rich cultures (056; dark green, 077; light green) and two PE-rich cultures (048; light
 195 red, 127; dark red) of *Synechococcus* sp. grown at 30, 90, 180, 300, 600, or 900 peak PAR $\mu\text{mol photons m}^{-2}\text{s}^{-1}$; and
 196 photoperiods of 8, 12, 16, or 24 h. The vertical lines represent the time when the cultures reached the maximum of
 197 the 1st derivative of OD_{680} , or maximum absolute hourly growth (tMaxAHG), taken as an index of transition from
 198 exponential to pre-stationary growth phases. The orange area represents the photoperiods, with peak PAR x 1/1000
 199 to scale to the Y axis.

200

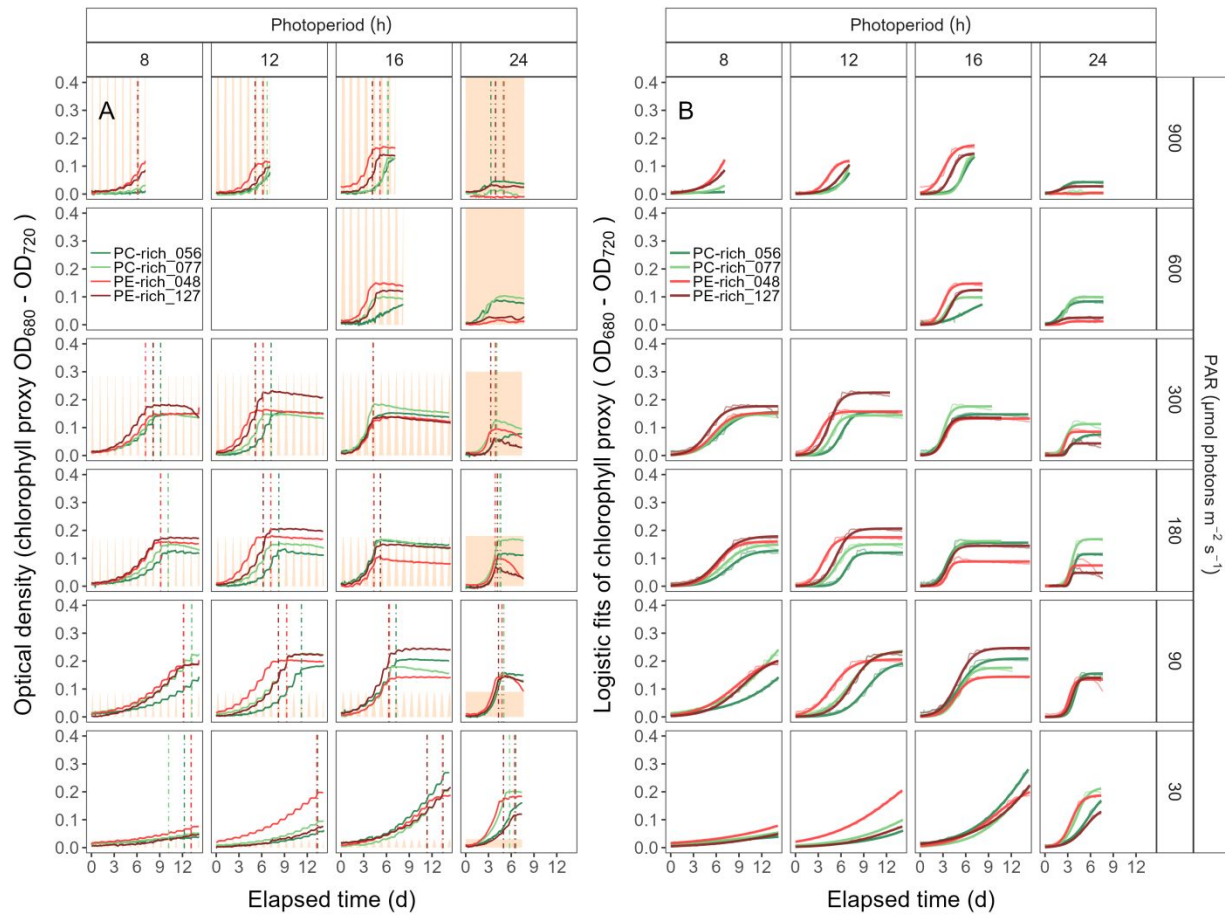
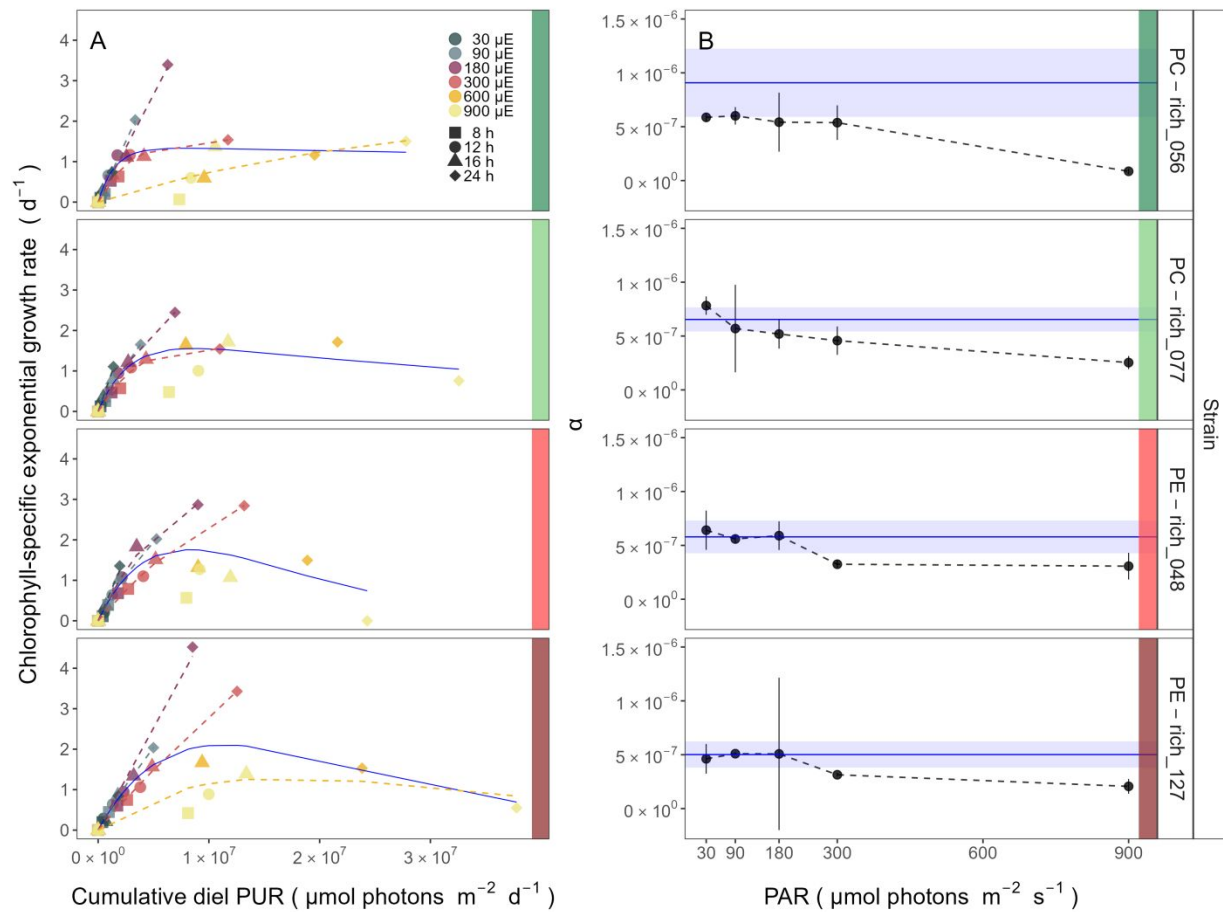


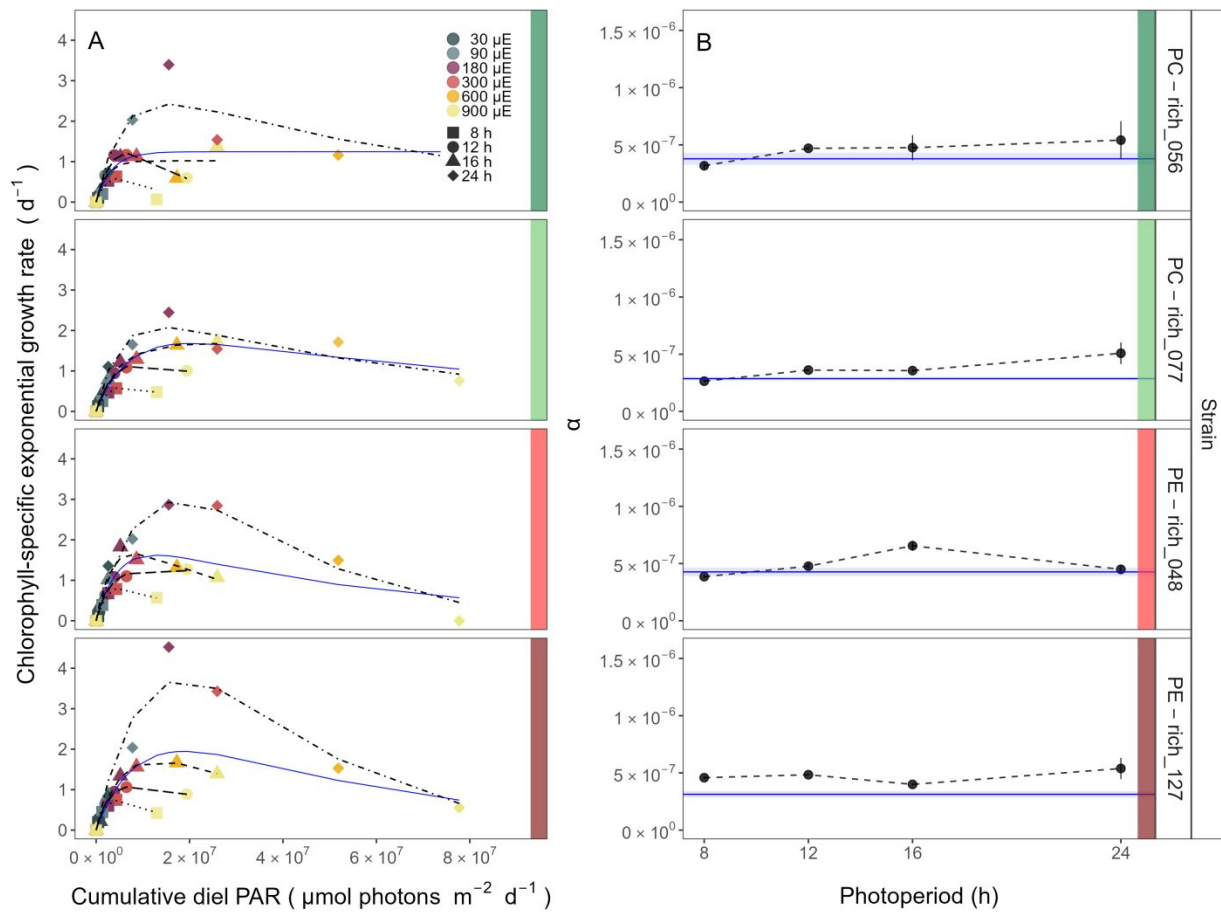
Fig. S3. (A) Growth curves (tracked as chlorophyll proxy $\text{OD}_{680}-\text{OD}_{720}$; Δ OD) vs. elapsed time (d). Growth curves were estimated over 5-min intervals for two PC-rich cultures (056; dark green, 077; light green) and two PE-rich cultures (048; light red, 127; dark red) of *Synechococcus* sp. grown at 30, 90, 180, 300, 600, or 900 peak PAR $\mu\text{mol photons m}^{-2}\text{s}^{-1}$; and photoperiods of 8, 12, 16, or 24 h. The vertical lines represent the time when the cultures reached the maximum of the 1st derivative of OD_{680} , or maximum absolute hourly growth (tMaxAHG), taken as an index of transition from exponential to pre-stationary growth phases. The orange area represents the photoperiods, with peak PAR $\times 1/2000$ to scale to the Y axis. (B) Logistic fits (thick lines) of chlorophyll proxy $\text{OD}_{680}-\text{OD}_{720}$ (Δ OD) vs. elapsed time (d). Growth curves (thin line) measured over 5-min intervals for each strain were also presented.



212

Fig. S4. (A) Chlorophyll-specific exponential growth rates (d^{-1}) vs. cumulative diel Photosynthetically Usable
Radiation (PUR, $\mu\text{mol photons m}^{-2}\text{d}^{-1}$). Growth rates (\pm SE falling within symbols) were estimated from logistic fits
of chlorophyll proxy OD₆₈₀ – OD₇₂₀ (ΔOD) vs. elapsed time (Fig. 1, Fig. S3B), for two PC-rich cultures (056; dark
green, 077; light green) and two PE-rich cultures (048; light red, 127; dark red) of *Synechococcus* sp. grown at 30
(dark gray), 90 (light gray), 180 (purple), 300 (red), 600 (orange), or 900 (yellow) peak PAR $\mu\text{mol photons m}^{-2}\text{s}^{-1}$
(μE); and photoperiods of 8 (square), 12 (circle), 16 (triangle), or 24 (diamond) h. Solid blue line shows a fit of the
pooled growth rates through peak PAR for each strain, with a three parameter model (Harrison and Platt, 1986). We
also fit the same model separately for 30 (dark gray), 90 (light gray), 180 (purple), 300 (red), 600 together with 900
(orange) peak PAR $\mu\text{mol photons m}^{-2}\text{s}^{-1}$, only when they were each significantly different (ANOVA, $p < 0.05$) from
the fit of pooled data. (B) Alpha parameters of the initial rise of growth rate (α) vs. cumulative diel
Photosynthetically Usable Radiation (PUR), estimated from data pooled for each peak PAR (points (\pm SE)
connected by dashed lines), and estimated for all data across all peak PAR, for each strain (solid blue horizontal line
 \pm SE).

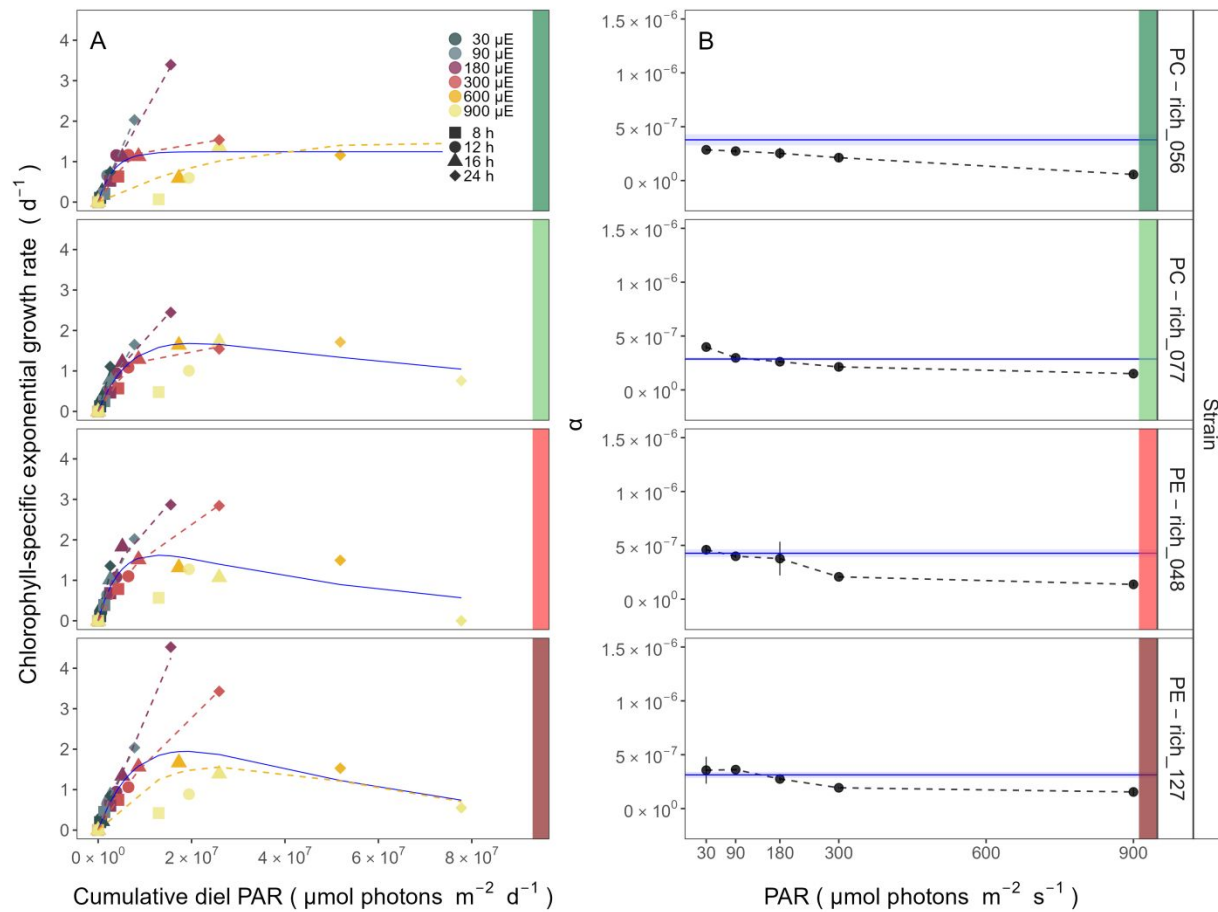
226



227

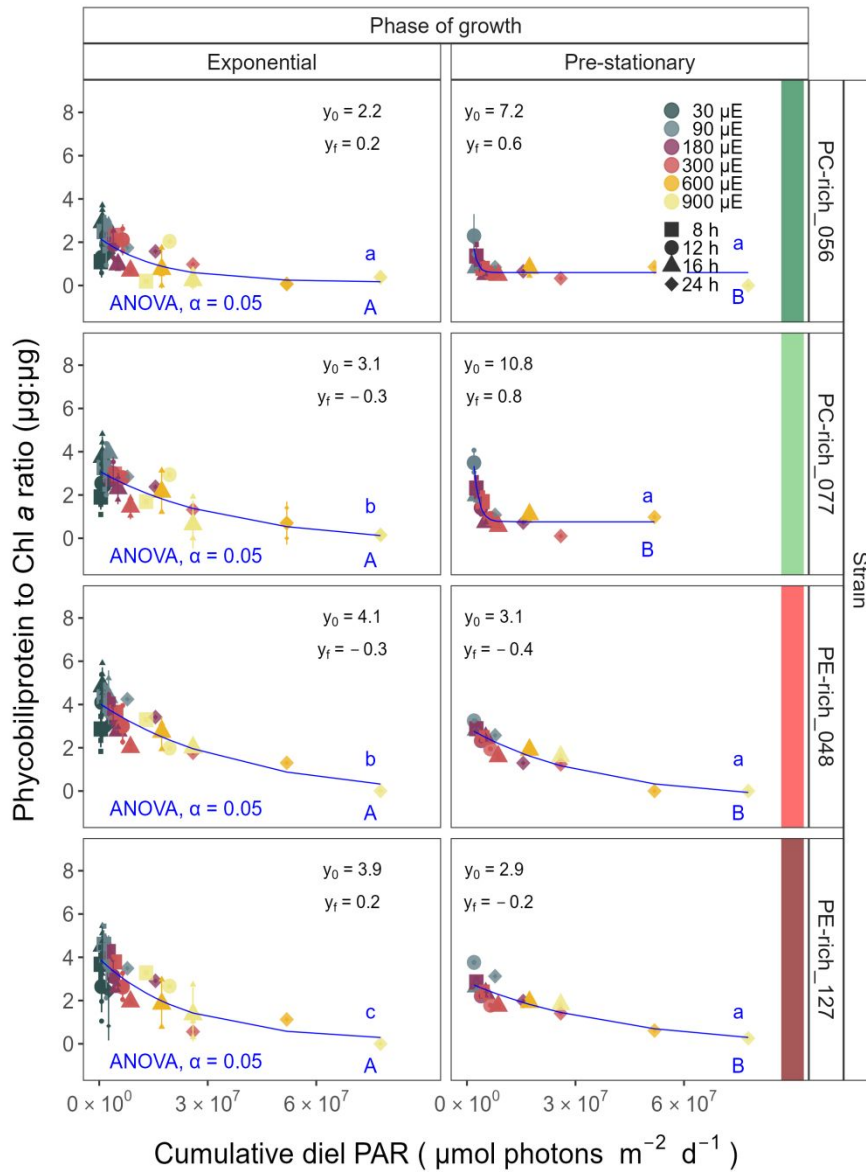
228 **Fig. S5.** (A) Chlorophyll-specific exponential growth rates (d^{-1}) vs. cumulative diel PAR ($\mu\text{mol photons m}^{-2} \text{d}^{-1}$).
 229 Growth rates (\pm SE falling within symbols) were estimated from logistic fits of chlorophyll proxy OD₆₈₀ – OD₇₂₀
 230 (ΔOD) vs. elapsed time (Fig. 1, Fig. S3B), for two PC-rich cultures (056; dark green, 077; light green) and two PE-
 231 rich cultures (048; light red, 127; dark red) of *Synechococcus* sp. grown at 30 (dark gray), 90 (light gray), 180
 232 (purple), 300 (red), 600 (orange), or 900 (yellow) peak PAR $\mu\text{mol photons m}^{-2}\text{s}^{-1}$ (μE); and photoperiods of 8
 233 (square), 12 (circle), 16 (triangle), or 24 (diamond) h. Solid blue line shows a fit of the pooled growth rates through
 234 photoperiod (h) for each strain, with a three parameter model (Harrison and Platt 1986). We also fit the same model
 235 separately for 8 (dotted line), 12 (long dash line), 16 (dashed line), or 24 (two dash line) h photoperiods, since for all
 236 strains they were each significantly different (ANOVA, $p < 0.05$) from the fit of pooled data. (B) Alpha parameters
 237 of the initial rise of growth rate (α) vs. cumulative diel PAR, estimated from data pooled for each photoperiod
 238 (points (\pm SE) connected by dashed lines), and estimated for all data across photoperiods (solid blue horizontal line
 239 \pm SE), for each strain.

240

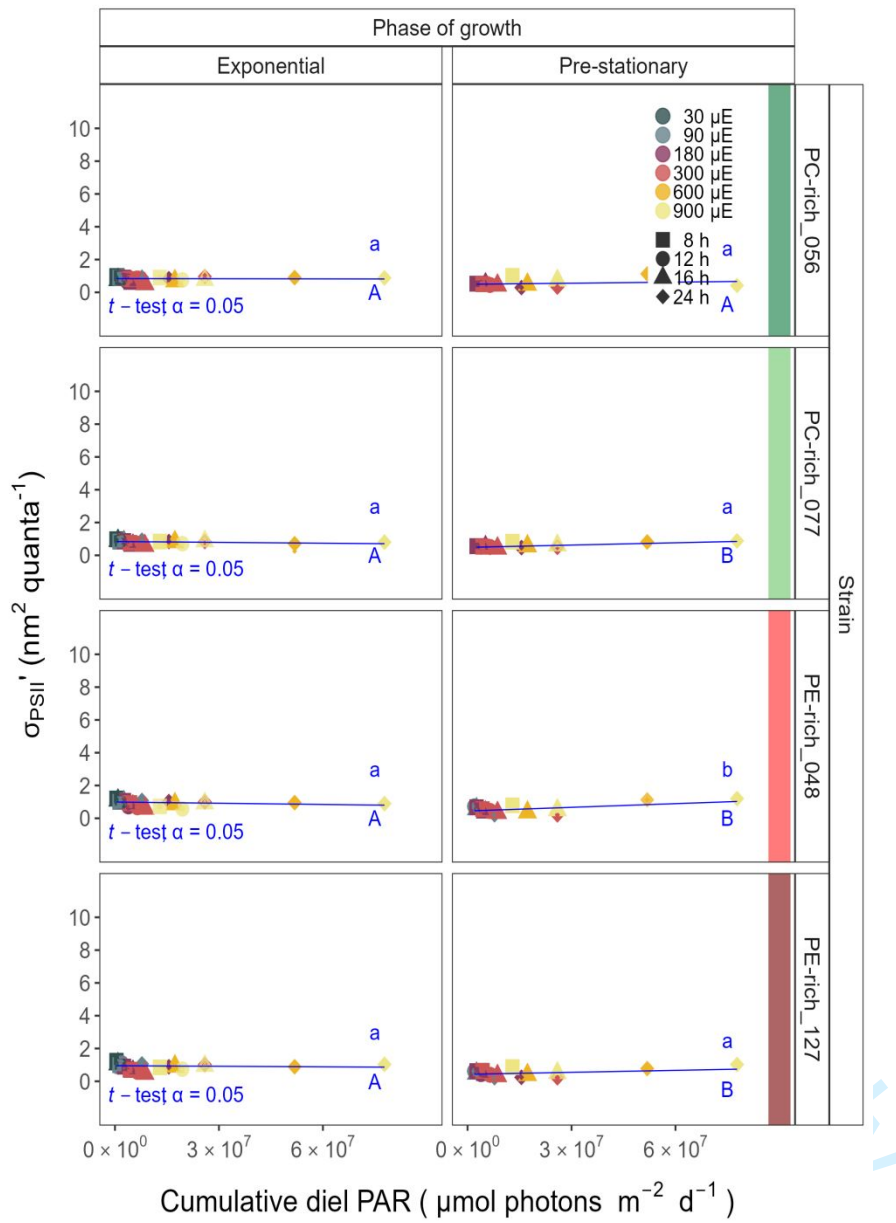


241
Fig. S6. (A) Chlorophyll-specific exponential growth rates (d^{-1}) vs. cumulative diel PAR ($\mu\text{mol photons m}^{-2}\text{d}^{-1}$).
242 Growth rates (\pm SE falling within symbols) were estimated from logistic fits of chlorophyll proxy OD₆₈₀ – OD₇₂₀
243 (ΔOD) vs. elapsed time (Fig. 1, Fig. S3B), for two PC-rich cultures (056; dark green, 077; light green) and two PE-
244 rich cultures (048; light red, 127; dark red) of *Synechococcus* sp. grown at 30 (dark gray), 90 (light gray), 180
245 (purple), 300 (red), 600 (orange), or 900 (yellow) peak PAR $\mu\text{mol photons m}^{-2}\text{s}^{-1}$ (μE); and photoperiods of 8
246 (square), 12 (circle), 16 (triangle), or 24 (diamond) h. Solid blue line shows a fit of the pooled growth rates through
247 peak PAR for each strain, with a three parameter model (Harrison and Platt, 1986). We also fit the same model
248 separately for 30 (dark gray), 90 (light gray), 180 (purple), 300 (red), 600 together with 900 (orange) peak PAR
249 $\mu\text{mol photons m}^{-2}\text{s}^{-1}$, only when they were each significantly different (ANOVA, $p < 0.05$) from the fit of pooled
250 data. **(B)** Alpha parameters of the initial rise of growth rate (α) vs. cumulative diel PAR, estimated from data pooled
251 for each peak PAR (points (\pm SE) connected by dashed lines), and estimated for all data across all peak PAR, for
252 each strain (solid blue horizontal line \pm SE).
253

254



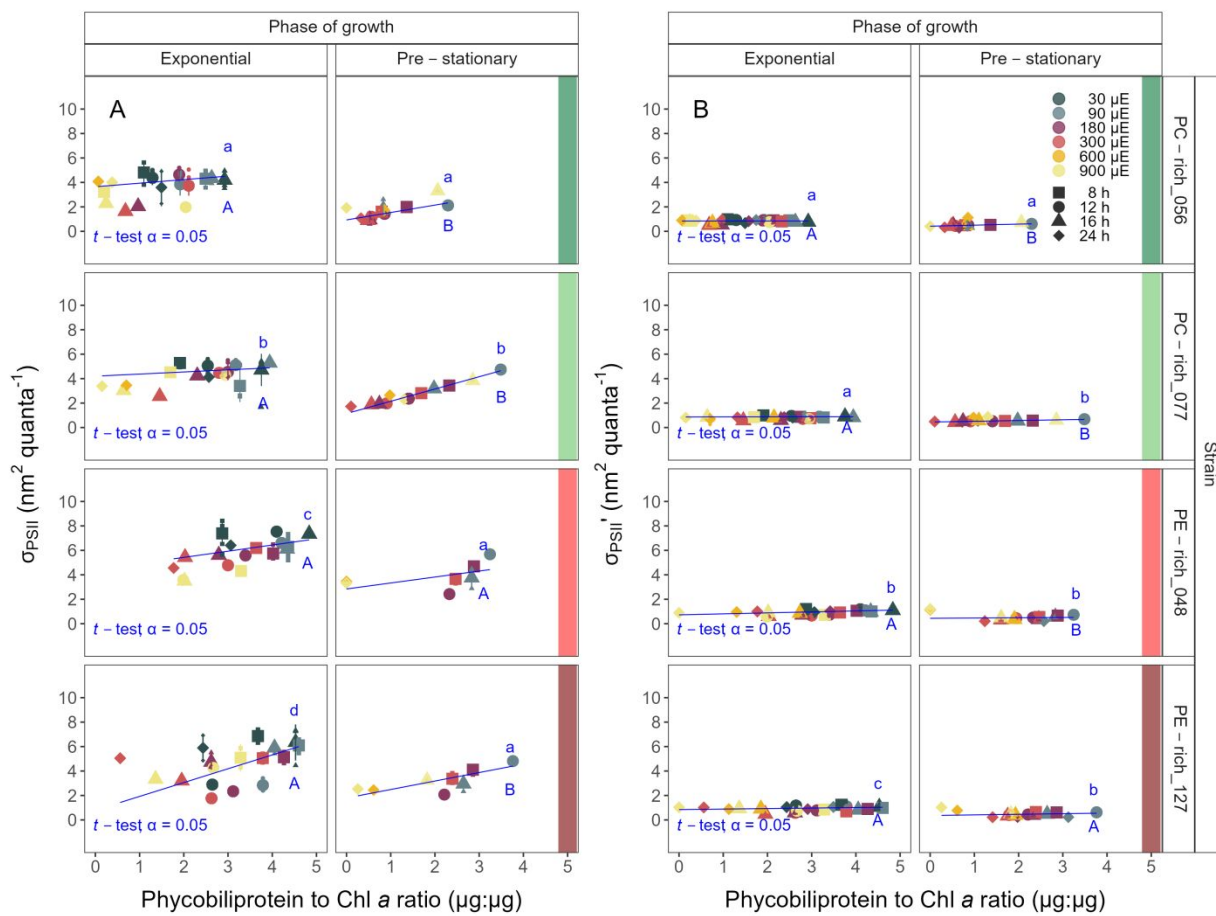
255
256 **Fig. S7.** Changes of Phycobiliprotein to Chl *a* ratio ($\mu\text{g}:\mu\text{g}$) vs. cumulative diel PAR ($\mu\text{mol photons m}^{-2}\text{d}^{-1}$).
257 Phycobiliprotein to Chl *a* ratio was estimated for two PC-rich cultures (056; dark green, 077; light green) and two
258 PE-rich cultures (048; light red, 127; dark red) of *Synechococcus* sp. grown at 30 (dark gray), 90 (light gray), 180
259 (purple), 300 (red), 600 (orange), or 900 (yellow) peak PAR $\mu\text{mol photons m}^{-2}\text{s}^{-1}$ (μE); and photoperiods of 8
260 (square), 12 (circle), 16 (triangle), or 24 (diamond) h. Figure presents data (smaller symbols) and means (bigger
261 symbols) from exponential or pre-stationary phase of growth. Blue solid line shows single phase exponential decay
262 fit for data from each strain and growth phase, fit parameters are presented. Different lowercase letters indicate
263 statistically significant differences between the fit models for different strains within a given phase of growth.
264 Different uppercase letters indicate statistically significant differences between the fit models for different phases of
265 growth within a given strain (ANOVA; $p < 0.05$).
266



267

268 **Fig. S8.** Effective absorption cross section of PSII ($\sigma_{\text{PSII}'}$; $\text{nm}^2 \text{ quanta}^{-1}$) measured under diel peak PAR growth light
 269 under blue ($\text{Ex}_{445\text{nm}}$) excitation vs. cumulative diel PAR ($\mu\text{mol photons m}^{-2} \text{ d}^{-1}$). $\sigma_{\text{PSII}'}$ was estimated for two PC-rich
 270 cultures (056; dark green, 077; light green) and two PE-rich cultures (048; light red, 127; dark red) of
 271 *Synechococcus* sp. grown at 30 (dark gray), 90 (light gray), 180 (purple), 300 (red), 600 (orange), or 900 (yellow)
 272 peak PAR $\mu\text{mol photons m}^{-2} \text{ s}^{-1}$ (μE); and photoperiods of 8 (square), 12 (circle), 16 (triangle), or 24 (diamond) h.
 273 Figure presents data (smaller symbols) and means (bigger symbols) from exponential or pre-stationary phase of
 274 growth. Blue solid line shows linear model fit for data from each strain and growth phase. Different lowercase
 275 letters indicate statistically significant differences between the fit models for different strains within a given phase of
 276 growth. Different uppercase letters indicate statistically significant differences between the fit models for different
 277 phases of growth within a given strain (t -test; $p < 0.05$).

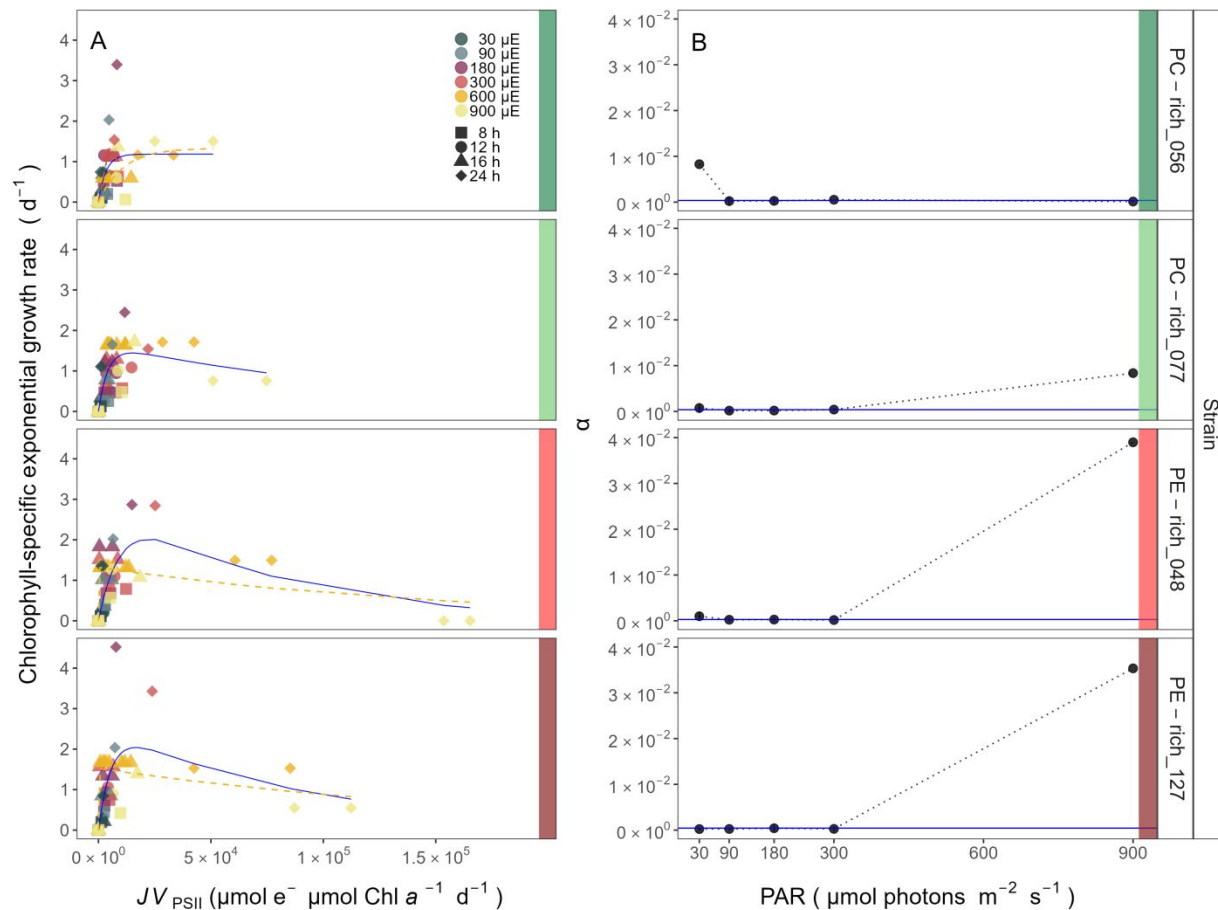
278



279

Fig. S9. (A) Changes of effective absorption cross section of PSII (σ_{PSII} ; $\text{nm}^2 \text{ quanta}^{-1}$) measured at the dark period under orange ($\text{Ex}_{590\text{nm}}$) excitation vs. the ratio of sum of μg phycobilins (PE, PC, APC protein, Phycobiliprotein) to μg Chl *a*. **(B)** Changes of effective absorption cross section of PSII (σ_{PSII}' ; $\text{nm}^2 \text{ quanta}^{-1}$) measured under diel peak PAR growth light under blue ($\text{Ex}_{445\text{nm}}$) excitation vs. the ratio of sum of μg phycobilins (PE, PC, APC protein, Phycobiliprotein) to μg Chl *a*. σ_{PSII}' was estimated for two PC-rich cultures (056; dark green, 077; light green) and two PE-rich cultures (048; light red, 127; dark red) of *Synechococcus* sp. grown at 30 (dark gray), 90 (light gray), 180 (purple), 300 (red), 600 (orange), or 900 (yellow) peak PAR $\mu\text{mol photons m}^{-2}\text{s}^{-1}$ (μE); and photoperiods of 8 (square), 12 (circle), 16 (triangle), or 24 (diamond) h. Figure presents data (smaller symbols) and means (bigger symbols) from exponential or pre-stationary phase of growth. Blue solid line shows linear model fit for data from each strain and growth phase. Different lowercase letters indicate statistically significant differences between the fit models for different strains within a given phase of growth. Different uppercase letters indicate statistically significant differences between the fit models for different phases of growth within a given strain (*t*-test; $p < 0.05$).

292



293

294 **Fig. S10.** (A) Chlorophyll specific exponential growth rates (d^{-1}) vs. cumulative diel PSII electron flux (JV_{PSII} ; μmol
 295 $e^- \mu\text{mol Chl } a^{-1} d^{-1}$) measured under diel peak PAR growth light. Growth rates (\pm SE falling within symbols)
 296 were estimated from logistic fits of chlorophyll proxy $OD_{680} - OD_{720}$ (ΔOD) vs. elapsed time (Fig. S3). PSII flux was
 297 estimated using FRRf induction curves with excitation of chlorophyll ($Ex_{445\text{nm}}$, blue), for two PC-rich cultures (056;
 298 dark green, 077; light green) and two PE-rich cultures (048; light red, 127; dark red) of *Synechococcus* sp. grown at
 299 30 (dark gray), 90 (light gray), 180 (purple), 300 (red), 600 (orange), or 900 (yellow) peak PAR $\mu\text{mol photons}$
 300 $\text{m}^{-2}\text{s}^{-1}$ (μE); and photoperiods of 8 (square), 12 (circle), 16 (triangle), or 24 (diamond) h. Solid blue line shows a fit
 301 of the pooled growth rates for each strain, with a three parameter model (Harrison and Platt 1986). We also fit the
 302 same model separately for 600 together with 900 (orange) peak PAR $\mu\text{mol photons m}^{-2}\text{s}^{-1}$, when they were
 303 significantly different (ANOVA, $p < 0.05$) from the fit of pooled data. (B) Alpha parameters of the initial rise of
 304 growth rate (α) vs. cumulative diel JV_{PSII} , estimated from data pooled for each peak PAR (points (\pm SE) connected
 305 by dashed lines), and estimated for all data across all peak PAR, for each strain (solid blue horizontal line \pm SE).

306

307 **References**

- 308 Harrison, W. G., and T. Platt. 1986. Photosynthesis-irradiance relationships in polar and
 309 temperate phytoplankton populations. Polar biology **5**: 153–164.